MECHANISM AND CONSEQUENCES OF CALCIUM INFLUX DURING DROSOPHILA EGG ACTIVATION

A Dissertation
Presented to the Faculty of the Graduate School
of Cornell University
In Partial Fulfillment of the Requirements for the Degree of
Doctor of Philosophy

by
Qinan Hu
May 2020

MECHANISM AND CONSEQUENCES OF CALCIUM INFLUX DURING DROSOPHILA EGG ACTIVATION

Qinan Hu, Ph. D.
Cornell University 2020

At the end of oogenesis, the mature oocyte is arrested in meiosis. It needs to be "activated" to transition to embryonic development. The egg activation process is largely conserved across organisms. It is accompanied by a rise of intracellular calcium in almost all species studied to date. This calcium rise is believed to trigger a series of downstream events in preparation for embryogenesis, including cell cycle resumption, maternal protein and mRNA processing, cytoskeleton rearrangement, egg covering modification and releases of intracellular zinc. In vertebrates, echinoderms, and *C. elegans*, egg activation is triggered by fertilization. In arthropods, however, egg activation is uncoupled from fertilization. *Drosophila* egg activation is triggered by mechanical pressure and oocyte-swelling during ovulation. Despite the different triggers, the presence of a calcium level rise and many downstream events are conserved. The calcium rise during *Drosophila* egg activation initiates through influx of external calcium. This influx nucleates a calcium wave that starts from the oocyte pole(s) and sweeps across the oocyte. The propagation of this calcium wave requires release of calcium from internal stores through IP_3R channels.

My research uncovered several aspects of *Drosophila* egg activation. I discovered that the TRP family channel, Trpm, mediates the calcium influx required for calcium wave initiation; I proposed a model for how Trpm is activated. I also

showed that Plc21c is required for calcium wave propagation, possibly through the IP_3 pathway. Downstream of the calcium wave, I detected a wave of F-actin reorganization that is interdependent with the calcium wave. I also found that zinc levels increase during oocyte maturation and decrease upon egg activation. These phenomena are analogous to those observed in echinoderms or mammals; their mechanisms have not been elucidated. My findings not only suggest conservation of multiple events during egg activation, but also demonstrate that *Drosophila* is an ideal model with which to dissect the molecular mechanisms of these events. In addition, I carried out experiments to optimize a germline-specific CRISPR/Cas9-mediated genome editing protocol in *Drosophila* that will facilitate future studies of *Drosophila* reproduction and germ cells.

BIOGRAPHICAL SKETCH

Qinan Hu grew up in Changzhou, a medium-sized city in southeast China. Eager to explore more of his potential, he signed up and passed the exam for admission to a special class for the gifted young in a junior high school located in a different city. Starting his boarding school life at the age of 13, Qinan finished his high school courses one year earlier than most of his peers and developed a passion for studying chemistry. He self-studied the college chemistry courses and won the first prize in National Olympiad Chemistry Competition, which guaranteed his admission to Peking University. In his undergraduate studies, he turned his interest to biochemistry and majored in life sciences. He gained his first appreciation for laboratory research working in the lab of Dr. Chengqi Yi, with whom he studied the mechanisms of methylation of specialized DNA bases. He continued his strong interest in research at Cornell University in pursuit of a Ph.D. degree, where he joined the lab of Dr. Mariana Wolfner and studied a fascinating process at the very beginning of life, egg activation, which involves a complex set of mechanisms that transition the oocyte to a developing embryo. After earning his Ph.D. degree, Qinan will continue his postdoc research back in China.

For Kexin and Zhixian

致 裴可心 与 胡知闲

ACKNOWLEDGMENTS

My time spent in Wolfner lab has been rewarding and exciting. Here, I learned how to come up with new ideas from previous research, how to design and perform experiments, how to collaborate with colleagues, and most of all, how to think like a scientist. None of these would have been possible without the inclusive and helpful environment of Wolfner lab, the inspiration and generosity of my collaborators, and Mariana, who has provided tremendous support for me throughout my graduate life, both in academics and in daily life. She discussed with me about research challenges, pointed me to the right direction, and helped me find the best people to collaborate with. She made me realize the qualities needed to be a good scientist and set a high-standard example for me to follow.

I would also like to thank my thesis committee members, Chun and Kelly, who were always there to provide their insightful suggestions whenever my research hit a bottleneck. In these years, I often trekked into unknown areas where none of our lab member was an expert. Thankfully, all the collaborators I met were patient and accommodating. Through working with them, I not only gained new perspectives to tackle my own problems, but also learned how to help build a supportive science community.

All of these experiences in my graduate school life will be invaluable assets for me in my future scientific career.

TABLE OF CONTENTS

LIST OF FIGURES

LIST OF TABLES

LIST OF ABBREVIATIONS

AB: activation buffer

ACA: *N*-(*p*-Amylcinnamoyl) anthranilic acid

APC: anaphase promoting complex

BAPTA: 1,2-bis(o-aminophenoxy) ethane-N,N,N′,N′-tetra acetic acid

CaMKII: Ca^{2+}/calmodulin-dependent protein kinase II

CG: cortical granule

CRISPR: clustered regularly interspaced short palindromic repeats

DAG: diacylglycerol

DSB: double strand break

ER: endoplasmic reticulum

FRAP: fluorescence recovery after photobleaching

FSC: follicle stem cell

GFP: green fluorescent protein

GSC: germline stem cell

HDR: homology directed repair

IB: isolation buffer

Indel: insertion/deletion

IP_3: inositol-1,4,5-triphosphate

IP_3R: inositol-1,4,5-triphosphate receptor

MAPK: mitogen-activated protein kinase

MI: meiosis I

MII: meiosis II

MPF: metaphase promoting factor

MS: mass spectrometry

NHEJ: non-homologous end joining

ORP2: Oregon-R-P2

PAM: protospacer adjacent motif

PI: propidium iodide

piRNA: Piwi-interaction RNA

PLC: phospholipase C

PM: plasma membrane

RB: modified Robb's buffer

ROI: region of interest

SEM: standard error of mean

TM: ammonium tetrathiomolybdate

TPEN: N,N,N′,N′-tetrakis(2-pyridylmethyl)-1,2-ethylenediamine

TRP: transient receptor potential

UAS: upstream activation sequence

UTR: untranslated region

VGCC: voltage-gated calcium channel

XFM: X-ray fluorescence microscopy

CHAPTER 1 INTRODUCTION

1.1 Oogenesis and egg activation in *Drosophila*

The *Drosophila melanogaster* ovary is a good model for studying germ cell development, meiosis and oocyte-to-embryo transition. Each *Drosophila* ovary consists of 16 to 20 ovarioles, which are assembly lines of oocytes. The germarium is located at the tip of the ovariole, including the area where the germline stem cells (GSCs) and follicle stem cells (FSCs) reside. GSCs divide asymmetrically, each division renews the GSC and give rise to a cystoblast. FSCs renew and give rise to the somatic follicle cells to surround the future egg chamber (reviewed in Wu et al., 2013). The cystoblast divides with incomplete cytokinesis for four times to produce 16 cystocytes, interconnected by ring canals and ensheathed by a layer of somatic follicle cells. This composite structure is called an egg chamber. Ring canals are maintained by a specialized type of organelle traversing them called the fusome (Lin et al., 1994). Each ovariole contains different stages of egg chambers, which develop through 14 morphologically distinct stages and the last stage, stage 14 (mature oocyte) is near the base of the ovary. It will ovulate into the oviduct.

Within the egg chamber, one of the 16 cystocytes will become the future oocyte. It is determined through a series of symmetry breaking events including asymmetric distribution of fusomes (de Cuevas and Spradling, 1998). Its other 15 sister cells become nurse cells that synthesize mRNAs, proteins and other molecules required for the future oocyte and embryo. As egg chambers mature, a series of cell-cell signaling, coordinated cell migrations and microtubule-based transfer of critical

molecules from nurse cells to the oocyte establish the proper polarity of the oocyte and egg chamber. This process is critical for the body axis determination of the future embryo (González-Reyes et al., 1995). The oocyte also takes up yolk from somatic tissues in a process called vitellogenesis. At late stages of oogenesis, the nurse cells "dump" all of their cytoplasm into the oocyte through ring canals and undergo apoptosis (reviewed in Buszczak and Cooley, 2000). The oocyte will enlarge significantly in size and ready to be ovulated.

The oocyte undergoes meiosis throughout oogenesis. Prophase I of meiosis occurs early during oogenesis when egg chamber is still in the germarium. The oocyte then arrests in the diplotene stage, at stage 5 of oogenesis, it remains arrested there until around stage 13. After stage 13, meiosis will progress to metaphase I. It arrests there again when the oocyte matures at stage 14 (reviewed in von Stetina and Orr-Weaver, 2011). The oocyte remains arrested in metaphase I until egg activation.

Egg activation is the process that releases mature oocytes from developmental arrest to transition to embryogenesis. The trigger of egg activation varies across species (reviewed in Horner and Wolfner, 2008a). In vertebrates, and some invertebrates like nematodes and echinoderms, egg activation is triggered by the fertilizing sperm (reviewed in Swann and Lai, 2016). In some marine invertebrates, egg activation is triggered by changes in pH and the ionic environment (Harada et al., 2003; Lindsay et al., 1992). In some insects, egg activation is independent of fertilization. In *Drosophila*, it is triggered by mechanical pressure from oviduct and/or fluid uptake during ovulation (Heifetz et al., 2001). The activated egg can then be fertilized by the sperm when the egg is in the uterus. *Drosophila* egg activation can be

mimicked *in vitro* by submerging dissected mature oocytes in a hypotonic buffer, in which the oocyte will swell and undergo several egg activation events (Horner and Wolfner, 2008b; Mahowald et al., 1983; Page and Orr-Weaver, 1997).

Egg activation encompasses a series of events in preparation for embryogenesis, including cell cycle resumption, maternal protein modification and/or degradation, maternal transcript translation or degradation, cytoskeletal rearrangement, eggshell and vitelline membrane modification and cellular zinc level decreases (**Figure 1.1**). Many of these events are conserved across species.

Before egg activation, the mature oocyte nucleus is arrested at species-specific stage during meiosis [metaphase II in mammals and *Xenopus* (Fan and Sun, 2004), metaphase I in *Drosophila* (von Stetina and Orr-Weaver, 2011)], mediated by cell cycle regulators such as maturation promoting factor (MPF). MPF consists of kinase Cdc2 and cyclin B; Its Cdc2 activity is dependent on cyclin B (Dunphy et al., 1988). Upon egg activation, the oocyte's meiotic cycle resumes from arrest via the activation of the anaphase promoting complex (APC). APC promotes the degradation of cyclin B and inactivation of MPF (reviewed in Acquaviva and Pines, 2006). MPF inactivation, along with the degradation of other proteins by APC, drives the progression of cell cycle, resulting in the formation of the haploid female pronucleus, ready to be fused with its male counterpart (reviewed in Gadella and Evans, 2011; Horner and Wolfner, 2008a; Krauchunas and Wolfner, 2013).

The oocyte proteome also undergoes drastic changes during egg activation. The transition from mature oocytes to embryos involves little if any transcription. Some protein activity changes rely on post-translational modification and/or

degradation of maternally deposited proteins in the oocyte. One prevalent protein modification is phosphorylation. In *Drosophila*, over three hundred proteins change their phosphorylation status during egg activation (Krauchunas et al., 2012). These phospho-proteins likely act as molecular switches controlling processes including cell cycle regulation and protein translation. Among them are key regulators of oogenesis and embryogenesis (Krauchunas et al., 2013; Zhang et al., 2018a, 2018b).

Mature oocytes are loaded with maternally deposited mRNAs. During egg activation, some of these maternal transcripts start to be translated. As mentioned above, early embryos experience a period of time with only little transcription. In *Drosophila*, this period can last about 2 hours until 13th mitotic cycle (Zalokar, 1976). Much of embryo development is driven by proteins translated from maternal transcripts during this period. A major regulator of mRNA translation during egg activation is the kinase Pan gu (*png*). Png activity is promoted by meiotic completion and extensively alters the translatome of activated eggs (Hara et al., 2017; Kronja et al., 2014). Poly(A) polymerase Wispy (*wisp*) is responsible for the polyadenylation of most maternally loaded mRNAs required for efficient translation during egg activation (Cui et al., 2008, 2013). On the other hand, some other maternal transcripts are removed during the transition to the totipotent embryo. In *Drosophila*, maternal protein Smaug (*smg*) and exonuclease Prage (*prage*) is responsible for destabilization and degradation of maternal transcripts during this process (Cui et al., 2016; Tadros et al., 2007).

The oocyte cytoskeleton is remodeled during egg activation. In mammals, protein kinase C reorganizes the intermediate filament network of the egg during

activation (Gallicano, 1995). In echinoderms, Actin cytoskeleton modulates calcium release during oocyte maturation and fertilization (Santella et al., 2015). In sea urchins, actin will polymerize around the sperm binding site to form a fertilization cone to facilitate the sperm-egg fusion (Tilney, 1980). Processes like these reshape the cytoskeleton of the egg in preparation for future embryo development.

Specialized egg coverings around mature oocytes serve multiple roles, including physical protection of the egg and embryo, sperm recognition and polyspermy blockage after fertilization. Egg coverings undergo major changes upon egg activation. In mammals and echinoderms, specialized secretory vesicles called cortical granules (CGs) in the oocyte undergo exocytosis and fuse with oocyte plasma membrane upon egg activation, releasing the enzymes within to modify the structure of extracellular egg coverings, serving as a blockage of polyspermy (Carroll Jr and Epel, 1975; Cheeseman et al., 2016; Gulyas, 1980). In *Drosophila*, egg coverings include inner vitelline membrane (vitelline envelope) and chorion. Crosslinking between vitelline membrane proteins and among chorion proteins occurs upon egg activation, hardening the eggshell, changing the eggshell's permeability and protecting the embryo from future environmental damage (Petri et al., 1979).

Finally, a rapid release of cellular zinc via exocytosis from activating oocytes is observed in mammals (Duncan et al., 2016; Kim et al., 2011; Que et al., 2019). This "zinc spark" is necessary for cell cycle progression during egg activation (Kim et al., 2011). The released zinc also modulates the hardening of extracellular matrix that acts as an initial prevention of polyspermy (Que et al., 2017a). The profile of zinc spark process thus can also serve as an indicator of embryo quality (Zhang et al., 2016).

1.2 Calcium dynamics during egg activation

A common feature that accompanies egg activation in almost all species studied to date is a rise of intracellular calcium level, preceding the abovementioned egg activation events (reviewed in Jaffe et al., 2001; Miao and Williams, 2012; Sartain and Wolfner, 2013). This elevated level of calcium can be due to influx of environmental calcium, release of internal Ca^{2+} from stores, or a combination of both (reviewed in Swann and Lai, 2016). The calcium level rises during egg activation take different forms and use different mechanisms across species.

In *C. elegans*, the fusion between sperm and egg delivers TRP-3 channels from the sperm plasma membrane to that of the egg. TRP-3 channel mediates the influx of external calcium and the onset of a calcium wave during egg activation (Takayama and Onami, 2016).

In *Xenopus*, a single calcium wave initiates from the point of sperm entry, travels through the entire oocyte and dies down within minutes (Busa and Nuccitelli, 1985). Fertilization induces the activation of phospholipase C γ(PLCγ), which catalyzes the cleavage of phosphatidylinositol 4,5-bisphosphate (PIP_2) to produce inositol-1,4,5-triphosphate (IP_3) and diacylglycerol (DAG). IP_3 then binds to and activates its receptor (IP_3R). IP_3R serves as an ion channel that releases Ca^{2+} from internal stores (Tokmakov et al., 2002). Thus, the calcium rise in *Xenopus* egg activation relies primarily on release from internal calcium stores.

In mouse, calcium rise during egg activation takes the form of multiple oscillations that can last several hours (reviewed in Swann and Lai, 2013; Wakai and

Fissore, 2013). The initial calcium rise also relies on IP_3 mediated calcium release. It is induced by a soluble factor introduced by the sperm during gamete membrane fusion. This factor is identified as PLCξ, which catalyzes the reaction that produces IP_3. IP_3 activates IP_3R to release internal calcium from stores, which travels across the activating egg in a wave (Kashir et al., 2014; Swann and Lai, 2013). However, since some of the calcium is pumped out of the egg as the wave passes, the subsequent calcium oscillations require influx of external calcium through TRPM7 and $Ca_V3.2$ channels (Bernhardt et al., 2018). Each oscillation correlates with more progression through a series of egg activation events (Ducibella et al., 2002; Miao and Williams, 2012). Therefore, the calcium oscillations during mouse egg activation depend on the combination of internal calcium stores and influx of external calcium.

In *Drosophila* egg activation, a transient calcium rise occurs in the form of a single calcium wave that initiates from the pole(s) and traverses the oocyte in 3-5 minutes (Kaneuchi et al., 2015; York-Andersen et al., 2015). This calcium wave can be visualized by expressing calcium sensors such as GCaMP in the female germline. Mechanical pressure during ovulation triggers egg activation *in vivo* (Heifetz et al., 2001), a calcium rise is seen upon ovulation, the wave initiates from the posterior end of the oocyte, which enters the oviduct first (Kaneuchi et al., 2015). Although osmotic pressure is applied to the entire oocyte in *in vitro* activation by allowing it to swell in hypotonic buffers, calcium waves still initiate mostly from posterior pole, although occasionally also from the anterior pole. The initiation of the calcium wave requires influx of external calcium, as depleting Ca^{2+} with the chelator 1,2-bis(o-aminophenoxy) ethane-N,N,N′,N′-tetra acetic acid (BAPTA) prevents calcium wave

initiation. The propagation of the calcium wave relies on release of internal calcium stores, as knockdown of IP_3R in the female germline allows a calcium rise to occur but not to sustain into a wave (Kaneuchi et al., 2015). Thus, *Drosophila* calcium wave during egg activation also relies on calcium sources from both the environment and internal stores.

How environmental calcium enters the activation *Drosophila* oocyte remained unknown. Chemical inhibitor tests suggested that mechanosensitive Transient Receptor Potential (TRP) family cation channels might be involved (Kaneuchi et al., 2015). It also remained to be elucidated why calcium waves always start from the oocyte poles and how the initial calcium influx is associated with calcium wave propagation and downstream egg activation events.

1.3 Calcium modulated molecular changes during egg activation

A likely way by which the calcium rise is associated with downstream egg activation events is through activation of calcium dependent kinases (such as Ca^{2+}/calmodulin-dependent protein kinase II, CaMKII) and/or phosphatases (such as calcineurin) (reviewed in Krauchunas and Wolfner, 2013). The activation of these enzymes drastically changes the phosphoproteome of the oocytes, leading to egg activation events such as cell cycle resumption and protein modification (Guo et al., 2015; Krauchunas et al., 2012; Presler et al., 2017).

In *Xenopus* and mouse activating oocytes, CaMKII activity increases rapidly concurrent with the elevation in calcium levels. In *Xenopus*, CaMKII activity spikes after the single calcium rise and is required for the transition from meiosis metaphase

II to anaphase II (Liu and Maller, 2005). CaMKII mediates the degradation of Emi2, an inhibitor of APC complex, to promote the progression of meiotic cycle (Liu and Maller, 2005). In mouse, CaMKII activity oscillates concurrent with calcium oscillations and also facilitates cell cycle progression (Markoulaki et al., 2003). CaMKII activates kinase Wee1B, which activates APC to facilitate transition to anaphase II of meiosis (Oh et al., 2011).

In *Xenopus* and *Drosophila*, calcineurin activity is required for multiple egg activation events. In *Drosophila*, the calcineurin regulator Sarah (*sra*) is needed for multiple aspects of egg activation including meiosis progression through anaphase I, maternal transcripts processing and maternal protein degradation (Horner et al., 2006; Takeo et al., 2006, 2010). Knockdown of the calcineurin regulatory unit CanB2 leads to a metaphase-like meiosis arrest (Takeo et al., 2010, 2012). Knockdown or overexpression of calcineurin also leads to dramatic changes in the phosphoproteome of activated eggs, including mis-regulation of multiple regulators of meiosis and protein translation (Zhang et al., 2018a). In *Xenopus*, inhibition of calcineurin leads to failure of cyclin B degradation and continued cell cycle arrest in metaphase II (Nishiyama et al., 2007).

1.4 Genetic manipulation of the *Drosophila* female germline

Most of our studies on *Drosophila* oogenesis and egg activation require precise and efficient temporal and spatial control of gene expression in the female germline. Thanks to the technical advantages of this highly tractable model organism, a rich pool of genetic tools is available to manipulate the genes expressed in *Drosophila* ovary,

and new approaches keep emerging.

The Gal4-UAS system is a widely used and highly versatile tool in *Drosophila melanogaster*. This system for inducible activation of gene expression utilizes tools originating from yeast and has been widely applied in *Drosophila*. Gal4-UAS is a binary system that includes the transcriptional activator Gal4 and its specific binding DNA sequence, upstream activation sequence (UAS). The expression of Gal4 can be controlled by a tissue-specific promoter in one fly line and UAS can be placed upstream of the gene of interest in another line. A simple cross between these two lines can yield progeny with desired tissue specific expression pattern of the gene of interest (**Figure 1.2 A**) (reviewed in Duffy, 2002). Additional temporal controls can be added by introducing a temperature sensitive Gal80 (Gal80ts) component to the Gal4 line. Gal80ts will bind Gal4 and inhibit its activity at lower temperatures. This inhibition can be released at higher temperatures, at which Gal80ts is released from Gal4. Transferring flies to higher temperature at desired developmental stage can achieve the additional temporal control of gene expression (Li et al., 2016). The Gal4-UAS system can be used to inhibit gene expression in combination with the RNA interference (RNAi) mechanism. By inducing the expression of double stranded RNA (dsRNA) against a gene of interest using an appropriately-expressed Gal4, tissue specific RNAi knockdown of genes can be achieved (Ni et al., 2011). The application of conventional Gal4-UAS system in the female germline is limited by the inefficiency of the standard UASt sequence in the germline. This is due to Piwi-interacting RNAs (piRNAs) in the female germline targeting Hsp70 promoter of UASt for inhibition (DeLuca and Spradling, 2018). To enhance the efficiency of this system

in the germline, another version of UAS sequence, UASp (Rørth, 1998), or a specialized expression vector, VALIUM construct (Ni et al., 2008), needs to be used.

Another system used for gene manipulation in the germline is the Flp-FRT system. This yeast site-specific recombination system utilizing FLPase (Flp) and its target sites, FRT, can be used to efficiently induce mitotic recombination in a single chromosome arm. This is an effective method to perform mosaic analysis. By inducing recombination between two chromosomes carrying either a visible marker (e.g. GFP) and a mutant allele and both carrying FRT sites at the same location proximal to the centromere, mitosis can yield two daughter cells homozygous for the mutant or marker allele. The absence of marker can be used to distinguish cells with homozygous mutant allele. By adding temporal or spatial control of Flp expression (e.g. with heatshock or tissue-specific promoter), this method allows analysis of phenotype of a homozygous lethal mutation in desired tissues or developmental stages (Theodosiou and Xu, 1998). In the female germline, Flp-FRT mosaic analysis can be further enhanced by replacing the visible marker with the dominant female sterile marker ovo^{D}. Germ cells carrying even one allele of ovo^{D} will not be able to develop normally. In *Drosophila*, ovo^{D} on the wildtype chromosome and a mutant on its ovo^{D+} homolog will make non-recombinant cells and cells that are homozygous wildtype for the gene of interest fail to develop, leaving only homozygous mutant germ cells in the germline for easy analysis (**Figure 1.2 B**) (Chou and Perrimon, 1996).

An emerging tool for genome editing is the clustered regularly interspaced short palindromic repeats (CRISPR)/Cas9 system. This bacteria-originated virus defense system (Horvath and Barrangou, 2010) can be used to induce DNA double

strand breaks (DSB) at precise desired locations in the genome. CRISPR/Cas9 requires two components to work: a synthetic single guide RNA (sgRNA) that has a recognition region that is complementary to the target sequence adjacent to a protospacer adjacent motif (PAM, e.g. NGG for Cas9) and a scaffold part for recruiting and binding Cas9; a Cas9 protein that functions as a nuclease, producing DSB near the sgRNA targeting site. This DSB can be repaired by imprecise non-homologous end joining (NHEJ) that is likely to introduce a random few base pair insertions/deletions (indels). If the indels are introduced in the critical coding region of the gene, causing a frameshift, a null allele of the gene can be generated. If two sgRNAs are used, a deletion can be created between the two target sites. Another way to repair the DSB is through homology directed repair (HDR). HDR involves introducing a donor DNA fragment that carries homologous sequences flanking the DSB site. The sequence between the homologous sequences can be integrated near the DSB site to achieve precise knockin of the desired DNA sequences (reviewed in Doudna and Charpentier, 2014; Jiang and Doudna, 2017; Ran et al., 2013). Both of these two approaches are powerful tools to perform gene knockout or knockin in both model and non-model organisms. With a tissue-specific promoter driving the expression of Cas9, genome editing can also be performed in specific tissues to avoid lethal effect of mutating essential genes (Poe et al., 2018; Xue et al., 2014a). CRISPR/Cas9 genome editing can be performed in the *Drosophila* female germline by driving Cas9 expression with a germline-specific promoter (e.g. *nos* promoter) (Sebo et al., 2014). Analogous to the tissue-specific GAL4-UAS system mentioned above, tissue-specific CRISPR/Cas9 genome editing can be achieved by crossing a line

expressing Cas9 in the desired tissue with a line that ubiquitously expresses sgRNAs targeting the gene of interest. The progeny of this cross will carry out editing of gene of interest in the desired tissue (**Figure 1.2 C**) (Poe et al., 2018). Unlike whole-fly editing in which one can obtain homozygous whole-fly mutants through crossing and screening of progenies, in germline-specific editing, since a bi-allelic null mutation is needed to knock out genes of interest to reveal their mutant phenotype, editing efficiency is critical to obtain a knockout. However, efficiency of germline CRISPR/Cas9 genome editing has not been optimal. Certain sgRNA expressing constructs that work efficiently in the soma do not do so in the germline. Thus, it is important to develop such tools to improve CRISPR/Cas9 editing efficiency.

1.5 Thesis outline

In this thesis, I describe my studies of how calcium enters oocytes during *Drosophila* egg activation, and subsequent events after the calcium wave. My studies identified Trpm as the channel that mediates calcium influx during *Drosophila* egg activation, explored the regulation mechanisms of Trpm activation in response to mechanical triggers, discovered an actin cytoskeleton reorganization wave interdependent with the calcium wave, and examined zinc dynamics during *Drosophila* oocyte maturation and egg activation. In addition, I participated in optimization of CRISPR/Cas9 genome editing in the *Drosophila* germline.

In Chapter 2, I genetically screened through the three TRP family channels expressed in the *Drosophila* ovary and identified Trpm as the only channel essential for calcium wave initiation. Calcium waves are diminished in oocytes from *trpm*

germline mutants in *in vitro* egg activation, but some egg activation events can still occur in these oocytes. I also found that *trpm* germline knockout reduces female fertility, but not because of failure of egg activation.

In Chapter 3, I examined possible explanations for why calcium waves always initiate from oocyte poles both *in vivo* and *in vitro*. I found that Trpm is uniformly distributed around plasma membrane of mature oocytes and de-localizes from the plasma membrane after egg activation. I further found that oocyte shape does not affect wave initiation site and that different parts of the oocyte display similar sensitivity to regional pressure. These results suggest that Trpm is under special regulation at the pole of mature oocytes so that it permits calcium influx only at the poles.

In Chapter 4, working with Adriana N Vélez-Avilés, I screened through the three phospholipase Cs (PLCs) encoded by the *Drosophila* genome and showed that Plc21C is necessary but not sufficient for calcium wave propagation during egg activation. This links the initial calcium influx during initiation with further propagation of the wave based on the release of calcium from internal stores.

In Chapter 5, in collaboration with Dr. Timothy Weil's lab at Cambridge University, I discovered a wave of actin reorganization cytoskeleton that closely follows the calcium wave during *Drosophila* egg activation. Inhibition of calcium wave blocks the actin wave, whereas inhibition of actin polymerization leads to incomplete calcium waves. I further found global pressure on the entire oocyte instead of regional pressure is required to trigger actin reorganization. Taken together, we revealed the interdependent regulatory network between calcium and actin in

Drosophila egg activation.

In Chapter 6, in collaboration with Drs. Francesca Duncan, Teresa Woodruff and Thomas O'Halloran's labs at Northwestern University and Olga Antipova at Argonne National Laboratory, I used X-ray Fluorescence Microscopy (XFM) to examine the content and distributions of transition metal elements during *Drosophila* oocyte maturation and egg activation. We found that zinc is the most abundant transition metal in *Drosophila* oocytes and eggs. Zinc level increases over oogenesis along with formation of zinc-enriched granules and decrease after egg activation.

In Chapter 7, in collaboration with Dr Chun Han's lab at Cornell University, we optimized the guide RNA (gRNA) expression construct for efficient CRISPR/Cas9-mediated genome editing in the *Drosophila* germline. We show that although certain gRNA expression construct designs improve editing efficiency in the soma, they do not perform as well in the germline.

Chapter 8 is a brief summary and discussion of my thesis work and provides possible directions for future experiments.

In Appendix A, I describe the approaches I have attempted to perform mechanical manipulation of *Drosophila* oocytes and document the results I observed. These works are collaborations with Drs. Jan Lammerding, Jonathan T. Butcher and Mingming Wu's lab at Cornell University.

In Appendix B, I describe the strontium induced calcium oscillations during *in vitro* activation of *Drosophila* oocytes.

In Appendix C, I describe the crossing scheme I designed to generate germline clone of *trpm* in an attempt to examine calcium waves in homozygous *trpm* mutant

oocytes.

Figure 1.1 Egg activation events.

Image via Biorender.com.

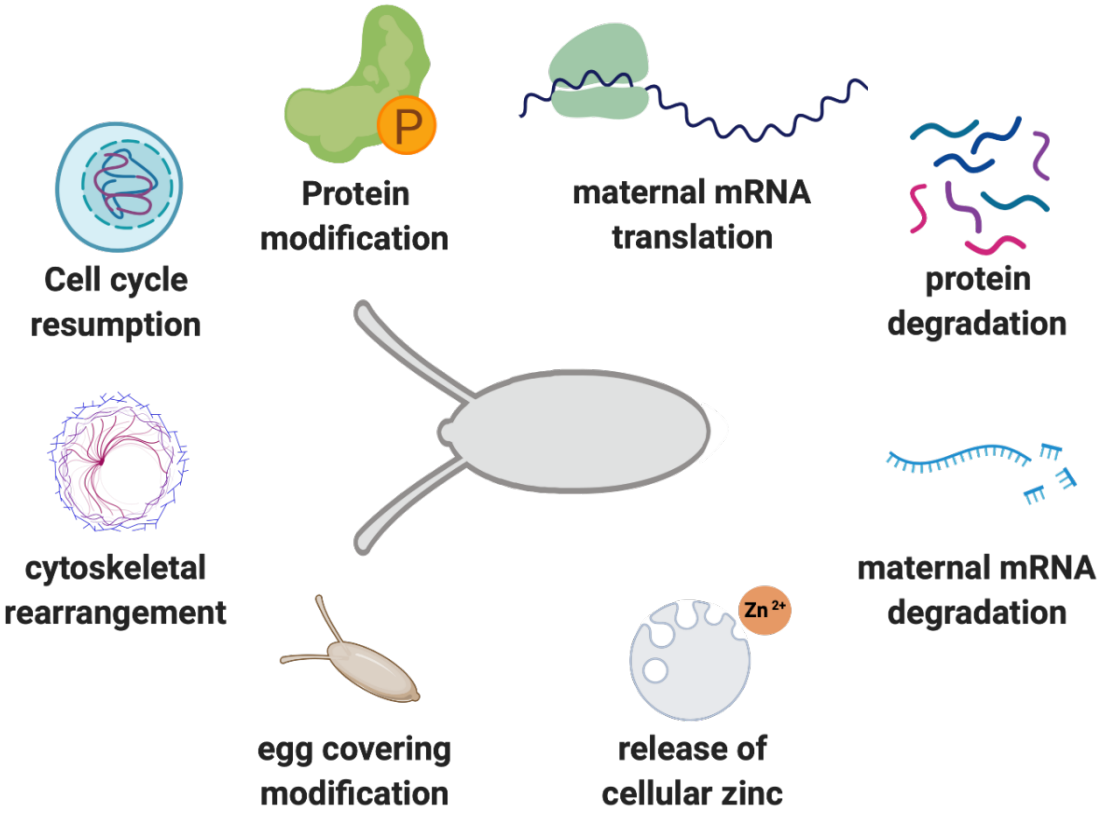
Cell cycle resumption
P
Protein modification
maternal mRNA translation
protein degradation
cytoskeletal rearrangement
maternal mRNA degradation
egg covering modification
Zn 2+
release of cellular zinc

Figure 1.2 Available tools for genetic manipulation of genes in the *Drosophila* female germline.

(A) Crossing scheme to achieve tissue specific gene expression using GAL4-UAS system. (B) Diagram of mosaic analysis using Flp-FRT mediated mitotic recombination. (C) Crossing scheme to achieve tissue specific genome editing using CRISPR/Cas9 system. TS: tissue-specific; UB: ubiquitous; mu: mutant allele. Image via Biorender.com.

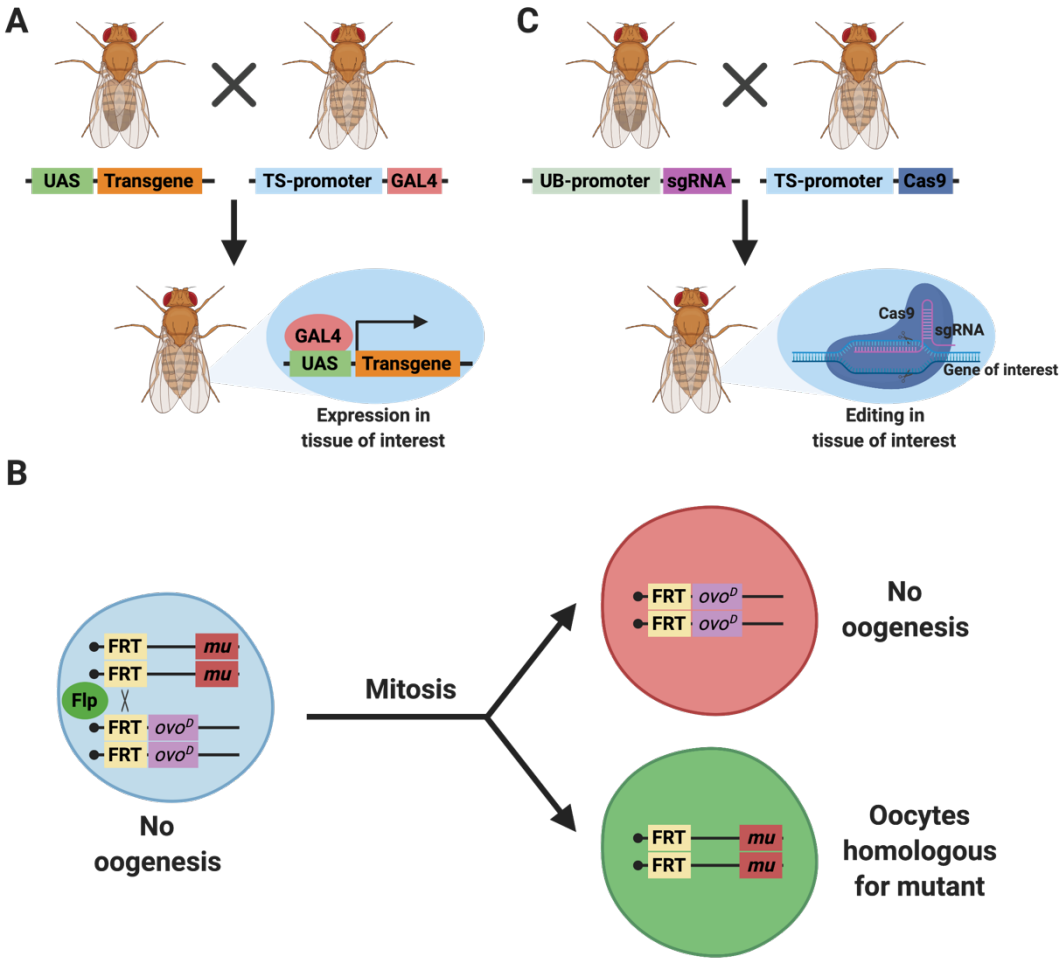
A
UAS
Transgene
TS-promoter
GAL4
GAL4
UAS
Transgene
Expression in
tissue of interest
C
UB-promoter
sgRNA
TS-promoter
Cas9
Cas9
sgRNA
Gene of interest
Editing in
tissue of interest
B
FRT
mu
FRT
mu
Flp
FRT
ovoD
FRT
ovoD
No
oogenesis
Mitosis
FRT
ovoD
FRT
ovoD
No
oogenesis
FRT
mu
FRT
mu
Oocytes
homologous
for mutant

CHAPTER 2 THE DROSOPHILA TRPM CHANNEL MEDIATES CALCIUM INFLUX DURING EGG ACTIVATION[1]

2.1 Introduction

In almost all animals, mature oocytes are arrested in meiosis at the end of oogenesis and require an external trigger to be activated and transition to start embryogenesis. This "egg activation" involves multiple events, including meiosis resumption and completion, maternal protein modification and/or degradation, maternal mRNA degradation or translation, and egg envelope changes (reviewed in Horner and Wolfner, 2008a; Kashir et al., 2014; Krauchunas and Wolfner, 2013; Sartain and Wolfner, 2013; Swann and Lai, 2016).

Triggers of egg activation vary across species. In vertebrate and some invertebrate species, fertilization triggers egg activation. However, changes in pH, ionic environment, or mechanical pressure can also trigger egg activation in other invertebrate species (reviewed in Horner and Wolfner, 2008a). A conserved response to these triggers is a rise of intracellular free Ca^{2+} levels in the oocyte. This calcium rise is due to influx of external calcium and/or release from internal storage, depending on the organism (reviewed in Swann and Lai, 2016). The elevated Ca^{2+} concentration is thought to activate Ca^{2+}-dependent kinases and/or phosphatases, which in turn change the phospho-proteome of the activated egg, initiating egg activation events (Krauchunas et al., 2012; Zhang et al., 2018a, reviewed in

[1] Published and reprinted with permission: Hu, Q., and Wolfner, M. F. (2019). The *Drosophila* Trpm channel mediates calcium influx during egg activation. *Proceedings of the National Academy of Sciences*, *116*(38), 18994-19000.

Krauchunas and Wolfner, 2013).

Drosophila eggs activate independent of fertilization, and the trigger is mechanical pressure. When mature oocytes exit the ovary and enter the lateral oviduct, they experience mechanical pressure from the reproductive tract. As the oocytes swell due to the influx of oviductal fluid, their envelopes become taut (Heifetz et al., 2001). *Drosophila* oocytes can be activated *in vitro* by incubation in a hypotonic buffer, although some egg activation events do not proceed completely normally *in vitro* (Kaneuchi et al., 2015; Page and Orr-Weaver, 1997). Intracellular calcium levels rise in oocytes during egg activation, as observed with the calcium sensor GCaMP. This calcium rise takes the form of a wave that starts at the oocyte pole(s) and traverses the entire oocyte (Kaneuchi et al., 2015; York-Andersen et al., 2015). *In vivo*, the wave starts with a calcium rise at the posterior pole; *in vitro* it also starts predominantly at the posterior pole but sometimes (also) at the anterior pole (Kaneuchi et al., 2015; York-Andersen et al., 2015). Initiation of this calcium wave requires influx of external Ca^{2+}, as chelating external Ca^{2+} in *in vitro* egg activation assays blocks the calcium wave and egg activation. Propagation of the calcium wave relies on the release of internal Ca^{2+} stores, likely through an Inositol 1,4,5-trisphosphate (IP_3)-mediated pathway as in other animals, because knocking down the endoplasmic reticulum (ER) calcium channel IP_3 receptor (IP_3R) prevents propagation of the calcium wave (Kaneuchi et al., 2015). How mechanical forces trigger calcium entry during *Drosophila* egg activation was unknown. However, the lack of initiation of a calcium wave in the presence of Gd^{3+}, an inhibitor of mechanosensitive ion channels (Millet, 1988), and *N*-(*p*-Amylcinnamoyl) anthranilic acid (ACA), an inhibitor of TRP-family

ion channels (Harteneck et al., 2007), suggested that TRP family ion channels (reviewed in Clapham et al., 2001) are likely involved (Kaneuchi et al., 2015). Further supporting this idea is the recent discovery that a TRP family channel, TRPM7, is needed for calcium influx that is necessary (but not sufficient) for calcium oscillations in activating mouse eggs (Bernhardt et al., 2018). The *Drosophila* genome encodes 13 TRP family channels (reviewed in Montell, 2005), but according to RNA-seq data, only 3 (Painless, Trpm, and Trpml) are expressed in the ovary (reviewed in Sartain and Wolfner, 2013). We used specific inhibitors, existing mutants, germline-specific RNAi knockdown, and knockouts that we created with CRISPR/Cas9 to screen these 3 candidates for their roles in the initiation of the calcium wave. We found that Trpm, the single *Drosophila* ortholog of mouse TRPM7, mediates calcium wave initiation, whereas the other 2 TRP channels are not necessary to initiate the calcium wave.

2.2 Materials and Methods

DNA constructs and transgenic flies. Calcium waves were visualized by expressing GCaMP sensors in the female germline using *matα4-GAL4-VP16; UASp-GCaMP3* (Kaneuchi et al., 2015), *matα4-GAL4-VP16; UAS-GCaMP6s*, or *nos-GCaMP6m*. The *nos-GCaMP6m* strain was constructed by replacing the GCaMP3 coding sequence in the previously described *nos-GCaMP3-attB* construct (Kaneuchi et al., 2015) with GCaMP6m coding sequence and integrating the construct into either the *attP2* or the *attP40* site.

Calcium wave incidence in each experiment was compared between perturbed and control oocytes using the same calcium sensor and exposure/gain

settings. Control oocytes showed lower incidence of calcium waves when expressing *GCaMP6s* or *GCaMP6m* compared to *GCaMP3*, likely due to weaker expression of our *GCaMP6s* or *GCaMP6m* constructs.

To create a null allele of *pain*, we generated *pU6-chiRNA* constructs following protocols described by FlyCRISPR website (Gratz et al., 2013). We generated 2 constructs to express sgRNAs with the following target sequences (PAM sequences are underlined): GTCTTGCAGCTGGTTGAGTCCGG, GACGCAGACTTAAGTAGTTCGGG. These 2 constructs were co-injected by Rainbow Transgenic Flies into *nos-Cas9-attP2* embryos. A strain carrying a 1,091-bp deletion (chr2R:24922130–24923220) in *pain* was isolated and stabilized to establish the null allele strain $pain^{TM\Delta}$.

To knock out *trpm*, we generated the U6:3-tRNA-gRNA1-tRNA-gRNA2 (Poe et al., 2018) and CR7T-gRNA1-U6:3-gRNA2 constructs (gifts from Chun Han, Cornell University, Ithaca, NY). We designed 3 sets of gRNAs targeting *trpm* to express in our constructs. sgRNA target sequences in the *trpm* gene are as follows (PAM sequences are underlined):

gRNA set 1: GGAACCATCGAGTTCCAGGGCGG; GATGTGGACACATGGCGAGGAGG; CTTTTGATCACCGTGCAGGGCGG; CTTGGACACGGAAATCTACGAGG

gRNA set 2: GATGAGCGAGGAGGGCACGATGG; ACCCATAACCAAGTTCTGGGCGG

gRNA set 3: GACTACAGGGATGAGCGAGGAGG; GAATACCACTCCTGCCACCGCGG

These constructs were injected by Rainbow Transgenic Flies into *yw, nos-phiC31; PBac{attP-9A}* embryos (**Figure 2.1**).

gRNA construct efficiency test. To confirm the efficiency of constructs expressing gRNAs, we employed the "Cas9-LEThAL" method (Poe et al., 2018) to validate the efficiency of our gRNA constructs. Males carrying gRNA constructs were crossed to *act-Cas9*, *lig4-* mutant females. Our gRNA set 3 construct caused 100% lethality in *lig4* mutant male offspring while the other 2 sets did not (Table 2.1), suggesting it has the highest efficiency.

Fly strains and maintenance. All *Drosophila* strains and crosses were maintained or performed on standard yeast-glucose-agar media at 25 °C [29 °C for all crosses involving the GAL4/UAS system to enhance its efficiency (Duffy, 2002)] on a 12/12 light/dark cycle. The following fly lines were obtained from Bloomington *Drosophila* Stock Center: $trpml^{1}$ (28992), $UAS\text{-}trpm^{RNAi}$ (57871), *matα4-GAL4-VP16* (7062), *20XUAS-IVS-GCaMP6s-attP40* (42746), *UAS-Cas9- attP2* (54595), *yw, nos-phiC31; PBac{attP-9A}* (35569).

Buffer reagents, drug and inhibitor treatment. IB was made as previously described (Kaneuchi et al., 2015). IB contains 55 mM NaOAc, 40 mM KOAc, 1.2 mM $MgCl_2$,1 mM $CaCl_2$, 110 mM sucrose, 100 mM Hepes in ddH_2O. IB is adjusted to pH 7.4 with NaOH and filter sterilized. We found that modified RB functioned as well as activation buffer [AB; (Kaneuchi et al., 2015)] for activating eggs, so we used RB for this purpose in our experiments. RB contains 55 mM NaOAc, 8 mM KOAc, 20 mM sucrose, 0.5 mM $MgCl_2$, 2 mM $CaCl_2$, 20 mM Hepes in ddH_2O. RB is adjusted to pH 6.4 with NaOH and filter sterilized. For tests of Trpm inhibitors, stock solutions of $MgCl_2$ (Mallinckrodt) and NS8593

(Sigma-Aldrich) were prepared and added to IB and RB to the indicated final concentrations, on the day of the experiment. The published concentration of Mg^{2+} (10 mM) was used to inhibit *Drosophila* Trpm (Georgiev et al., 2010). For NS8593, we tried a series of concentrations starting from published results on mammalian TRPM7 (30 μM) (Chubanov et al., 2012). We found that 100 μM is the optimal concentration for *Drosophila* Trpm inhibition.

Stage 14 oocytes, dissected from virgin females that had been aged on yeast for 3 to 5 d, were incubated in inhibitor containing IB or control IB for 30 min before experiments. Inhibitor treated oocytes were then switched to incubation in RB that also contained the inhibitor at the same concentration, and oocytes incubated in control IB were activated in control RB lacking the inhibitor.

Imaging. For calcium wave visualization, oocytes were imaged using a Zeiss Elyra Super Resolution Microscope with a 5× or 10× lens with Zen software. The detection wavelength was set to 493 to 556 nm for GCaMP signal.

For immunostaining, fixed and stained embryos were imaged using a Zeiss LSM880 Confocal Multiphoton Microscope with a 10× lens and the Zen software. The detection wavelength was set to 495 to 634 nm for FITC signal, and 410 to 495 nm for DAPI. Z-stack images were taken from the shallowest to the deepest visible planes with a pinhole of 100. Maximum intensity projection of captured images was performed using the Zen software.

To examine ovary morphology, ovaries were dissected from 3- to 5-d-old virgin females aged on yeast. Their images were captured using an Echo Revolve Microscope, with a 4× lens and brightfield imaging settings. Ovary images were processed with the Echo Revolve App.

All acquired images were processed with ImageJ software (Schindelin et al., 2012) as needed.

***In vitro* egg activation assay.** Oocytes were dissected from the indicated female flies and induced to activate *in vitro* following methods as described previously (Kaneuchi et al., 2015). For imaging, oocytes were placed in a drop of IB in a glass- bottomed Petri dish. After imaging parameters were configured, IB was replaced by RB to induce egg activation (Kaneuchi et al., 2015). Time-lapse images were taken at 1-s or 10-s intervals, for 10 to 20 min after the addition of RB. The distance traveled by the wavefront was measured using ImageJ software, and the elapsed time was recorded. The propagation rate of the calcium wave was calculated as distance traveled by the wavefront divided by time.

Egg-laying and egg hatchability assay. Virgin females of the indicated genotypes were aged on yeasted food vials for 3 to 5 d, before mating with Oregon-R-P2 (ORP2) WT males. Matings were observed and the males were removed after a single mating had completed. Females were allowed to lay eggs in the mating vial for 24 h and were then transferred to a new vial. Females were transferred 3 times before they were discarded. The number of eggs and pupae were counted. Egg hatchability was calculated by the number of pupae divided by the number of eggs. To confirm there was no post-embryonic developmental arrest in eggs laid by mutants that could have affected our hatchability score, we counted the number of unhatched eggs for 3 d after egg laying and thus determined the number of hatched eggs. This number equaled the number of pupae, indicating that our method of calculating egg hatchability was reliable.

RT-PCR. RNA was extracted from 4 to 5 pairs of ovaries from virgin

females aged in yeasted vials for 3 to 5 d using TRIzol/chloroform. Seven hundred and fifty nanograms of RNA from each sample underwent DNase (Promega) treatment and cDNA synthesis using SuperScript II Reverse Transcriptase (Invitrogen) following the manufacturer's instructions. A 30-cycle PCR amplification was performed with GoTaq polymerase (Promega) with the following conditions: 95 °C at 2 min, 95 °C at 40 s, 54 °C at 40 s, 72 °C at 40 s, 72 °C at 10 min. PCR products were run on 1% agarose gels, and the DNA was stained with 1 μg/mL ethidium bromide. Captured gel images were processed with ImageJ software.

The expression level of ribosome protein gene *rpl32* was used as a normalization control (Ponton et al., 2011). The following primers were used for RT-PCR: *trpm*-F: TCACTGTGCTGGTGAAGATG; *trpm*-R: CCAGAGGTCCCAGGTATTTATTC (amplicon size with cDNA as template is 324 bp. The reverse primer spans an exon-exon junction and will amplify a 513-bp band with genomic DNA as template.). *rpl32*-F: CACCAGTCGGATCGATATGC; *rpl32*-R: CGATCCGTAACCGATGTTG (amplicon size with cDNA as template is 120 bp. The primers flank an exon-exon junction and will amplify a 182-bp band with genomic DNA as template.).

Immunostaining. Embryos and eggs from the indicated mating were collected from grape juice/agar plates. Embryos were dechorionated in 50% commercial bleach, fixed in methanol/heptane (Rothwell and Sullivan, 2007), and stored at 4 °C until use. Fixed embryos were washed with phosphate buffered saline with 0.1% Tween-20 (PBST) 3 times for 5 min each and blocked with PBST containing 5% vol of normal goat serum (PBST-NGS). Embryos were then

incubated overnight at 4 °C in PBST-NGS containing mouse monoclonal anti-α-Tubulin- FITC antibody (Sigma-Aldrich) at a dilution of 1:200 and RNaseA (Roche Applied Science) at a concentration of 5 μg/mL. Embryos were then washed with PBST 3 times for 5 min each. DNA was stained with 1 μg/mL DAPI (Molecular Probes) in PBST for 5 min, and embryos were mounted on glass microscope slides in antifade mounting buffer.

Bleach resistance assay. Mature oocytes were dissected in IB from the indicated females. Eggs laid by indicated females after mating to indicated males were collected from grape juice/agar plates. Both oocytes and embryos were incubated in 50% commercial bleach for 2 min (Page and Orr-Weaver, 1997). Numbers of oocytes and embryos before and after incubation were counted to calculate the percentage that survived bleach treatment.

Statistics. Pearson's χ^2 test was used to compare the incidence of calcium waves and ovary morphology defects. Student's *t* test was used to compare the propagation speed of calcium waves and egg hatchability.

Mutant verification. The deletion in $pain^{TM\Delta}$ allele was confirmed by PCR and sequencing using the following primers: *pain*-C1F: GTATCACCACAAACGGAGAGAG; *pain*-C1R: GGTGCCACTTGAGGAATAGAA; *pain*-C2F: ACCAACGTCCTTAGTCGGTA; *pain*-C2R: GTCCTCATTTCGAAGGGATCG (**Figure 2.2 A-C**).

$trpml^{1}$ carries a 1097bp deletion which removes nucleotides -456 to +641 relative to the *trpm*l translation start site (Venkatachalam et al., 2008). The deletion was confirmed with the following primers: *trpm*l-F:

CTGACCACGATGTTTATCGC; *trpm*l-R: AACGGCGGAATTTGGAATAC (**Figure 2.2 D**).

A 32 cycle PCR amplification was performed with GoTaq polymerase (Promega) with the following conditions: 95°C 2 minutes, 95°C 40 seconds, 54°C 40 seconds, 72°C 1 minute 30 seconds, 72°C 10 minutes. PCR products were run on 1% agarose gels, and the DNA was stained with 1 μg/mL ethidium bromide. Captured gel images were processed with ImageJ software.

Single oocyte RT-PCR. RNA was extracted from single mature oocytes from virgin *trpm* germline knockout females (*nos-Cas9-attP2/gRNA-trpm*^{1}) aged in yeasted vials for 3-5 days using Trizol/chloroform and underwent DNase (Promega) treatment and cDNA synthesis using SuperScript™ II Reverse Transcriptase (Invitrogen) following the manufacturer's instructions. Three rounds of nested PCR amplification (30 cycles/round, product of the last round was used as the template for the next round) was performed with iProof Hi-Fidelity polymerase (Bio-Rad) with the following conditions: 98°C 30 seconds, 98°C 10 seconds, 56°C 30 seconds, 72°C 15 seconds, 72°C 10 minutes. The first round of PCR was performed using outer primers: *trpm*-outerF: GGAGTTCGAGAGCAAAGGTAAG; *trpm*-outerR: GAACGATCCGAGTCATCATTGT. The second and the third round of PCR were performed using inner primers: *trpm*-innerF: GAGCTACACTCCTGGTCAAATC; *trpm*-innerR: GTCAAGCTGCCTGATGTAGAA.

The final round of PCR product was run on 1% agarose gels, and the DNA was stained with 1 μg/mL ethidium bromide. Captured gel images were processed

with ImageJ software (**Figure 2.3 A**). The product bands were cut out and purified with gel extraction kit (Invitrogen) for sequencing (**Figure 2.3 B**).

2.3 Results

Painless and Trpml are not essential for the calcium wave initiation or propagation

Three TRP channels [Painless (Pain), Trpm, and Trpml] are expressed in the *Drosophila* ovary and are candidates for involvement in calcium wave initiation. To examine the roles of these channels in the calcium wave during egg activation, we performed *in vitro* activation assays on mature oocytes dissected from WT, mutant, and/or knockdown females, and imaged the calcium waves with fluorescence microscopy (Materials and Methods). Since calcium influx is required for calcium wave initiation (Kaneuchi et al., 2015), we used the incidence of calcium waves as an indicator of calcium influx and assessed the role of candidate channels with it.

Among the 3 candidates, Pain is reported to display mechanosensitivity (Tracey et al., 2003). To examine the role of Pain, we made a CRISPR knockout line, $pain^{TM\Delta}$, by deleting the region that encodes Pain's transmembrane domains. Since *pain* loss-of-function mutants are viable (Gorczyca et al., 2014), we were able to examine the calcium wave phenotype in oocytes from homozygous $pain^{TM\Delta}$ females that also carried a *nos-GCaMP6m-attP2* transgene. The incidence of a calcium wave *in vitro* in mature oocytes of homozygous $pain^{TM\Delta}$ females did not differ significantly from that of heterozygous controls (**Figure 2.4 A**). The propagation rate of the calcium wave, as measured at its wave-front, was also not significantly different from

control (**Figure 2.4 B**).

To examine the role of Trpml, we tested an existing null mutant, *trpml*^{1} (Venkatachalam et al., 2008). We crossed into *trpml*^{1} the *nos-GCaMP6m- attP40* transgene and examined the calcium wave phenotype in mature oocytes from homozygous mutants or heterozygous controls. Again, we did not find a difference in the calcium wave incidence (**Figure 2.4 C**) or in calcium wave propagation rate between oocytes from homozygous mutant and those from heterozygous control females (**Figure 2.4 D**).

Thus, neither Pain or Trpml is essential for the initiation or propagation of the calcium wave. These channels thus are either not involved in calcium wave initiation, or they function redundantly with other channels.

Inhibitor and RNAi perturbations of *trpm* inhibit calcium wave initiation

To test whether Trpm is needed for the calcium wave, we first examined the effect of known inhibitors of this channel. Ten millimolar Mg^{2+} is reported to inhibit several TRP channels including mouse TRPV3 (Luo et al., 2012), TRPM6, TRPM7 (Gwanyanya et al., 2004), and *Drosophila* Trpm (Georgiev et al., 2010). In the presence of 10 mM Mg^{2+} in isolation buffer (IB) and modified Robb's Buffer (RB), the incidence of a calcium wave *in vitro* was significantly reduced (**Figure 2.5 A**, **B**, and **E**). We also tested the effect of NS8593, a specific inhibitor of mouse TRPM7 channels (Chubanov et al., 2012). One hundred micromolar NS8593 in IB and RB completely blocked calcium wave initiation *in vitro* (**Figure 2.5 C** and **F**).

Since *trpm* homozygous mutants are lethal before adult stage (Hofmann et al., 2010), we next tested the role of *trpm* in calcium wave initiation using germline-

specific RNAi. We crossed *matα4-GAL4-VP16; UASp-GCaMP3* to *UAS-trpm*^{RNAi}. The female offspring expressed both GCaMP3 and *trpm* shRNA in the germline. We examined the calcium waves in *in vitro* activation assays with mature oocytes from these females. Oocytes from *trpm* germline knockdown females displayed a significantly lower incidence of calcium waves *in vitro* (**Figure 2.5 D and G**). To validate the efficiency of germline knockdown, we performed RT-PCR with ovary mRNA from these females. RT-PCR results showed that more than 90% of *trpm* transcripts were removed in germline knock- down females compared to control (**Figure 2.5 H**).

Inhibitors of Trpm and germline knockdown of *trpm* both reduced the incidence of calcium waves in *in vitro* egg activation assays. Thus, our data strongly suggested that Trpm is necessary for calcium influx during *Drosophila* egg activation.

Germline-specific CRISPR/Cas9 knockout of *trpm* inhibits calcium wave initiation

To further validate the role of Trpm in the initiation of the calcium wave, we attempted to perform germline-specific biallelic knockout of *trpm* using the CRISPR/Cas9 system. We designed 3 sets of gRNAs targeting *trpm* (Materials and Methods). We used the "Cas9-LEThAL" (Poe et al., 2018) method to evaluate the efficiency of our gRNA expression constructs. Among them, gRNA set 3 displayed the highest efficiency (Table 2.1). Using this set of gRNAs, we made a dual-gRNA transgenic line based on a polycistronic gRNA design (U6:3-tRNA-gRNA1- tRNA-gRNA2, gRNA-*trpm*^{1}) and a dual transcription unit design (CR7T-gRNA1-U6:3-gRNA2, gRNA-*trpm*^{2}), both ubiquitously expressing the gRNAs (**Figure 2.1 A**).

We crossed each of these transgenic fly strains to *nos-Cas9; matα4-GAL4-VP16; UASp-GCaMP3* to achieve germline–specific knockout of *trpm* at early oogenesis stages, via *nos-Cas9*, and calcium visualization at the same time (**Figure 2.1 B**). By sequencing amplicons generated by single oocyte RT-PCR, we confirmed the presence of CRISPR/Cas9-generated indels (**Figure 2.3**). With gRNA-*trpm*^{1}, 34% of the female offspring displayed defects in ovary morphology (**Figure 2.6 A-B**). With gRNA-*trpm*^{2}, 96% of the female offspring displayed similar defects (**Figure 2.6 C**). These data showed that *trpm* is required for early female germline development. Since Trpm is involved in maintaining cation homeostasis in cellular environments and tissue development (Georgiev et al., 2010; Hofmann et al., 2010), we hypothesize that early knockout of *trpm* by *nos-Cas9* interferes with normal germline development. The less-than-100% incidence of this phenotype is likely due to lack of 100% efficiency in generating biallelic null mutations of *trpm* in the germline with les efficient gRNA expression constructs.

Some early *trpm* germline knockout females had ovaries with grossly normal morphology, perhaps because null mutations were generated at both *trpm* alleles only after a critical developmental point. We tested their mature oocytes for activation *in vitro*. We observed that the incidence of calcium waves was significantly reduced in oocytes from these females (**Figure 2.7 B** and **D**) compared to Cas9 control (**Figure 2.7 A**). Since efficient CRISPR/Cas9-mediated *trpm* knockout caused ovary development defects, flies with normal-looking ovaries may have less efficient *trpm* biallelic knockout in the germline, which could explain the incomplete elimination of calcium waves in oocytes from these flies.

To bypass the critical stage in early oogenesis that may require *trpm* function, we knocked out *trpm* at only later stages of oogenesis by crossing the *UAS-GCaMP6s; gRNA-trpm*^{1} strain to the *matα4-GAL4-VP16; UAS-Cas9* strain (**Figure 2.1 B**). Since *matα4-GAL4-VP16* does not drive expression of UAS constructs until mid to late oogenesis (Häcker and Perrimon, 1998), female offspring of this cross will initiate germline knockout of *trpm* at later stages of oogenesis in contrast to crosses using *nos-Cas9*, which initiate knockout early in oogenesis. None of these germline knockout females displayed gross ovary morphology defects (**Figure 2.6 D-E**), suggesting that *trpm* knockout occurred after a critical stage in early oogenesis. We examined the calcium wave phenotype of mature oocytes from these females in *in vitro* egg activation assays. We observed a significant decrease in the incidence of calcium waves (**Figure 2.7 C** and **E**).

Taken together, these results further support that Trpm is required for calcium wave initiation. In addition, our results also suggest that Trpm plays essential roles in early oogenesis.

Egg activation events occur in *trpm* knockout eggs *in vivo*

We next asked whether egg activation requires normal *trpm* function. Almost all 1- to 5-h embryos from *trpm* germline knockout females displayed resistance to 50% bleach, an indicator of vitelline membrane cross-linking after egg activation (Mahowald et al., 1983) (**Figure 2.7 F**). This suggests that egg envelope hardening, one aspect of egg activation, still occurs in embryos from *trpm* germline knockout females.

Since bleach resistance does not always completely reflect the state of egg

activation (Page and Orr-Weaver, 1997), we examined whether embryos from *trpm* germline knockout females were able to enter mitosis, implying successful completion of meiosis and fertilization. Surprisingly, anti-Tubulin and DAPI staining of 1- to 5-h-old embryos laid by *trpm* germline knockout females mated with ORP2 WT males showed they had all undergone early embryo mitoses (n = 88 for early germline knockout mutants, n = 36 for late germline knockout mutants, **Figure 2.8 A**). This indicated that cell cycles can resume in embryos from *trpm* germline knockout females mated with WT males.

We then asked if egg hatchability (percent of eggs that hatched into larvae) is affected by *trpm* germline perturbations. Germline knockdown of *trpm* did not impair egg hatchability (**Figure 2.8 C**). Since this knockdown, despite being highly efficient, did not completely abolish *trpm* function in oocytes, we examined the hatchability of eggs from *trpm* germline knockout females. Germline *trpm* knockout females displayed significantly reduced egg hatchability compared to control, with either early (**Figure 2.8 D**) or late (**Figure 2.8 E**) germline-specific knockout, suggesting that the lack of maternal Trpm function or a calcium wave compromised development events after initiation of the embryos' mitotic phase. Since the fathers of these embryos were wildtype, a WT *trpm* allele was present in the embryos. Thus, defects in hatchability must be due to the lack of maternal *trpm* product, because after zygotic genome activation, these embryos will express WT Trpm.

Taken together, these observations indicate that fertilized eggs are able to resume cell cycles and harden egg envelopes in the absence of Trpm function. The reduced hatchability of eggs laid by *trpm* germline knockout females suggests that

lack of oocyte Trpm function or a calcium wave affects embryogenesis after egg activation.

Sperm is not an alternative trigger of egg activation in the absence of *trpm* function

Because fertilized eggs from *trpm* germline knockout females proceeded to mitotic stages, we wondered whether sperm could act as an alternative trigger for the calcium rise and egg activation (reviewed in Horner and Wolfner, 2008a) in *Drosophila*. We mated control and *trpm* germline knockout females to spermless males (Boswell, 1985). Eggs laid by females after the mating would experience the normal egg-activating environment *in vivo* but remain unfertilized. We then examined if meiosis resumption and vitelline membrane cross-linking occur in unfertilized eggs from *trpm* germline knockout females. We observed 100% resistance to 50% bleach in these unfertilized eggs (**Figure 2.7 F**). We also observed normal production of polar bodies in all unfertilized eggs from control (n = 14) and *trpm* germline knockout females (n = 20) (**Figure 2.8 B**). These results indicated that vitelline membrane cross-linking and meiosis resumption still occur in eggs from *trpm* germline knockout mutants independent of sperm, ruling out the possibility that sperm could overcome the lack of calcium influx triggered by mechanical pressure and activate eggs in the absence of Trpm function.

2.4 Discussion

Egg activation is an essential step for oocytes to transition to embryogenesis. In all species studied to date, egg activation involves a rise in

intracellular calcium. In *Drosophila*, this calcium rise takes the form of a wave that is triggered by mechanical pressure. The initiation of this calcium wave requires influx of calcium from the environment through mechanosensitive TRP family channel(s) (Kaneuchi et al., 2015).

Here, we determined that Trpm channel is necessary for this calcium wave. Of the 3 TRP channels expressed in ovaries (Pain, Trpm, and Trpml), only impairment of Trpm affects the initiation of the calcium wave. Calcium wave phenotypes are normal in oocytes from *pain* or *trpml* null mutants. However, the incidence of the calcium wave is diminished in WT oocytes in the presence of Trpm inhibitors and in oocytes from *trpm* germline knockdown or knockout mutants. These results consistently indicated that Trpm mediates the calcium influx that initiates the calcium wave during *Drosophila* egg activation. Given the short time frame of calcium wave propagation and limitations of the inhibitor test technique, we cannot determine if Trpm also plays a role in calcium wave propagation. *trpm* germline knockout females also displayed significantly decreased egg hatchability, due to defects after cell cycle resumption. The reduced egg hatchability suggested that maternal *trpm* function or the calcium wave is required for further embryogenesis after egg activation.

The *Drosophila* Trpm channel plays important reproductive roles

TRP family cation channels are nonselective and respond to a wide array of environmental stimuli. *Drosophila* Trpm has been reported to play multiple roles throughout larval development, including maintaining Mg^{2+} and Zn^{2+} homeostasis (Georgiev et al., 2010; Hofmann et al., 2010), and sensing noxious cold in larval class III md neurons (Turner et al., 2016). However, the role of Trpm in

reproduction had not been investigated because of the pupal lethality of *trpm* null mutants (Hofmann et al., 2010). Here, our germline-specific RNAi knockdown and CRISPR/Cas9-mediated knockout revealed 3 functions of *Drosophila* Trpm: supporting early oogenesis, mediating influx of environmental calcium to initiate the calcium wave during egg activation, and maternally supporting embryonic development after egg activation.

Our previous study suggested that calcium influx during *Drosophila* egg activation is mediated through mechanosensitive ion channels (Kaneuchi et al., 2015). Both *Drosophila* Trpm and mouse TRPM7 are reported to be constitutively active and permeable to a wide range of divalent cations (Fleig and Chubanov, 2014; Georgiev et al., 2010). Mouse TRPM7 is known to respond to mechanical pressure (Liu et al., 2015; Xiao et al., 2014), but further study will be needed to determine whether *Drosophila* Trpm is similarly responsive to mechanical triggers, such as those that occur during ovulation.

Requirement for Trpm during *Drosophila* embryogenesis

Germline knockout of *trpm* significantly reduced the incidence of calcium waves in *in vitro* egg activation assays and egg hatchability. However, this reduced egg hatchability was not due to failure of cell cycle resumption during egg activation. There are 2 possible explanations for the reduced egg hatchability of *trpm* germline knockout females.

First, it is possible that *trpm* plays a maternal role, independent of its role in initiating the calcium wave, such that lack of maternally deposited Trpm proteins leads to defects during embryogenesis. In mouse, TRPM7 is also required for normal early embryonic development, apart from its role in calcium

oscillations. Inhibition of TRPM7 function impairs preimplantation embryo development and slows progression to the blastocyst stage (Carvacho et al., 2016). *Drosophila trpm* mutant lethality had been reported to occur during the pupal stage (Hofmann et al., 2010). However, those homozygous mutants were offspring of heterozygous mothers and, thus, did not lack maternal Trpm function. Our germline-specific depletion of *trpm* reveals a possible maternal role for Trpm in embryogenesis.

Alternatively, or in addition, it is possible that oocytes lacking Trpm do not pass sufficient Ca^{2+} from the environment to form a calcium wave, but that at least some events of egg activation can occur despite this. In mouse, an initial calcium rise is induced by sperm delivered Phospholipase C ζ (PLCζ) via the IP_3 pathway (Saunders et al., 2002). Yet although sperm from PLCζ null males fails to trigger normal calcium oscillations, some eggs fertilized by those sperm develop (Hachem et al., 2017). Multiple oscillations following fertilization require influx of external calcium (Miao and Williams, 2012), mediated by TRPM7 and $Ca_V3.2$ (Bernhardt et al., 2018). Although these oscillations had been reported to be needed for multiple postfertilization events (Ducibella et al., 2002), some TRPM7 and $Ca_V3.2$ double-knockout embryos still develop, albeit not completely normally (Bernhardt et al., 2018). Together, these data suggest that egg activation can still occur in mouse with diminished intracellular calcium rises, analogous to what we see in *Drosophila* in the absence of maternal Trpm function.

Insufficient influx of calcium in the absence of Trpm function could disrupt later (but maternally dependent) embryogenesis. The oocyte-to-embryo transition involves multiple events. In mouse egg activation, these events take place

sequentially as calcium oscillations progress, with developmental progression associated with more oscillations and more total calcium signal. Some of the events start after a certain number of oscillations but require additional oscillations to complete (Ducibella et al., 2002). It is possible that mechanisms critical for *Drosophila* embryo development also depend on reaching a precise level of calcium. A low-level calcium rise might be sufficient to trigger some egg activation mechanisms such as vitelline membrane cross-linking and cell cycle resumption, but high levels of calcium may be required for further progression.

Alternative pathways for calcium influx during egg activation

Given the importance of calcium in egg activation (Miao and Williams, 2012; Page and Orr-Weaver, 1997), we were surprised that although *trpm* knockout eggs lacked a calcium wave *in vitro*, *in vivo* such eggs could progress in cell cycles and even, sometimes, hatch. As discussed above, there may be insufficient calcium influx in the absence of Trpm for full and efficient development, but some egg activation events may still occur. Alternatively, it is possible that redundant mechanisms permit a sufficient calcium level increase without producing a detectable wave form. Despite being able to trigger a series of egg activation events including meiosis resumption and protein translation (Horner and Wolfner, 2008b; Page and Orr-Weaver, 1997), osmotic pressure during *in vitro* activation may have different properties from mechanical pressure exerted on mature oocytes during ovulation. The latter might allow opening of other calcium channels to initiate a normal calcium rise and complete egg activation. Two channels, TRPM7 and $Ca_v3.2$, are needed for the calcium oscillations following mouse fertilization, but the *Drosophila* ortholog of mouse $Ca_v3.2$, Ca-α1T, is not

detectably expressed in fly ovaries (Brown et al., 2014). From RNA-seq database, another mechanosensitive, nonselective cation channel, Piezo (Coste et al.), is expressed in *Drosophila* ovaries (Brown et al., 2014). Piezo and/or other unknown channels might play this redundant role of mediating calcium influx *in vivo*. In this light we note that levels of basal GCaMP fluorescence varied among oocytes incubated in IB that were inhibited from forming a wave, suggesting the possibility of a calcium increase by a redundant mechanism (**Figure 2.9**).

Conserved role of TRPM channels in egg activation

We are intrigued that *Drosophila* Trpm is essential for the calcium rise at egg activation, given that mouse TRPM7 was recently reported to be required (along with $Ca_V3.2$) for the calcium influx needed for post-fertilization calcium oscillations that are, in turn, required for egg activation events (Bernhardt et al., 2018; Ducibella et al., 2002). This apparent conservation in mechanisms in egg activation involving orthologous Trpm channels in a protostome (*Drosophila*) and a deuterostome (mouse) prompts us to wonder whether Trpm mediated calcium influx is a very ancient and basal aspect of egg activation, with other more variable aspects such as sperm triggered calcium rises being more derived, if better known, features. It is interesting in this light that a sperm delivered TRP channel (TRP-3) has also been reported to mediate calcium influx and a calcium rise in another protostome, *Caenorhabditis elegans* (Takayama and Onami, 2016).

Figure 2.1 Scheme for gRNA expression plasmid construction and crosses to achieve germline CRISPR/Cas9-mediated knockout.

(A) Two designs of gRNA transgenesis vectors that allow ubiquitous expression of multiple gRNAs (Poe et al., 2018); element lengths and positions are not drawn to scale. CR7T and U6:3: ubiquitous promoters; sgRNA1 and 2: utilizes gRNA set 3 (Materials and Methods) targeting *trpm*; tRNA: *Drosophila* glycine tRNA; U6 fl: U6 promoter 3' flanking sequence. The vectors were incorporated into the *Drosophila* genome by phiC31 mediated chromosomal integration. (B) Crossing scheme to achieve germline-specific CRISPR/Cas9-mediated knockout of *trpm*.

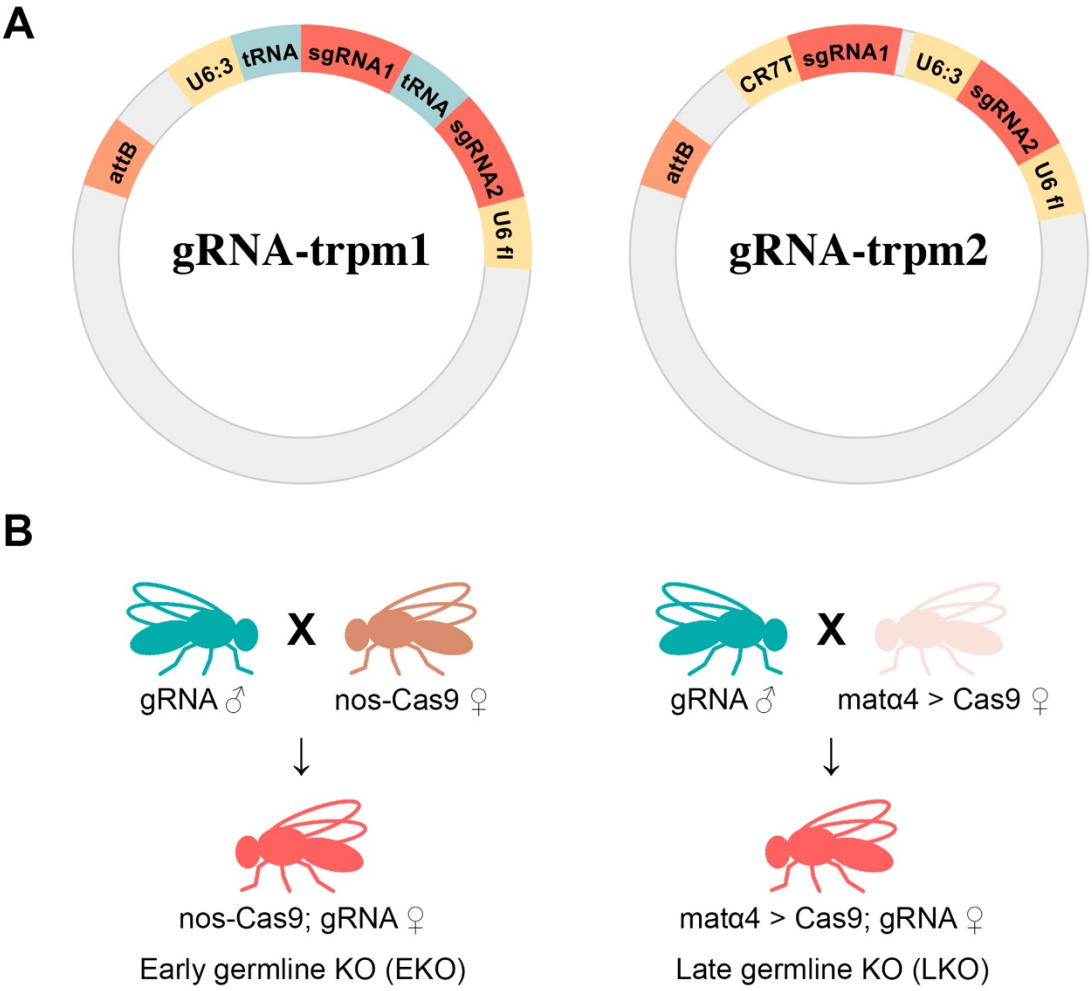
A
attB
U6:3
tRNA
sgRNA1
tRNA
sgRNA2
U6 fl
gRNA-trpm1
attB
CR7T
sgRNA1
U6:3
sgRNA2
U6 fl
gRNA-trpm2
B
gRNA ♂
X
nos-Cas9 ♀
nos-Cas9; gRNA ♀
Early germline KO (EKO)
gRNA ♂
X
matα4 > Cas9 ♀
matα4 > Cas9; gRNA ♀
Late germline KO (LKO)

Figure 2.2 Verification of *pain* and *trpml* null mutants.

(A) Scheme of $pain^{TM\Delta}$ deletion. Locations of gRNA targets and PCR primers relative to the deletion are shown; (B) Sequencing results of $pain^{TM\Delta}$ allele. Bases labeled in cyan are gRNA targets in the wildtype allele. Red labels mismatching bases and deletion resulted from CRISPR/Cas9-mediated editing; (C) PCR verification of $pain^{TM\Delta}$ allele. Expected amplicon sizes: C1F+C1R (207bp in WT allele, none in mutant allele), C2F+C2R (203bp in WT allele, none in mutant allele), C1F+C2R (1268bp in wildtype allele, 177bp in mutant allele); (D) PCR verification of $trpml^{1}$ allele. Expected amplicon sizes: 1347bp in wildtype allele, 250bp in mutant allele.

A

B

gRNA target 1 gRNA target 2

WT AGAGAGACTCCGGACTCAACCAGCTGCAAGAC...1065bp...CCCGAACTACTTAAGTCTGCGTCAGATTTCCGTGC

pain$^{TM\Delta}$ AGAGAGACTCCGGG----------ACTTAAGTCTGCGTCAGATTTCCGTGC

C

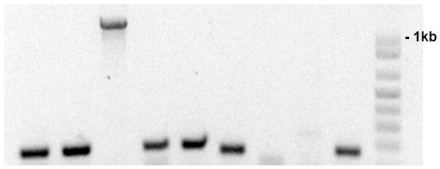

DNA	+/+			*pain*$^{TM\Delta}$/+			*pain*$^{TM\Delta}$/*pain*$^{TM\Delta}$		
Primer pair	C1F C1R	C2F C2R	C1F C2R	C1F C1R	C2F C2R	C1F C2R	C1F C1R	C2F C2R	C1F C2R

D

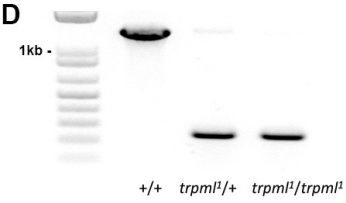

Figure 2.3 Verification of CRISPR/Cas9 generated indels in oocytes from *trpm* germline knockout females.

(A) Representative gel of final products from single oocyte RT-PCR followed by nested PCR using oocytes from *trpm* germline knockout females (*nos-Cas9-attP2/gRNA-trpm*^{1}). Amplicon size of *trpm* inner primers is 256bp. Oocyte 1, 3, 8 and 9 successfully generated PCR products. Oocyte 2, 4, 5, 6 and 7 failed to generate PCR products likely due to low copy number of mRNA in a single egg. Genomic DNA of ORP2 wildtype flies was used as positive control. A sham sample undergoing the same RNA extraction, RT-PCR and nested PCR process was used as a negative control; (B) Representative sequencing results of the PCR product in (A). Highlighted bases are one of the gRNA targets in gRNA set 3. Mixed sequencing peaks showed up after the gRNA target in 6 out of 8 oocyte samples sequenced, suggesting successful introduction of indels near the gRNA target by CRISPR/Cas9. We were unable to determine whether these indels caused frameshift, because it was difficult to untangle the mixed readings: depending on the timing of the editing, multiple species of *trpm* mRNA can be present in an oocyte.

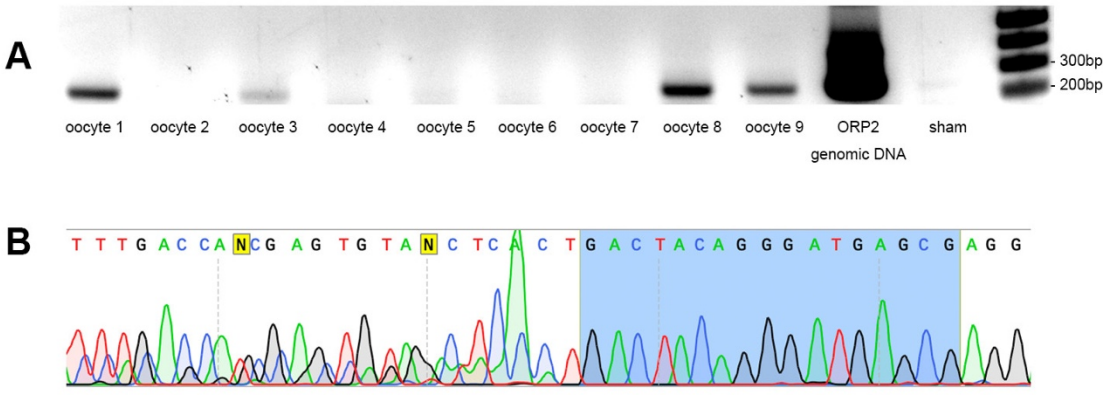
A
300bp
200bp
oocyte 1
oocyte 2
oocyte 3
oocyte 4
oocyte 5
oocyte 6
oocyte 7
oocyte 8
oocyte 9
ORP2
genomic DNA
sham
B
T T T G A C C A N C G A G T G T A N C T C A C T G A C T A C A G G G A T G A G C G A G G

Figure 2.4 Pain and Trpml are not essential for calcium wave initiation or propagation.

(A) The incidence of a calcium wave in *in vitro* activation assays does not differ between control ($pain^{TM\Delta}$/+, n = 33/49) and *pain* null mutant ($pain^{TM\Delta}/pain^{TM\Delta}$, n = 33/48), p = 1. (B) The propagation speed of the calcium wave does not differ between control (2.37 ± 0.38 μm/s) and *pain* null mutant (2.49 ± 0.78 μm/s), p = 0.59. (C) The incidence of a calcium wave in *in vitro* activation assays does not differ between control ($trpml^{1}$/+, n = 17/21) and *trpm*l null mutant ($trpml^{1}/trpml^{1}$, n = 15/25), p = 0.22. (D) The propagation speed of the calcium wave does not differ between control (2.97 ± 0.74 μm/s) and *trpm*l null mutant (2.78 ± 0.77 μm/s), p = 0.51. N.S., not significant (p > 0.05).

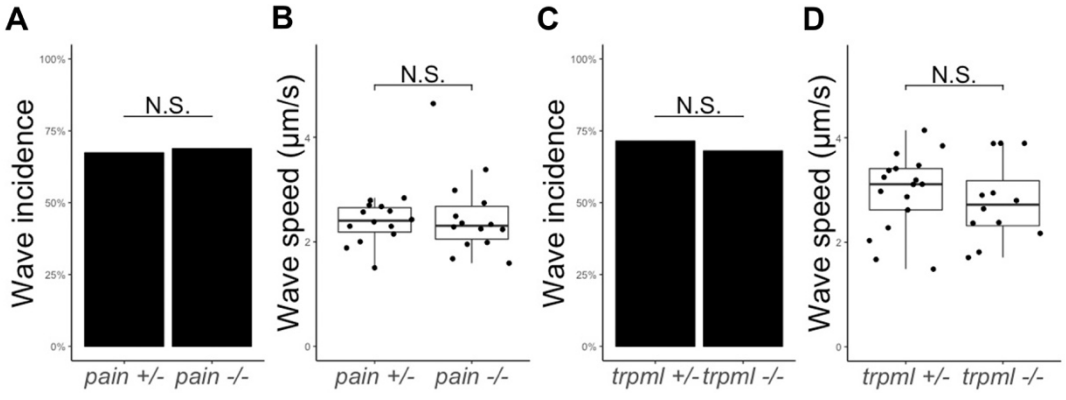
A
B
C
D
Wave incidence
Wave speed (µm/s)
N.S.
100%
75%
50%
25%
0%
4
2
0
pain +/-
pain -/-
trpml +/-
trpml -/-

Figure 2.5 Disrupting *trpm* function reduces calcium wave incidence *in vitro*.

(A–C) Representative calcium waves, or lack thereof, in *matα4-GAL4-VP16; UASp-GCaMP3* stage 14 oocytes in *in vitro* activation assays. Oocytes were incubated in: unmodified IB and RB (A); IB and RB with 10 mM of $MgCl_2$ (B); IB and RB with 100 μM NS8593 (C). (D) Representative pictures showing lack of calcium waves in stage 14 oocytes from *trpm* germline knockdown females (*matα4-GAL4-VP16/UAS-trpm*^{RNAi}*; UASp-GCaMP3*) incubated in unmodified IB and RB. An increase of calcium signal without a discernible wave is observed in some of the oocytes, possibly because of incomplete removal of Trpm channels by RNAi. (Scale bars: 50 μm.) (E–G) Quantification of calcium wave incidence in oocytes as in B–D: n = 16/18 for control (IB and RB with 30 mM sucrose to provide the same osmolarity change as 10 mM $MgCl_2$), n = 2/20 for 10 mM $MgCl_2$, $p = 5.69 \times 10^{-6}$ (E); n = 27/29 for control (DMSO), n = 0/29 for 100 μM NS8593, $p = 2.15 \times 10^{-11}$ (F); n = 26/28 for control (*matα4-GAL4-VP16; UASp-GCaMP3*), n = 11/70 for *trpm* germline knockdown mutants (*matα4-GAL4-VP16/UAS-trpm*^{RNAi}*; UASp-GCaMP3*), $p = 5.74 \times 10^{-12}$ (G). (H) RT-PCR quantification of *trpm* germline knockdown. Normalized expression level of *trpm* was calculated by normalizing *trpm* band intensity with that of ribosome protein gene rpl32 (C: control, KD: *trpm* germline knockdown). Transcript levels of *trpm* are decreased by >90% in knockdown ovaries and mature oocytes. Both sets of primers flank an exon-exon junction and will amplify a bigger band with genomic DNA as templates. This ensures that the bands we quantified were amplified from cDNA only. ***, $p < 0.001$.

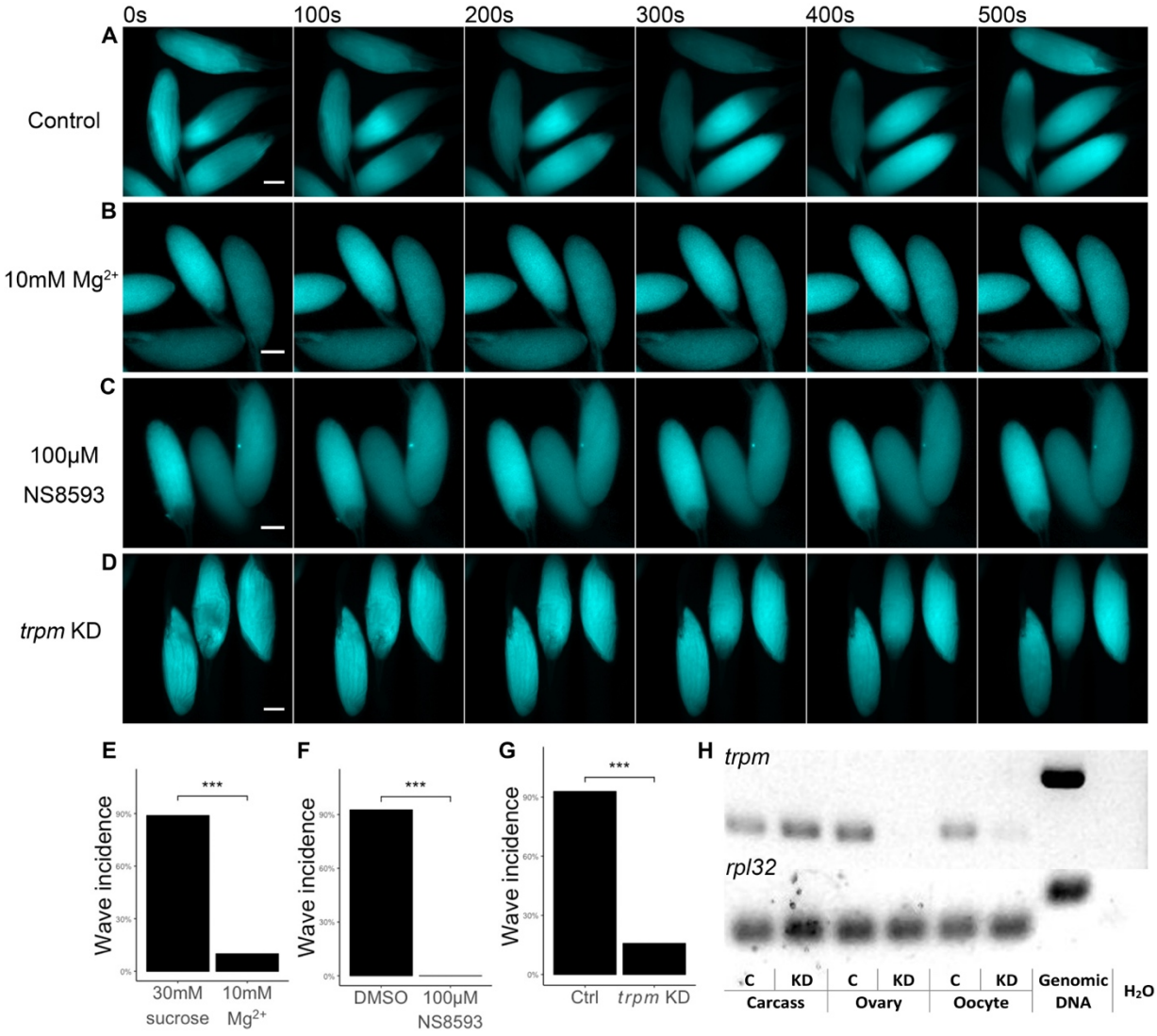
0s
100s
200s
300s
400s
500s
A
Control
B
10mM Mg2+
C
100μM
NS8593
D
trpm KD
E
Wave incidence
***
30mM
sucrose
10mM
Mg2+
F
Wave incidence
***
DMSO
100μM
NS8593
G
Wave incidence
***
Ctrl
trpm KD
H
trpm
rpl32
C
KD
C
KD
C
KD
Genomic
DNA
H2O
Carcass
Ovary
Oocyte

Figure 2.6 Ovary morphology of germline-specific *trpm* knockout females.

(A) *nos-Cas9* control females display normal ovary morphology (representative picture of n = 25); (B) 34% of the early germline *trpm* knockout females (*nos-Cas9; gRNA-trpm*^{1}) display ovary morphology defects (representative picture of n = 13/38, p = 0.003); (C) 96% of the early germline *trpm* knockout females (*nos-Cas9; gRNA-trpm*^{2}) display ovary morphology defects (representative picture of n = 22/23, p = $2.18X10^{-8}$); (D) *matα4-GAL4-VP16 > UAS-Cas9* control females display normal ovary morphology (representative picture of n=11); (E) Late germline *trpm* knockout females (*matα4-GAL4-VP16 > UAS- Cas9; gRNA-trpm*^{1}) display normal ovary morphology (representative picture of n=18). All scale bars = 500 μm.

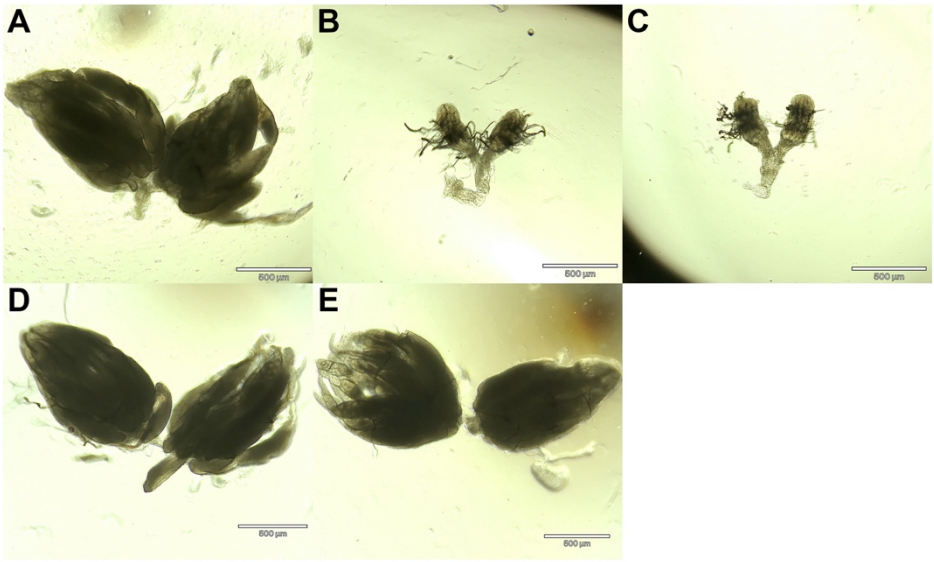
A
B
C
D
E
500 µm
500 µm
500 µm
500 µm
500 µm

Figure 2.7 *trpm* germline specific CRISPR knockout reduces calcium wave incidence.

(A–C) Representative calcium waves, or lack thereof, in *in vitro* activation assays. Stage 14 oocytes were dissected from: *nos-Cas9; matα4-GAL4-VP16; UASp-GCaMP3* control (A); early germline *trpm* knockout (*nos-Cas9; matα4-GAL4-VP16; UASp-GCaMP3/gRNA-trpm*^{1}) (B); late germline *trpm* knockout (*matα4- GAL4-VP16/UAS-GCaMP6s; gRNA-trpm*^{1}*/UAS-Cas9*) (C). (Scale bars: 50 μm.) (D and E) Quantification of calcium wave incidence in oocytes as in B and C: n = 36/39 for control (*nos-Cas9; matα4-GAL4-VP16; UASp-GCaMP3*), n = 38/87 for early *trpm* germline knockout (*nos-Cas9; matα4-GAL4-VP16; UASp-GCaMP3/gRNA-trpm*^{1}), p = 4.64×10^{-7} (D); n = 20/27 for control (*matα4-GAL4-VP16/UAS-GCaMP6s; UAS-Cas9*), n = 5/62 for late *trpm* germline knockout (*matα4-GAL4-VP16/UAS-GCaMP6s; gRNA-trpm1/ UAS-Cas9*), p = 3.68×10^{-11} (E). (F) Resistance to 50% bleach by mature oocytes, 1- to 5-h embryos and unfertilized eggs from control (*nos-Cas9-attP2*, C), *trpm* early germline knockout (*nos-Cas9-attP2/gRNA-trpm*^{1}, EKO), and late germline knockout (*matα4-GAL4-VP16; UAS-Cas9/gRNA- trpm*^{1}, LKO) females. All pre-activation oocytes are vulnerable to bleach. One- to 5-hour embryos and unfertilized eggs from both control and *trpm* germline knockout mutants displayed resistance to bleach treatment. C oocyte n = 132, EKO oocyte n = 152, LKO oocyte n = 119, C embryo n = 76, EKO embryo n = 73, LKO embryo n = 64, C unfertilized egg n = 66, EKO unfertilized egg n = 58, LKO unfertilized egg n = 71. N.S., not significant ($p > 0.05$); *** $p < 0.001$.

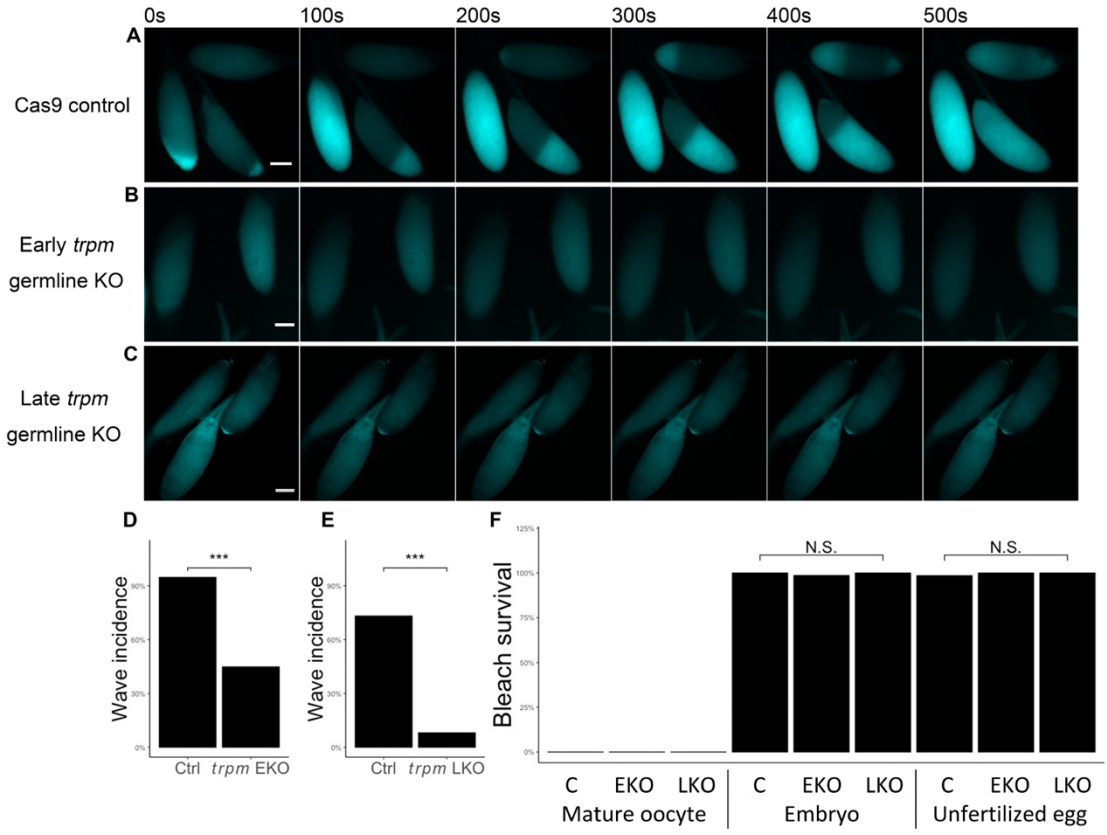
0s
100s
200s
300s
400s
500s
A
Cas9 control
B
Early trpm
germline KO
C
Late trpm
germline KO
D
Wave incidence
***
Ctrl trpm EKO
E
Wave incidence
***
Ctrl trpm LKO
F
Bleach survival
N.S.
N.S.
C EKO LKO
Mature oocyte
C EKO LKO
Embryo
C EKO LKO
Unfertilized egg

Figure 2.8 Cell cycle resumption and vitelline membrane cross-linking occur normally in eggs and embryos from *trpm* germline knockout females.

(A) Representative pictures of anti-Tubulin and DAPI staining of 1- to 5-h embryo laid by control and *trpm* germline CRISPR knockout females. Focal planes vary across samples. All embryos from *trpm* germline knockout females have started mitosis and progressed to multicellular stages (n = 88 for early germline knockout, n = 36 for late germline knockout). (B) Representative pictures of anti-Tubulin and DAPI staining of unfertilized eggs laid by control (*nos-Cas9-attP2*, n = 14) and *trpm* germline knockout (*nos-Cas9-attP2/gRNA-trpm*^{1}, n = 20) females. All eggs from both control and germline knockout females have completed meiosis, indicated by production of a normal polar body (Scale bars: A, 50 μm; B, 5 μm.) (C) *trpm* germline RNAi (*matα4-GAL4-VP16/UAS-trpm*^{RNAi}*; UASp-GCaMP3*, n = 18) does not significantly affect female egg hatchability relative to control (*matα4-GAL4-VP16; UASp-GCaMP3*, n = 18), p = 0.15. (D) Early *trpm* germline knockout (*nos-Cas9-attP2/gRNA-trpm*^{1}, n = 21) significantly reduces female egg hatchability relative to control (*nos-Cas9-attP2*, n = 16), p = 2.08×10^{-15}. (E) Late *trpm* germline knockout (*matα4-GAL4-VP16; UAS-Cas9/gRNA-trpm*^{1}, n = 17) significantly reduces female egg hatchability relative to control (*matα4-GAL4-VP16 > UAS-Cas9*, n = 9), p = 5.13×10^{-5}. N.S., not significant (p > 0.05); *** p < 0.001.

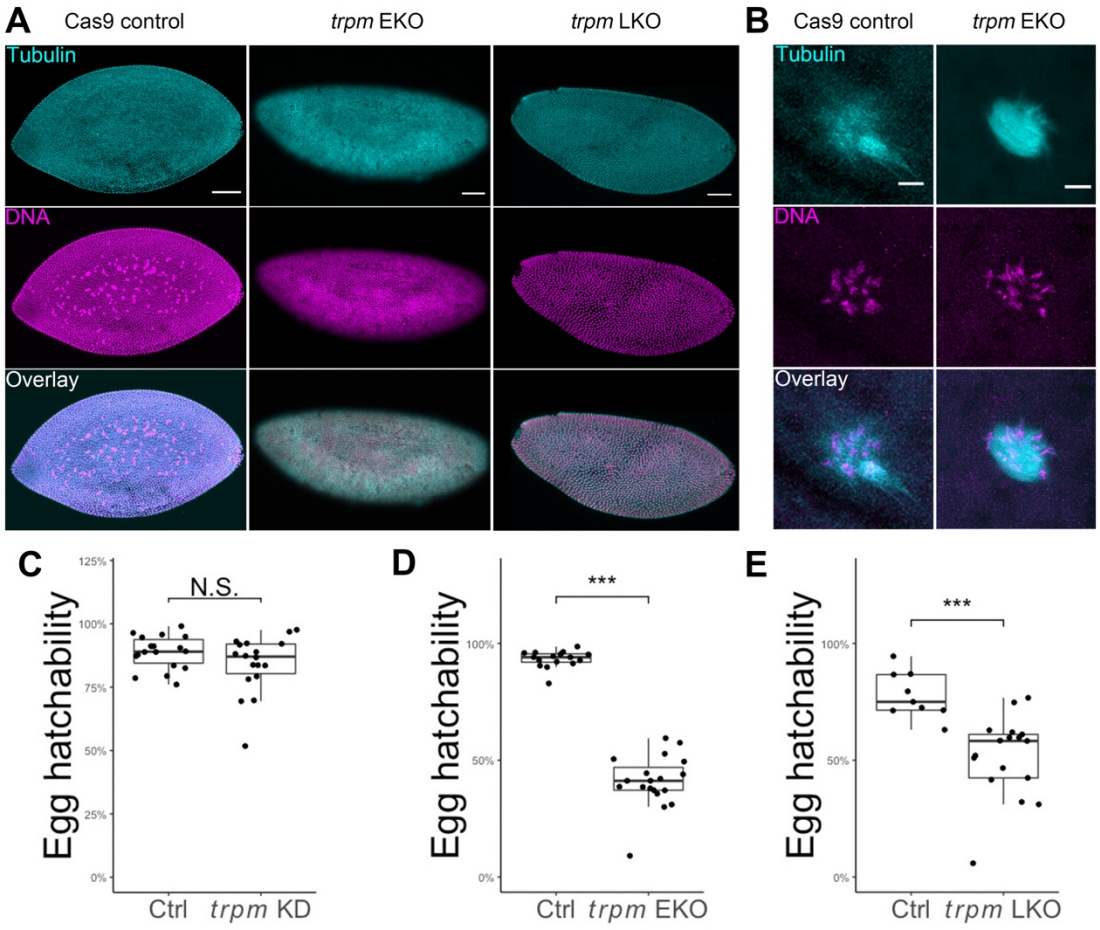
A
Cas9 control
trpm EKO
trpm LKO
Tubulin
DNA
Overlay
B
Cas9 control
trpm EKO
Tubulin
DNA
Overlay
C
Egg hatchability
125%
100%
75%
50%
25%
0%
N.S.
Ctrl
trpm KD
D
Egg hatchability
100%
50%
0%
***
Ctrl
trpm EKO
E
Egg hatchability
100%
50%
0%
***
Ctrl
trpm LKO

Figure 2.9 Variation in basal calcium levels in mature oocytes without a calcium wave.

(A) Two mature oocytes dissected from the same 3 to 5-day old *matα4-GAL4-VP16; UAS-GCaMP3* virgin female, incubated in IB. Difference in GCaMP3 signal suggests variation in basal calcium levels in mature oocytes. Scale bar = 50 μm; (B) Quantification of GCaMP3 signal intensity in (A).

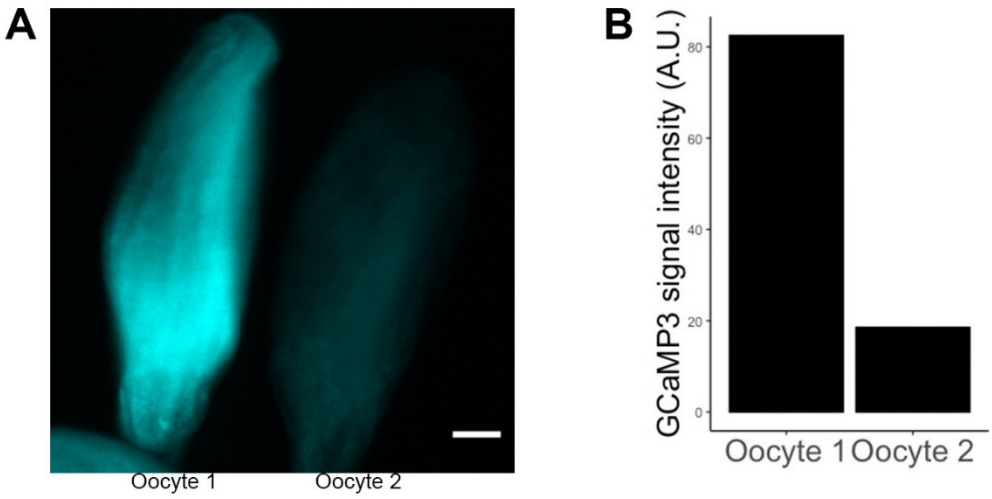
A
Oocyte 1
Oocyte 2
B
GCaMP3 signal intensity (A.U.)
0
20
40
60
80
Oocyte 1
Oocyte 2

Table 2.1 Efficiency test of gRNA sets targeting *trpm* using "Cas9-LEThAL" method.

act-Cas9, lig4- mutant females were crossed to males carrying U6:3-tRNA- gRNA1-tRNA-gRNA2 plasmid with different sets of gRNAs (Poe et al., 2018). Number of female and male progenies from the crossing were counted. Higher gRNA efficiency results in higher male lethality.

Efficiency test of gRNA sets targeting *trpm* using "Cas9-LEThAL" method			
gRNA-*trpm*	Number of female progenies	Number of male progenies	Male/female ratio
Set 1	65	6	0.092
Set 2	72	4	0.056
Set 3	68	0	0

CHAPTER 3 REGULATION OF CALCIUM WAVE INITIATION DURING DROSOPHILA EGG ACTIVATION

3.1 Introduction

Egg activation releases mature oocytes from developmental arrest so that they can proceed into embryogenesis (reviewed in Kashir et al., 2014; Krauchunas and Wolfner, 2013). Most of this process is conserved in species studied to date. A common feature of egg activation is a rise in levels of intracellular calcium, due to influx of external calcium and/or release of internal calcium from stores (reviewed in Swann and Lai, 2016). The trigger of this calcium rise varies across species, from mechanical stimulation from the reproductive tract in arthropods, to the fertilizing sperm in vertebrates, echinoderms and nematodes (reviewed in Horner and Wolfner, 2008a).

In *Drosophila* egg activation, environmental calcium enters the oocyte through Transient receptor potential, family M (Trpm) channels in response to mechanical triggers (Hu and Wolfner, 2019), such as pressure from the reproductive tract and/or swelling of the oocyte due to fluid uptake from the oviducts (Heifetz et al., 2001). *Drosophila* egg activation can be induced *in vitro* by incubating mature oocytes in hypotonic buffer so that they swell (Horner and Wolfner, 2008b; Page and Orr-Weaver, 1997). The calcium influx initiates a wave of calcium that propagates across the oocyte and can be visualized with the fluorescent calcium sensor GCaMP expressed in the germline (Kaneuchi et al., 2015; York-Andersen et al., 2015). The propagation of this calcium wave requires calcium release from internal stores, through the activation of the inositol 1,4,5-trisphosphate receptor (IP_3R) (Kaneuchi et

al., 2015). Both *in vivo* and *in vitro*, calcium waves initiate from one or both poles of the *Drosophila* oocyte. *In vivo*, they initiate only from the posterior end 95% of the time (Kaneuchi et al., 2015). The posterior end of the oocyte enters the oviduct first and experiences the pressure from passing through the pedicel and swelling in the oviduct first. *In vitro*, incubation in a hypotonic buffer results in swelling throughout the oocyte, but calcium waves still initiate from the poles for the majority of the time (Kaneuchi et al., 2015; York-Andersen et al., 2015). These observations raise the question of how the oocyte poles are specially regulated to allow calcium wave initiation. Since the calcium influx occurs through Trpm channels, we were curious to know whether Trpm is found only at the poles of the oocytes, explaining its local activation, or whether it is distributed evenly around the oocyte but only activated at the poles.

Here, we show that Trpm is uniformly localized around the mature oocyte. We then test and rule out two models for this activation at the poles: the ellipsoidal shape of the oocyte and differential sensitivity to regional pressure around the oocyte. This suggests that there is local special regulation of Trpm at oocyte poles to allow it to open for calcium influx only there.

3.2 Materials and Methods

Fly strains and maintenance. All *Drosophila* strains and crosses were maintained or performed on standard yeast-glucose-agar media at 25 °C on a 12/12 light/dark cycle. *matα-GAL4-VP16 > UAS-GCaMP3*, *nos-GCaMP6m*, *matα-GAL4-VP16 > UAS-Cas9*, and *matα-GAL4-VP16 > UAS-Cas9; trpm-gRNA*^{1} transgenic line

were as previously described (Hu and Wolfner, 2019; Kaneuchi et al., 2015). The *kugelei*$^{N103-2}$ strain (Horne-Badovinac et al., 2012) was a gift from Dr. Sally Horne-Badovinac at the University of Chicago. The *kramer*^{2} strain (Shami Shah et al., 2019) was a gift from Dr. Jeremy Baskin at Cornell Unniversity. *trpm* MiMIC insertion strain (Nagarkar-Jaiswal et al., 2015) (64467) was obtained from Bloomington *Drosophila* Stock Center.

Microneedle manipulation. Microneedles were fabricated and manipulated as previously described (York-Andersen et al., 2019). Indicated regions of wildtype mature oocytes carrying *matα-GAL4-VP16 > UAS-GCaMP3* transgene were pressed with the microneedle until a calcium rise occurred as visible with GCaMP3 signal increase. Propidium iodide was used as an indicator of plasma membrane integrity to prevent false calcium signals due to plasma membrane damage. Oocyte calcium dynamics were observed for 20 min.

Immunostaining. Mature oocytes from the indicated genotype were fixed and stained following established protocols (Radford and McKim, 2016). Embryos or eggs from Oregon-R-P2 (ORP2) wildtype females mated with either ORP2 males (for early embryos) or with the spermless male offspring of *tudor*^{1} females (Mahowald and Boswell, 1983) (for activated but unfertilized eggs) were collected from grape juice/agar plates . Embryos and eggs were dechorionated in 50% sodium hypochlorite (commercial Clorox bleach), fixed in methanol/heptane, and stored at 4°C until use. Fixed embryos and eggs were washed with phosphate-buffered saline, 0.1% Tween (PBST) 3 times for 5 minutes each and blocked with PBST containing 5% vol of normal goat serum (PBST-NGS). Embryos were then incubated overnight at 4 °C in

PBST-NGS containing primary antibody [rabbit anti-Trpm (Hofmann et al., 2010) (a kind gift from Dr. Craig Montell at University of California, Santa Barbara) at a dilution of 1:500, mouse anti-FLAG (MilliporeSigma) at 1:500, or rabbit anti-phospho-ERK (Cell Signaling) at 1:250]. Embryos and eggs were then washed with PBST 3 times for 5 minutes each and incubated at room temperature in PBST-NGS containing the corresponding secondary antibody [AlexaFluor 594 anti-rabbit, AlexaFluor 594 anti-mouse or AlexaFluor 488 anti-rabbit (Thermo Fisher)] for 4 h. Samples were then washed with PBST 3 times and mounted on glass microscope slides in anti-fade mounting buffer.

Imaging. Fixed and stained oocytes, embryos and eggs were imaged using a Zeiss LSM880 Confocal Multiphoton Microscope with a 10X lens and Zen software. The detection wavelength was set to 585-733 nm for AlexaFluor 594 signals and 493-556 nm for AlexaFluor 488 signals. Mature oocytes were dissected from females of indicated genotypes. They were activated *in vitro* as previously described. During *in vitro* activation, oocytes were imaged using a Zeiss Elyra Super Resolution Microscope with a 5X or 10X lens and Zen software. The detection wavelength was set to 493-556 nm for GCaMP6m signal. Images were processed with ImageJ software when needed.

3.3 Results

Trpm is evenly distributed around the periphery of mature oocytes

To examine the cellular distribution of Trpm, we used a validated anti-Trpm antibody (Hofmann et al., 2010) to visualize the distribution of Trpm in mature

oocytes, activated but unfertilized eggs and early embryos from Cas9 control and *trpm* germline knockout mutants (Hu and Wolfner, 2019). In Cas9 control, Trpm channels displayed an even distribution around the plasma membrane, with no concentration at oocyte poles (**Figure 3.1 A**). Trpm channels appeared more diffuse around the plasma membranes after *in vivo* egg activation and were not seen on the plasma membrane in 1-5 h early embryos (**Figure 3.1 A**). Samples from *trpm* germline knockout females did not show significant staining under the same imaging settings (**Figure 3.1 B**). To verify this distribution change, we used anti-FLAG to probe Trpm in *trpm* MiMIC insertion lines that carry multi-tag insertion including FLAG in frame with the endogenous *trpm* gene (Nagarkar-Jaiswal et al., 2015). We observed similar FLAG distributions and pattern changes in mature oocytes and unfertilized eggs (**Figure 3.1 C-D**).

Taken together, our results suggested that Trpm is evenly distributed around the plasma membrane of the mature oocytes and gets gradually de-localized from plasma membrane after egg activation, coinciding with the timing of its function in mediating the initial calcium influx at egg activation. The even distribution of Trpm channels around mature oocytes rules out the possibility that calcium initiation site is determined by specialized localization of Trpm channels mediating calcium influx. Thus, Trpm channels must be under special regulation or encounter special conditions at the poles to allow them to open only there in response to global mechanical triggers.

Oocyte shape does not determine calcium wave initiation site

The ellipsoidal shape of *Drosophila* oocyte could make its poles and waist experience different levels of mechanical pressure when passing through the

reproductive tract *in vivo* or swelling in hypotonic buffer [modified Robb's buffer (RB) (Hu and Wolfner, 2019)] *in vitro*. To determine if oocyte shape affects the site of calcium wave initiation, we examined the calcium wave phenotype in oocyte from *kugelei* (*kug*, Fat2) mutants. *kugelei* is required for the follicle cell migration around the oocyte that shapes the oocyte. Its mutants fail to elongate egg chamber during oogenesis, resulting in near-spherical oocytes (Horne-Badovinac et al., 2012; Viktorinová et al., 2009). These oocytes would experience similar pressures at their poles and waistline during swelling *in vitro*. We crossed into $kugelei^{N103\text{-}2}$ null mutants the *nos-GCaMP6m-attP40* transgene that expresses a fluorescent calcium sensor in the germline and visualized the calcium waves in the spherical mature mutant oocytes in *in vitro* egg activation. All calcium waves still initiated from the poles in spherical oocytes (**Figure 3.2 A**), indicating that calcium wave initiation site is not determined solely by oocyte shape.

Oocyte poles and waist display similar sensitivity to regional mechanical pressure

We asked if oocyte poles and waist display similar sensitivity to mechanical pressure. In our previous studies, we showed that a regional calcium rise can be induced with a microneedle in mature oocytes incubated in hypertonic isolation buffer (IB), which prevents oocytes from swelling and activation (York-Andersen et al., 2019). This calcium rise stays regional without propagation. Here, we extended this experiment by applying microneedle pressure at the anterior end, waist and posterior end of mature oocytes respectively. We observed that regardless of the pressing site, a regional calcium rise can always be induced (**Figure 3.2 B-D**), but it did not spread

into a wave. This suggested that the oocyte poles and waist display similar responses to regional pressure. When exposed to global pressure such as that from swelling in RB, oocytes are likely to use other mechanisms to regulate calcium rises to cause calcium waves to initiate only from the poles.

3.4 Discussion

Egg activation is a conserved process that is needed to initiate embryogenesis. It is accompanied by a rise in the egg's level of free intracellular calcium, in most species. Trpm channels mediate the influx of environmental calcium to initiate a calcium rise that nucleates into a wave as the *Drosophila* oocyte activates; homologous channels also induce calcium rises in activating mouse eggs. The *Drosophila* calcium wave initiates from the oocyte poles, primarily the posterior pole. It was unknown whether this local calcium wave initiation reflected the localization of Trpm channels at the poles, or local activation of otherwise uniformly distributed Trpm channels. Here, we showed that Trpm channels are uniformly distributed around the periphery of the mature oocyte, indicating that the second model is correct.

The uniform localization of Trpm channels around the *Drosophila* oocyte periphery raises the question of how these channels are only activated at the poles. Previous data showed that mechanical force external to, or by swelling of, the oocyte caused the Trpm-mediated calcium influx. Yet, the fluid nature of cytoplasm determines that different regions of the plasma membrane should experience equivalent pressure around the oocyte when it swells in response to the activation trigger, regardless of its shape. Consistent with this model, our observation that the

wave initiates at the poles of *kug* mutant oocytes, where the curvature is significantly smaller, argues against a model that the curvature of the oocyte regulates the likelihood of Trpm channel activation, at least in a form that can initiate a calcium wave. Our data also argue against a model that localized pressure alone (such as that exerted by a microneedle) is sufficient to activate mechanosensitive channels in a way that can nucleate a calcium wave. In an ideal situation, a cell containing fluid cytoplasm would adopt a spherical shape to minimize its surface tension. The ellipsoid shape of mature oocytes indicates that there must be structural differences between the poles and the waist (e.g. cytoskeletal network, membrane proteins or lipid composition) that hold the otherwise spherical cell in an elongated shape. Therefore, it is possible that structural molecules or molecular differences at the oocyte poles and/or their plasma membrane cause local activation of Trpm channels.

In *Drosophila* early embryos, developmental studies provide precedent for molecular differences between the oocyte poles and the rest of the oocyte. For example, some molecules that specify the terminal region of embryos are pole-localized, such as Fork head (*fkh*) (Weigel et al., 1989). Some other molecules are non-localized but are locally activated at the poles, such as Torso (*tor*) (Brönner and Jäckle, 1991), after egg activation and fertilization. Our data indicate that non-localized Trpm is locally activated at oocyte poles during egg activation, raising the possibility that terminal pattern formation might also be initiated prior to the start of embryogenesis.

In light of this hypothesis, we tested two possibilities: Kramer (*kmr*) and mitogen-activated protein kinase (MAPK). According to the BioGRID protein

interaction database (Stark et al., 2006), Trpm has a potential physical interaction with Kramer, a regulator of the Wnt signaling pathway (Shami Shah et al., 2019). We visualized Trpm localization in *kmr* null background and observed that Trpm is still evenly distributed around the *kmr* null oocytes (**Figure 3.3 A**). We also visualized calcium waves in *kmr* null oocytes and observed that calcium waves still initiate primarily from the poles of these oocytes. Thus, Kmr is unlikely to regulate Trpm localization or calcium wave initiation. The MAPK pathway can also activate in response to mechanical cues (Komuro et al., 1996) and its activity changes during *Drosophila* egg activation (Sackton et al., 2014). We examined the localization of the active form of ERK, phospho-ERK, in mature oocytes and activated eggs from ORP2 wildtype females and observed that phospho-ERK was also evenly distributed in wildtype mature oocytes and eggs (**Figure 3.3 B-C**). This suggests that MAPK pathway does not regulate Trpm activity via polarized distribution of active ERK in the oocyte.

The mammalian ortholog of *Drosophila* Trpm, TRPM7, is also involved in calcium influx during egg activation (Bernhardt et al., 2018). TRPM7 displays mechanosensitivity (Liu et al., 2015; Xiao et al., 2014) and can interact with cytoskeleton through non-muscle myosin II (Clark et al., 2006). Actin may be involved in the structural determination of the ellipsoid oocyte. We recently reported that the cortical actin is less concentrated at the posterior end of *Drosophila* mature oocytes and it is possible that lack of actin rigidity allows opening of calcium channels (York-Andersen et al., 2019). Given these observations, we believe a more likely candidate for local activation of Trpm at oocyte poles is the actin cytoskeleton. Future

studies are needed to determine how ubiquitously localized mechanically gated channels can be activated only in certain parts of a large cell like *Drosophila* oocyte.

Figure 3.1 Localization of Trpm before and after egg activation.

(A-B) Representative images of anti-Trpm staining of mature oocytes (n=16 for Ctrl, n=15 for *trpm* KO), unfertilized eggs (n=10 for Ctrl, n=10 for *trpm* KO) and 1-5 h early embryos (n=13 for Ctrl, n=9 for *trpm* KO) from (A) *matα-GAL4-VP16 > UAS-Cas9* control females and (B) *matα-GAL4-VP16 > UAS-Cas9; trpm-gRNA*^{1} *trpm* germline knockout females (*trpm* KO). (C-D) Representative images of anti-FLAG staining of mature oocytes (n=9 for *trpm* MiMIC, n=8 for WT) and unfertilized eggs (n=11 for *trpm* MiMIC, n=7 for WT) from *trpm* MiMIC insertion females and ORP2 wildtype females. Scale bars = 100 μM.

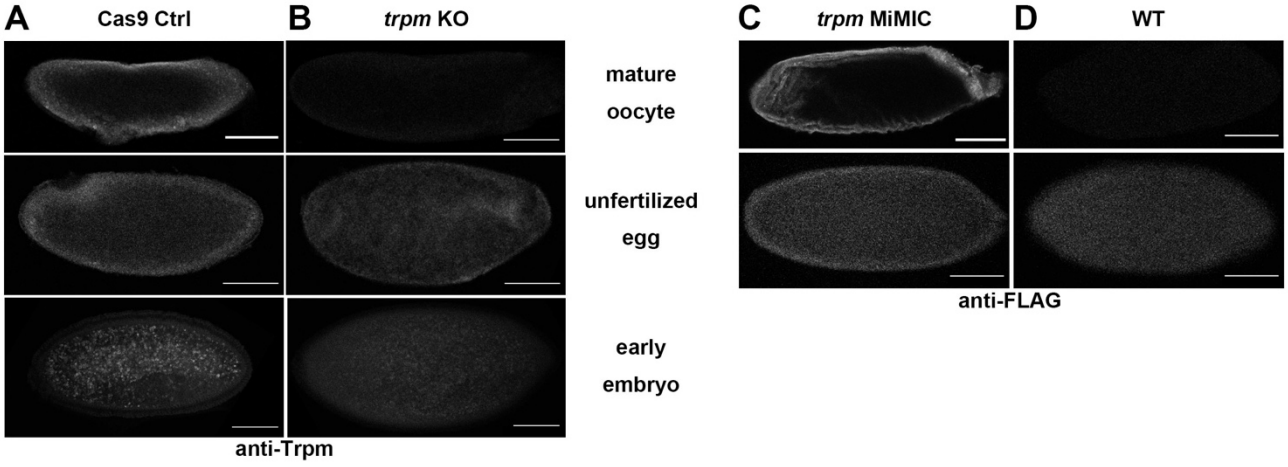
A
Cas9 Ctrl
B
trpm KO
C
trpm MiMIC
D
WT
mature
oocyte
unfertilized
egg
early
embryo
anti-Trpm
anti-FLAG

Figure 3.2 Calcium waves in *kug* mutant oocytes and regional calcium rise induced by microneedles in wildtype oocytes.

(A) Representative images showing calcium waves propagating from the ends of *kug* mutant near-spherical shaped mature oocytes (n=15). All scale bars = 100 μm. (B-D) Representative images showing regional calcium rises that do not propagate into waves induced by microneedle pressing at (B) anterior (n=7), (C) waist (n=4), and (D) posterior (n=4) regions of wildtype mature oocytes.

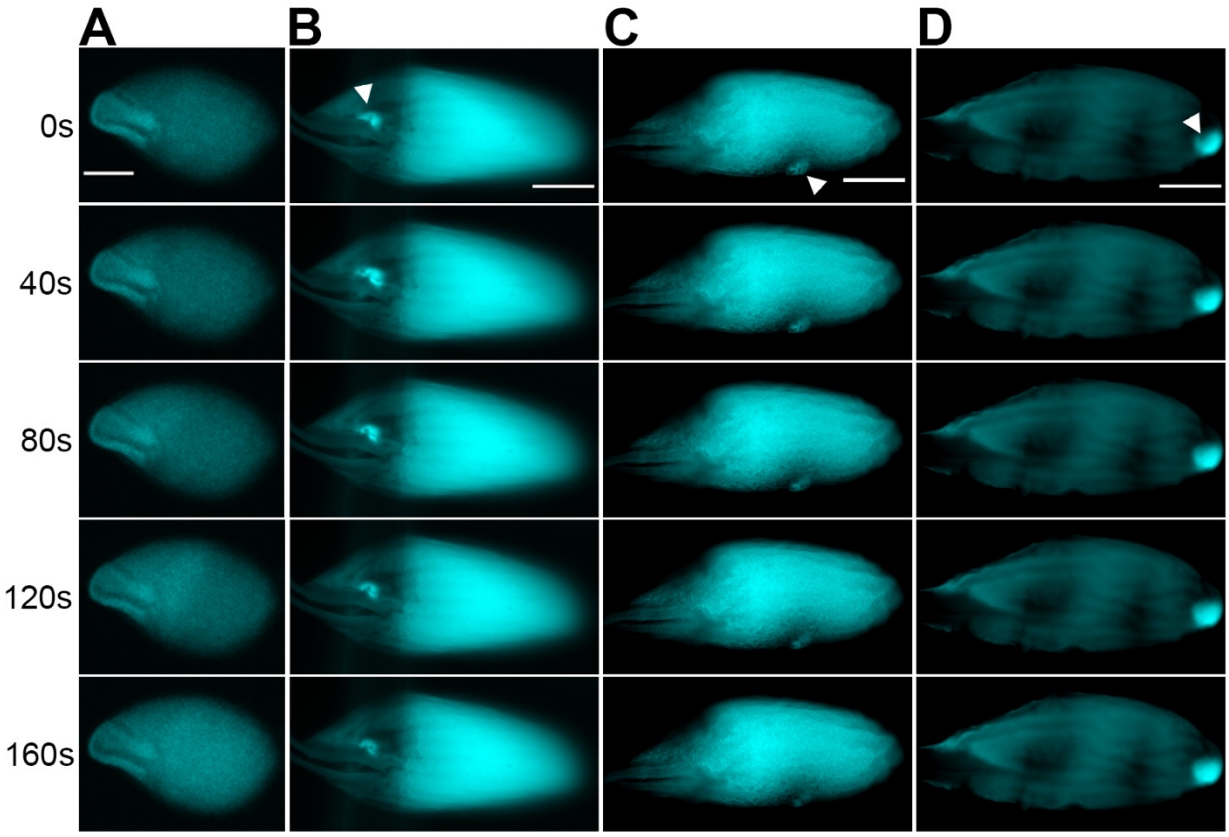
A
B
C
D
0s
40s
80s
120s
160s

Figure 3.3 Localization of Trpm in *kmr* mutant oocytes and localization of pERK before and after egg activation.

(A) Representative images of anti-Trpm staining in mature oocytes from *kmr*^{2} (n=13) females. (B-C) Representative images of anti-pERK staining in (C) mature oocytes (n=12) and (D) unfertilized eggs (n=10) of ORP2 wildtype females. All scale bars = 100 μm.

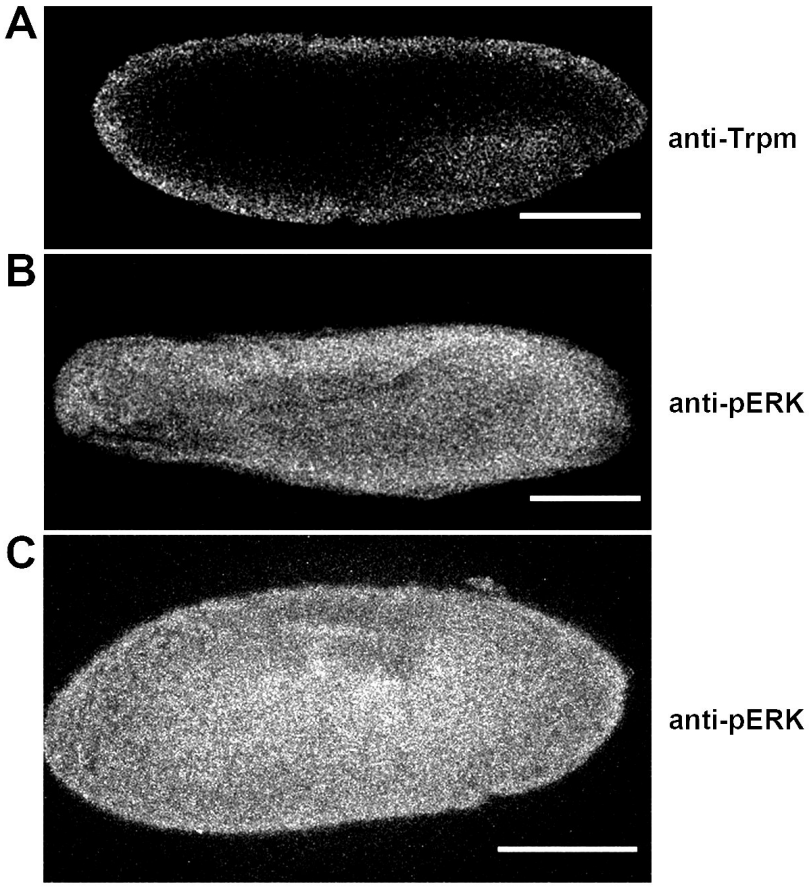
A
anti-Trpm
B
anti-pERK
C
anti-pERK

CHAPTER 4 DROSOPHILA PLC21C IS INVOLVED IN CALCIUM WAVE PROPAGATION DURING EGG ACTIVATION[2]

4.1 Introduction

Mature oocytes arrest in meiosis by the end of oogenesis and need to be activated in order to proceed to embryonic development. This egg activation process encompasses a series of events that transition the oocyte to a developing embryo, including meiosis resumption, maternal protein translation/modification, maternal mRNA processing, and cytoskeleton and eggshell changes (reviewed in Avilés-Pagán and Orr-Weaver, 2018; Horner and Wolfner, 2008a; Kashir *et al.*, 2014; Krauchunas and Wolfner, 2013). The triggers of egg activation vary across species, from mechanical pressure in arthropods to the fertilizing sperm in nematodes, echinoderms and vertebrates (reviewed in Horner and Wolfner, 2008a). Despite differences in trigger, a rise of intracellular calcium levels preceding downstream events is found in most species studied to date (reviewed in Swann and Lai, 2016). In *Drosophila* egg activation, the intracellular calcium rise is triggered by mechanical cues, which can be pressure exerted by the oviduct or from oocyte swelling *in vivo* (Heifetz *et al.*, 2001) or *in vitro* due to osmotic pressure from a hypotonic buffer (Horner and Wolfner, 2008b; Page and Orr-Weaver, 1997). This calcium rise takes the form of a transient calcium wave starting from the pole(s) and traversing the oocyte (Kaneuchi *et al.*, 2015; York-Andersen *et al.*, 2015). This calcium wave is initiated by influx of

---

[2] Published and reprinted with permission: Hu, Q.; Vélez-Avilés, A.N. and Wolfner, M.F. (2020). *Drosophila* Plc21C is involved in calcium wave propagation during egg activation. *microPublication Biology*. 10.17912/micropub.biology.000235

I contributed to designing and performing experiments, and data analysis.

environmental calcium through Trpm channels in response to the mechanical trigger (Hu and Wolfner, 2019). Further propagation of the calcium wave requires release of internal calcium from stores through the inositol 1,4,5-trisphosphate (IP_3) receptor (IP_3R) calcium channel (Kaneuchi *et al.*, 2015). It remains unclear how the initiation of calcium waves triggers the activation of IP_3R during this process.

Phospholipase Cs (PLCs) are membrane-associated enzymes that mediate the cleavage of phospholipids, specifically the cleavage of phosphatidylinositol 4,5-bisphosphate (PIP_2) to produce diacylglycerol (DAG) and IP_3. This reaction is involved in multiple signal transduction pathways (reviewed in Kadamur and Ross, 2013). In mammalian egg activation, a sperm-delivered PLC (PLCζ) is responsible for activating IP_3R to start the initial calcium rise (Saunders *et al.*, 2002).

Because the propagation of calcium waves in *Drosophila* egg activation also requires IP_3R, we hypothesized that this is also mediated by PLC and the IP_3 pathway. The *Drosophila* genome encodes three PLCs: No receptor potential A (*norpA*), Small wing (*sl*) and Phospholipase C at 21C (*plc21C*). According to the RNAseq database, all three are expressed in *Drosophila* ovaries (Leader *et al.*, 2017). It is possible that one or more of the three PLCs is involved in transducing the initial calcium influx signal to the IP_3 pathway to allow the calcium wave to propagate. Some PLCs can directly bind to Ca^{2+} and get activated in response to calcium signals (reviewed in Katan, 1998). All three *Drosophila* PLCs contain EF hand domains, which can potentially bind Ca^{2+} and directly transduce the ionic signal to downstream pathways (Lewit-Bentley and Réty, 2000).

4.2 Materials and Methods

Fly strains and maintenance. All *Drosophila* strains and crosses were maintained or performed on standard yeast-glucose-agar media at 25C° on a 12/12 light/dark cycle. The *nos-Cas9; matα-GAL4-VP16; UAS-GCaMP3* transgenic line was made by crossing *yw, nos-Cas9* into a previously described *matα-GAL4-VP16; UAS-GCaMP3* transgenic line (Kaneuchi *et al.*, 2015). The *nos-GCamP3* and *nos-GCaMP6m* transgenic lines were as previously described (Hu and Wolfner, 2019; Kaneuchi *et al.*, 2015). $norpA^{36}$ (9048) and *yw, nos-Cas9* (54591) fly lines were obtained from the Bloomington *Drosophila* Stock Center.

DNA constructs and transgenic flies. Calcium waves were visualized by expressing GCaMP calcium sensors in the female germline using *matα4-GAL4-VP16; UASp-GCaMP3* or *nos-GCaMP6m* as previously described (Hu and Wolfner, 2019; Kaneuchi *et al.*, 2015). To generate CRISPR/Cas9 knockouts of *plc21C* and *sl*, we followed the previously described germline specific CRISPR/Cas9 genome editing protocol (Hu and Wolfner, 2019; Poe *et al.*, 2018). The offspring of the germline knockout females were isolated and sequenced to establish stable lines of *plc21C* and *sl* null mutants. The following gRNA target sequences were used:

gRNA-plc21C: CTACATCTCCACCGCCAGCG; CTTCTGGAACGGACGCACCG

gRNA-sl: ACCATTGGTATGCTGGAGCG; CTCCAGTGAATCCTCCTGCG

These gRNA expression constructs were injected by Rainbow Transgenic Flies, Inc. into *yw, nos-phiC31; PBac{attP-9A}* embryos. Flies carrying correct insertions were isolated to establish gRNA expression transgenic lines. To generate

whole fly knockout strains for *plc21C* and *sl*, we crossed germline knockout females to males carrying balancer chromosomes. The F1 progeny were single-pair mated with balancer flies. Once the crosses began producing offspring the parent containing a putative PLC mutation was individually genotyped with PCR. Primers flanking the gRNA targeting sites were used in PCR to detect deletions. Primer sequences are as follows: *plc21C*-F: TCGGATACCAACCAGGACTATG, *plc21C*-R: TATCTCGGGCACGAACGTATAG; *sl*-F: CGGATGAGAACTGGATTCGATAG, *sl*-R: GTGCAGTATGACAAAGCACTTG. The F2 progeny of crosses from the confirmed-mutant F1s were brother-sister mated to establish stable mutant lines. $plc21C^{1}$ carries a ~19kb deletion from exon 1 to exon 8, covering the majority the gene. sl^{12} carries a 44 bp deletion in exon 1 that leads to a frameshift and premature stop codon.

***In vitro* egg activation assay and imaging.** Oocytes were dissected from the indicated female flies fattened on yeast and were induced to activate *in vitro* following methods as previously described (Hu and Wolfner, 2019; Kaneuchi *et al.*, 2015). Before imaging, oocytes were placed in a drop of Isolation Buffer (IB) (Page and Orr-Weaver, 1997) in a glass-bottomed Petri dish. IB was then replaced by modified Robb's buffer (RB) (Hu and Wolfner, 2019) to induce egg activation at the start of imaging. Time-lapse images were taken at every 1s for 20 min after the addition of RB, using Zeiss Elyra Super Resolution Microscope with a 10X lens and Zen software. The detection wavelength was set to 493-556 nm, for the GCaMP signal.

Statistics. Pearson's χ^2 test was used to compare the incidence of calcium waves. Student's *t* test was used to compare the propagation speeds of the calcium

waves.

4.3 Results and Discussion

To determine the role of phospholipase C (PLC) in calcium wave propagation during *Drosophila* egg activation, we screened each of the PLCs. We started by examining the role of Plc21C. We examined the calcium wave phenotype in oocytes from germline-specific CRISPR/Cas9 *plc21C* knockout females. These females were offspring from *nos-Cas9; matα-GAL4-VP16; UAS-GCaMP3* crossed to *gRNA-plc21C* (see Methods). We observed a significant decrease in calcium wave incidence in oocytes from *plc21C* germline knockout females compared to controls (**Fig.1A**). To confirm these results, we isolated a null allele of *plc21C* (*plc21C^{1}*) from the offspring of the germline-knockout females (see Methods). This mutation is homozygous viable. We crossed it into the *nos-GCaMP6m* transgenic background (Hu and Wolfner, 2019) to allow us to visualize calcium dynamics in the germline of *plc21C^{1}* females. We examined oocytes dissected from *plc21C^{1}* homozygous females during *in vitro* egg activation and again found a significant decrease in calcium wave incidence compared to heterozygous controls (**Fig.1A and C**). In the few homozygous *plc21C^{1}* oocytes that did show calcium waves, we did not observe a significant difference in calcium wave propagation speed compared to controls (**Fig.1B**). Taken together, our data show that calcium waves during *Drosophila* egg activation require Plc21C.

Since there were still calcium waves in a minority of *plc21C^{1}* mutant oocytes, we suspected that Plc21C might function redundantly with other molecule(s). We thus examined the role of the two other PLCs encoded by the *Drosophila* genome, NorpA

and Sl. *norpA* has an available, viable, null allele $norpA^{36}$ (Riesgo-Escovar *et al.*, 1995). We crossed it into it the *nos-GCaMP3-attP2* transgenic background (Kaneuchi *et al.*, 2015) to visualize calcium dynamics in the germline. We isolated mature oocytes from $norpA^{36}$*; nos-GCaMP3-attP2* females and imaged them during *in vitro* egg activation. We observed that calcium wave incidence and propagation speed did not differ between the oocytes of homozygous $norpA^{36}$ mutants and heterozygous controls (**Fig.1A-B**). Next, we examined calcium waves in *sl* germline knockout oocytes during *in vitro* activation. Mutant oocytes did not differ from control oocytes in calcium wave incidence or propagation speed (**Fig.1A-B**). We also isolated a null allele of *sl* (sl^{12}) from the offspring of *sl* germline-knockout females (see Methods) and attempted to visualize calcium waves in oocytes from sl^{12} females. However, sl^{12} appeared to have combinatorial lethality with the *nos-GCaMP6m* transgene, as we were unable to isolate homozygous sl^{12}*; nos-GCaMP6m* flies. The fluorescence signal strength of heterozygous *nos-GCaMP6m* was too low for us to visualize calcium waves. Although oocytes from germline specific *sl* knockout females displayed normal calcium wave incidence and propagation speed, it is possible that this knockout did not efficiently cause biallelic null mutations in most oocytes to reveal the function of Sl. Thus, we were unable to determine a requirement of *sl* for calcium wave propagation.

The presence of calcium waves in a minority of *plc21C* null oocytes suggests that Plc21C functions redundantly with other PLCs such as Sl or with other calcium signal relaying mechanisms to facilitate calcium wave propagation. These redundant mechanisms require further investigation. It also remains to be elucidated how Plc21C

is activated by the initial calcium influx, whether through direct binding of Ca^{2+} to Plc21C or through other signal relaying molecules. Finally, we note that lack of Plc21C activity did not lead to the presence of initiated but only partially-propagated calcium waves, as was seen for IP3R knockdowns (Kaneuchi *et al.*, 2015). The complete absence of calcium waves seen in most *plc21C* null oocytes suggests that Plc21C activity is needed at the earliest stages of (or to initiate) wave propagation in response to the Trpm-mediated calcium influx.

In wing imaginal discs, Plc21C is required for the intercellular calcium waves that regulate wing development via the IP_3 pathway (Brodskiy *et al.*, 2019). Thus, Plc21C and the IP_3 pathway mediate both intracellular calcium waves during egg activation and intercellular calcium waves during tissue development.

This study identified the connection between calcium wave initiation and propagation during *Drosophila* egg activation. Based on this and our previous studies (Hu and Wolfner, 2019; Kaneuchi *et al.*, 2015), we propose the following model for the mechanism of the calcium wave during *Drosophila* egg activation: mechanical pressure activates Trpm channels located on the plasma membrane of mature oocytes, allowing influx of external calcium. These Ca^{2+} ions then directly or indirectly activate Plc21C (and possibly other signal-relaying molecules), which catalyzes the reaction producing IP_3. IP_3 then binds to and activates its receptor to release calcium from internal stores, facilitating propagation of the calcium wave (**Fig.1D**). Our demonstration of the use of PLC to relay egg activation triggering signals to intracellular calcium rises reveals an important conservation in egg activation mechanisms between *Drosophila* and mammals.

Figure 4.1 *plc21C*, but not *norpA* or *sl*, is necessary but not sufficient for calcium wave incidence *in vitro*.

(A) The incidence of calcium waves in oocytes from (left to right): *plc21C* germline-knockout females (*nos-Cas9; gRNA-plc21C*, n=16, p=0.007); $plc21C^{1}$ null mutant females (n=35, p=0.0018); $norpA^{36}$ null mutant females (n=18, p=1); *sl* germline knockout mutant (*nos-Cas9; gRNA-sl*, n=16, p=0.93) compared with controls (*nos-Cas9*, n=21; $plc21C^{1}$/+, n=22; $norpA^{36}$/+, n=15; *nos-Cas9*, n=21, respectively) during *in vitro* egg activation. (B) The propagation speed of calcium waves in (left to right): the few oocytes from $plc21C^{1}$ null mutant females that had calcium waves (n=4, 1.87±0.51 μm/s, p=0.47); oocytes from $norpA^{36}$ null mutant females (n=10, 2.13±0.41 μm/s); oocytes from *sl* germline knockout females (1.68±0.50 μm/s, n=11), p=0.72, all compared with their controls ($plc21C^{1}$/+, 1.62±0.62 μm/s, n=9; $norpA^{36}$/+, 1.85±0.39 μm/s, n=13; *nos-Cas9*, 1.74±0.26 μm/s, n=13, respectively) **(C)** Representative images of calcium waves, or lack thereof, in control (top, $plc21C^{1}$/+, n=15/22) and $plc21C^{1}$ null mutant (bottom, n=8/35). A pseudocolor look-up table was applied to make the signals easier to see. **(D)** Proposed model of the initiation and propagation of calcium waves during *Drosophila* egg activation. Image made using Biorender.com. All scale bars = 100 μM. **: p<0.01, N.S.: not significant, gKO: germline-specific knockout.

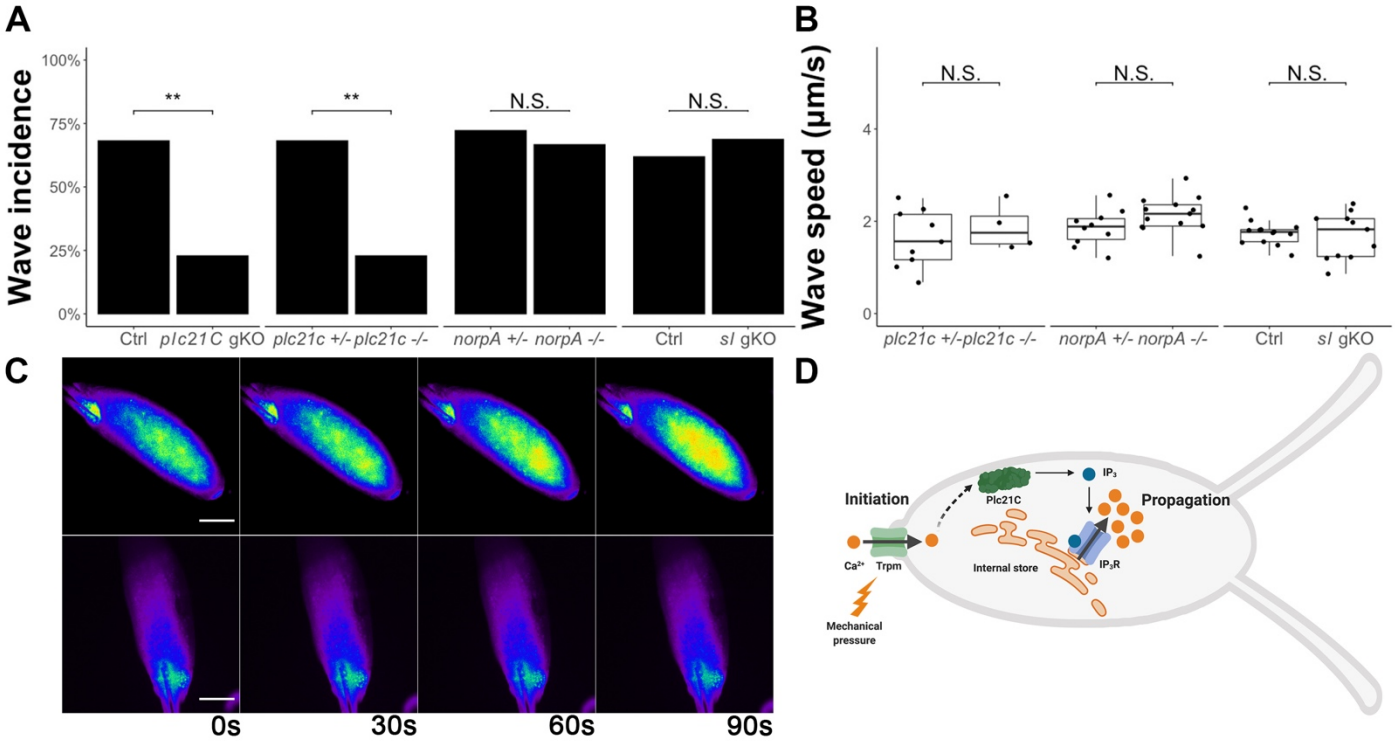
A
Wave incidence
100%
75%
50%
25%
0%
**
**
N.S.
N.S.
Ctrl
plc21C gKO
plc21c +/-
plc21c -/-
norpA +/-
norpA -/-
Ctrl
sl gKO
B
Wave speed (μm/s)
4
2
0
N.S.
N.S.
N.S.
plc21c +/-
plc21c -/-
norpA +/-
norpA -/-
Ctrl
sl gKO
C
0s
30s
60s
90s
D
Initiation
Plc21C
IP3
Propagation
Ca2+
Trpm
Internal store
IP3R
Mechanical pressure

CHAPTER 5 A CALCIUM-MEDIATED ACTIN REDISTRIBUTION AT EGG ACTIVATION IN DROSOPHILA[3]

5.1 Introduction

Production of female gametes is an important part of the faithful passage of genetic information from parents to offspring. Upon completion of oogenesis, mature oocytes remain developmentally arrested. They are triggered to resume development by egg activation, a series of conserved processes that include completion of meiosis to generate a haploid female pronucleus, structural changes in the extracellular matrix of the oocyte, translation and degradation of maternal messenger RNAs (mRNAs), rearrangement of the cytoskeleton, and modification of proteins (Horner and Wolfner, 2008a; Kaneuchi et al., 2015; Kashir et al., 2014; Krauchunas and Wolfner, 2013; Miao and Williams, 2012; Swann and Lai, 2016). All of these events are preceded by a transient rise in the intracellular level of free calcium (Bernhardt et al., 2018; Kaneuchi et al., 2015; Kubota et al., 1987; Miao and Williams, 2012; York-Andersen et al., 2015). This calcium rise, which can result from influx of extracellular calcium and/or the release of calcium from internal stores, leads to dramatic changes in the mature oocyte that prepare it for further development. Many of these changes require the activity of calcium-dependent kinases and phosphatases (Horner et al., 2006; Mochida and Hunt, 2007; Takeo et al., 2006, 2010), which alter the phospho-proteome

[3] Published and reprinted with permission: York-Andersen, A. H.*, Hu, Q.*, Wood, B. W., Wolfner, M. F., and Weil, T. T. (2019). A calcium-mediated actin redistribution at egg activation in *Drosophila*. *Molecular Reproduction and Development*. *Equal contribution authors.
I contributed to designing and performing experiments (data in Figure 3.6, Figure 3.7 b, b', c, c', Figure 3.8 d, d', e).

of the egg (Guo et al., 2015; Krauchunas et al., 2012; Presler et al., 2017; Roux et al., 2008; Zhang et al., 2018a, reviewed in Krauchunas and Wolfner, 2013).

The trigger that initiates egg activation varies across species. In vertebrates and some invertebrates, egg activation requires sperm entry. Significantly, in other invertebrates, egg activation is independent of fertilization and can be initiated by changes in the ionic environment, variation in external pH, or mechanical pressure (reviewed in Horner and Wolfner, 2008a).

In *Drosophila melanogaster*, egg activation is triggered by mechanical pressure during ovulation and does not require sperm (Heifetz et al., 2001; Horner and Wolfner, 2008b). When a mature oocyte is ovulated and moves from the ovary to the lateral oviduct, it is thought to experience pressure and fluid uptake. This results in its swelling and a transient wave of increased cytoplasmic calcium that initiates from oocyte poles, predominantly the posterior, due to calcium influx through Trpm channels (Horner and Wolfner, 2008b; Hu and Wolfner, 2019; Kaneuchi et al., 2015). This calcium influx and wave can be recapitulated *ex vivo* by submerging dissected mature oocytes in certain hypotonic buffers (Kaneuchi et al., 2015; York-Andersen et al., 2015). This experimental approach has shown that initiation of the calcium wave requires a functional actin cytoskeleton, as the presence of the actin polymerization inhibitor cytochalasin D results in a loss of the full calcium wave in the majority of oocytes (York-Andersen et al., 2015).

Changes in the actin cytoskeleton have previously been observed at fertilization and egg activation in multiple systems. In sea urchins, actin polymerizes around the sperm binding site to form a fertilization cone and facilitates the sperm-egg

fusion that initiates egg activation events (Tilney, 1980). In mouse oocytes, actin is required for TRPV3-mediated calcium influx during parthenogenetic egg activation with strontium chloride, as the actin polymerization inhibitor latrunculin A blocks the calcium rise through TRPV3 activation (Lee et al., 2016). Furthermore, starfish eggs treated with ionomycin to raise the intracellular level of calcium show a perturbed actin cytoskeleton and fail to display the centripetal movement of filamentous actin (F-actin) (Vasilev et al., 2012). Together, these data highlight potential regulatory interactions between the actin cytoskeleton and calcium at egg activation. However, a clear mechanistic understanding and detailed characterization of the interplay between calcium and actin at egg activation is lacking.

Here we use live imaging, pharmacological disruption, mechanical manipulation, and genetics to determine the relationship between calcium and actin at egg activation in *Drosophila*. We show that actin has a broad distribution, filling in ridges that cover the cortex of the mature oocyte. Upon egg activation, we report dispersal of the actin cytoskeleton concurrent with rounding of the cortex as the egg swells. The change in the actin cytoskeleton is required for the calcium wave. The calcium wave, in turn, is required for the reorganization of the actin cytoskeleton, which also proceeds in a wavelike manner. Moreover, we found that cortical actin is dynamic before and after egg activation as well. Regional pressure on mature oocytes can induce a local calcium rise with no increase of the local actin signal. Together, our data suggest that increased cytoplasmic calcium is necessary for actin reorganization. The co-dependence of the calcium wave and actin reorganization enables the mature

oocyte to undergo the dramatic physiological and molecular changes required for the initiation of further development. Since our model links calcium, a ubiquitous secondary messenger, to actin, a key cytoskeletal component, we expect that the interactions established in this study will be conserved in other species.

5.2 Materials and Methods

Fly stocks and reagents. The following fly stocks were used*: matα4-GAL-VP16>UASp-GCaMP3* [as previously described in (Kaneuchi et al., 2015)]; *UAS-Lifeact::mCherry* (a gift from from Palacios Lab, QMUL); *UAS-Spire B.tdTomato* (a gift from the Quinlan Lab, UCLA); *UASp-F-Tractin.tdTomato* (RRID:BDSC_58988, 58989*); UASp-Act5C-GFP* (RRID:BDSC_7309); *UAS-SCAR.RNAi* (RRID:BDSC_36121). All UAS constructs were driven with *matα4-GAL-VP16* (RRID:BDSC_7062, 7063).

Fly stocks were raised on either standard cornmeal–agar medium or yeast-glucose agar medium at 21°C or 25°C, mainly on a 12-light/dark cycle. Before dissection of the mature oocytes, female flies were fattened on yeast for 48–72 hr at 25°C. BAPTA (Sigma-Aldrich) was used at 10 mM, cytochalasin D (Sigma-Aldrich) at 10 μg/ml, Phalloidin (Sigma-Aldrich) at 3.3 nM, latrunculin A (Sigma-Aldrich) at 10 μg/ml, 2-APB (Sigma-Aldrich) at 200 μM, and RFP/mCherry booster (Atto 594) at 1:200 (ChromoTek).

Oocyte and embryo collection. Mature oocytes were dissected from the ovaries from fattened flies using a probe and fine forceps as described previously (Kaneuchi et al., 2015; York-Andersen et al., 2015). Embryos were collected for 30

min on apple or grape juice agar plates with yeast and then dechorionated in 50% bleach.

***Ex vivo* egg activation assay.** Oocytes were activated with different, but equivalent preparation methods: Dissected oocytes were placed in series 95 halocarbon oil (KMZ Chemicals) on 22 × 40 coverslips, aligned parallel to each other to maximize the acquisition area for imaging and left to settle for 10–15 min before addition of AB and imaging (Derrick et al., 2016); AB contains 3.3 mM NaH_2PO_4, 16.6 mM KH_2PO_4, 10 mM NaCl, 50 mM KCl, 5% polyethylene glycol 8000, 2 mM $CaCl_2$, brought to pH 6.4 with a 1:5 ratio of NaOH:KOH (Mahowald et al., 1983). Oocytes were dissected in IB (Page and Orr-Weaver, 1997) in a glass-bottomed Petri dish and activated by replacing IB with modified RB. IB contains 55 mM NaOAc, 40 mM KOAc, 1.2 mM $MgCl_2$, 1 mM $CaCl_2$, 110 mM sucrose, 100 mM HEPES in ddH2O. IB is adjusted to pH 7.4 with NaOH and filter sterilized. RB contains 55 mM NaOAc, 8 mM KOAc, 20 mM sucrose, 0.5 mM $MgCl_2$, 2 mM $CaCl_2$, 20 mM HEPES in ddH_2O. RB was adjusted to pH 6.4 with NaOH and filter sterilized (Hu and Wolfner, 2019).

For the high-resolution 3D live imaging oocytes were mounted in a glass-bottomed culture dish (MatTek) in Schneider's insect culture medium (GIBCO-BRL) with a 1 mm2 coverslip on the oocyte. For activation, Schneider's medium was removed and replaced with AB (Weil et al., 2008).

Imaging. Mature oocytes were imaged using a Zeiss LSM880 confocal microscope with Zen software under 10 × 0.45 NA water immersion objective with a detection wavelength of 493–556 nm for GCaMP signal, and 566–691 nm for F-tractin

signal. Z-stacks were taken from the shallowest to deepest visible plane of the oocyte. Z-stacks and time series of images taken were 3D reconstructed in Imaris software for final output. Image processing and analysis were performed using ImageJ (Schindelin et al., 2012).

Alternatively, images were acquired with an inverted Leica SP5 confocal microscope, under 20 × 0.7NA immersion objective with acquisition parameters of 500–570 nm, 400 Hz. Similar settings were used for the F-tractin cytoskeleton, with acquiring parameters of 570–700 nm. The Z-stacks were taken from the shallowest visible plane of the oocyte and were acquired at 2 μm per frame 40-μm deep. The Z-stacks were presented as maximum projections of 40 μm, unless stated otherwise.

High-resolution 3D images of the cortex were collected using an Olympus FV3000 confocal microscope with Schneider's mounting and activation preparation. Parameters for image collection were: 60x silicon immersion objective, 60 μm Z-stack, 0.34 μm between each Z-slice, 2,048 × 2,048 resolution of varying ROIs at the cortex, approximately 8–10 min per complete acquisition. The display has an initial angle of 0°, total rotation of 150° and a rotation angle increment of 1°. Image processing and analysis were performed using ImageJ and displayed as a maximum Z-projection or 3D projections.

FRAP was carried out on the cortex of the mature oocyte using a UV laser on the Olympus FV3000 microscope for 15 s. The fluorescence recovery was recorded using Olympus FV3000 for 20 min. Samples were imaged under a 30 × 1.05NA silicon immersion objective. Despite technical challenges due to swelling of activated eggs, we were able to visualize the bleached region clearly for approximately 100 s

after photobleaching. A partial calcium wave is defined as one that initiates but fails to completely traverse the entire oocyte; A full (or complete) calcium wave is defined as one that is able to traverse the entire oocyte.

Microneedle manipulation. Microneedles were fabricated from borosilicate glass rods (Catalog no. BR-100-15; Sutter Instrument), in a Sutter model P97 flaming/brown micropipette puller, with the following program: heat = 490, pull = 0, velocity = 25, time = 250. Mature oocytes of the indicated genotype were incubated in a glass-bottom Petri dish in 100 µl of IB that contained PI (Molecular probes) at a final concentration of 1 µg/ml as an indicator of PM integrity. Since the PM is not permeable to PI, PI staining at the microneedle pressing site would suggest damage to the PM and false calcium signal by calcium in IB entering through PM breach. To manipulate the oocyte, the microneedle was attached to and manipulated with an Eppendorf Injectman NI 2 micromanipulator. The indicated regions of mature oocytes were pressed with the microneedle until a calcium rise occurred as visible with GCaMP. Oocyte calcium and actin dynamics were observed for 20 min.

5.3 Results

Actin reorganizes and is more dynamic during *Drosophila* egg activation

Throughout *Drosophila* oogenesis, actin plays a role in tissue morphogenesis, signaling cascades, localization of mRNAs, and maintaining the integrity of the cortex (Spracklen et al., 2014a; Wang and Riechmann, 2007; Weil et al., 2008). To establish the distribution of the actin cytoskeleton before egg activation in the mature oocyte, we used the actin indicator F-tractin. Generated from the rat actin-binding inositol

1,4,5-trisphosphate 3-kinase A, F-tractin has been shown to closely correlate with Phalloidin staining and is suggested to be the least invasive actin probe in *Drosophila* follicle development (Schell et al., 2001; Spracklen et al., 2014b). To observe the dynamics of the actin cytoskeleton at live egg activation, we took advantage of an established *ex vivo* egg activation protocol (Weil et al., 2008) which enabled us to collect high-resolution three-dimensional (3D) images at different time points. This showed that before egg activation, actin is finely distributed around well-defined ridges in the dehydrated mature oocyte (**Figure 3.1 a–a″**). Following egg activation *ex vivo*, actin initially dispersed and was then reorganized into larger, more widely distributed foci (**Figure 3.1 b–c″**). We observed the same reorganization of actin in the *in vivo*-activated egg (**Figure 3.1 d–d″**) and in the early embryo (**Figure 3.2**).

To test the dynamics of actin before and after egg activation, we performed fluorescence recovery after photobleaching (FRAP) on mature oocytes expressing GFP-moesin, which is comprised of the C-terminal actin-binding domain of moesin, a transmembrane protein, and member of the ERM family, labeling only actin at the cortex (Edwards et al., 1997). By measuring the mean fluorescence intensity, we observed a more rapid recovery of GFP-moesin after photobleaching in activated versus mature eggs. Pre-activation, GFP-moesin has recovery halftime of 45 s, compared with post-activation, where the recovery halftime is 14 s (n = 5; **Figure 3.3 a, b**). We have also tested the recovery of the actin marker Act5C-GFP (Weil et al., 2006), and find similar FRAP recovery times before and after egg activation [41 vs. 20 , respectively (n = 5; **Figure 3.4**)]. The difference in GFP-moesin (and Act5C-GFP) recovery before and after egg activation suggests an increased turnover of cortical

actin and/or stabilization of F-actin, either of which could result in increased recruitment of actin markers.

Dynamic actin is required for a calcium wave during egg activation

The dispersal of actin appeared to occur before the previously established timing of the calcium wave associated with egg activation (Kaneuchi et al., 2015; York-Andersen et al., 2015). Moreover, previous work suggested that the calcium wave might depend on a freely dynamic actin cytoskeleton (York-Andersen et al., 2015). To confirm this relationship, we treated mature oocytes expressing the calcium indicator GCaMP3 with activation buffer (AB) mixed with phalloidin, a class of filament stabilizing phallotoxins (Cooper, 1987). Upon the addition of this solution, the mature oocytes swelled but exhibited a disrupted calcium wave in 68% of the oocytes, as the majority of phenotypes observed were partial or no waves (**Figure 3.3 c**, n = 35). We also elaborated on previous data and showed that when mature oocytes were treated with AB and cytochalasin D, 72% displayed a disrupted calcium wave (**Figure 3.3 c**, n = 35; (York-Andersen et al., 2015)). Notably, full calcium waves, defined as a wave of calcium which traverses the entire oocyte, were observed in some oocytes. This is likely due to incomplete inhibition by the drug, and in these cases, swelling of the oocyte occurred as normal. Higher concentrations of the drugs did not change the observed calcium wave phenotypes.

In addition to disrupting F-actin, we tested the effect of reducing the pool of globular actin (G-actin) monomers by treating mature oocytes with AB and latrunculin A, which binds the G-actin monomers and prevents actin assembly (Yarmola et al., 2000). Upon the addition of this solution, the majority of oocytes showed a full

calcium wave (75%; n = 20), not significantly different from wildtype. Together, these pharmacological disruptions suggest that the calcium wave is dependent on a dynamic F-actin network and can occur without de novo actin assembly from G-actin monomers (**Figure 3.3 c**).

We next hypothesized that excess polymerized F-actin in the mature oocyte would disrupt the calcium wave. To test this, we overexpressed the actin nucleation factor Spire B (Dahlgaard et al., 2007; Quinlan et al., 2005; Wellington et al., 1999) and observed the calcium wave. We found that additional Spire B leads to a reduction (42% vs. 85%) in the number of mature oocytes that showed a wild- type calcium wave (**Figure 3.3 d**; n = 12 and n = 30). In those eggs that did show a calcium wave, we observed a delay of 5–10 min in the initiation of the wave. These results corroborate the phalloidin data that showed excess or a stabilized actin cytoskeleton to be inhibitory to the calcium wave at egg activation.

Finally, we tested if reducing F-actin assembly before egg activation would allow for faster entry of calcium into the egg at activation. We used RNAi against *scar*, which encodes an activator of the Arp2/3 complex, to disrupt the nucleation of the actin network (Zallen et al., 2002). We showed that while the number of mature oocytes that showed a normal calcium wave is equal to wildtype, knockdown of scar resulted in calcium entering the egg more quickly than in controls (**Figure 3.3 e**). Moreover, we observed a decrease in the concentration of actin at the cortex in scar knockdown egg chambers (**Figure 3.3 f–f′**). This supports a model where a spreading or reduction of actin at the cortex allows for calcium entry. In addition, we observed that the cortical actin marker GFP-moesin was less concentrated at the posterior pole

(**Figure 3.3 g**), and in some cases at the anterior pole (**Figure 3.3 g′**). This could explain why there is a higher occurrence of calcium waves from the posterior pole of mature oocytes when activated *ex vivo*.

Taken together, these data support a model in which an intact and dynamic F-actin cytoskeleton, but not de novo assembly of F-actin, is essential to regulate the initiation of the calcium wave.

A wavefront of actin follows the calcium wave during egg activation

We next examined actin dynamics following the calcium wave in *ex vivo* egg activation. We used a germline driver to express markers for both calcium and F-actin simultaneously during *Drosophila* egg activation. Using AB to activate the mature oocyte, we observed and analyzed a calcium wave and a wavefront of actin (**Figure 3.5 a–a′**). The analysis shows that the actin wavefront (**Figure 3.5 b**) lags behind the calcium wave at initiation by approximately 2 min and completes propagation across the oocyte approximately 4 min after the calcium wave. A similar phenomenon is observed with the recovery of both waves, actin trailing calcium (see **Figure 3.5 a** legend for details). We confirmed this result using modified Robb's Buffer [RB, (Hu and Wolfner, 2019)] to initiate egg activation and show that the speed of the F-tractin wavefront is similar to that of the calcium wave (0.56 μm/s; **Figure 3.6**). The average completion times of the calcium wave and the F-actin wavefront highlights the similarities between the dynamics of these waves.

To verify the discovery of an actin wavefront at *Drosophila* egg activation, we also tested the widely used *in vivo* actin marker Lifeact, a 17-amino acid peptide from yeast Abp140 (Riedl et al., 2008). At egg activation, Lifeact showed an increase in

fluorescence from the posterior pole that propagated across the oocyte in a wavelike manner (**Figure 3.5 c**). The speed of the wave was consistent with that seen with F-tractin. Overall, using multiple activation methods and F-actin markers, we demonstrate that the calcium wave during egg activation is followed by a wavefront of F-actin reorganization.

The calcium wave is necessary to sustain the actin wavefront

Our previous observation that the actin wavefront follows the calcium wave with similar speed and direction, suggests that the actin wavefront may be dependent on the calcium wave. To test this dependence, we used a genetic approach to assess the requirement of a calcium increase for the F-actin wavefront at egg activation. Our previous work has shown that the calcium wave does not occur in a *sarah* mutant (York-Andersen et al., 2015). *sarah* encodes a key protein in the calcium signaling pathway that regulates the calcium-dependent phosphatase calcineurin (Horner et al., 2006; Takeo et al., 2006, 2010). F-actin visualized in a *sarah* mutant background revealed normal swelling of the mature oocyte but no change in the in F-actin distribution or levels (**Figure 3.7 a**; n = 12).

Next, we inhibited the calcium wave upon egg activation with the addition of 2-aminoethoxydiphenyl borate (2-APB). Calcium waves initiate at the oocyte pole(s) due to the influx of external calcium through the TRPM channel (Hu and Wolfner, 2019). Propagation of the waves through the oocyte requires the inositol trisphosphate receptor [IP_3R, (Kaneuchi et al., 2015)]. 2-APB is a known ion channel inhibitor that has been experimentally used to block both TRP channels and IP_3R (Clapham et al., 2001; Maruyama et al., 1997). We observed that the addition of 2-APB results in no

calcium wave or F-actin wavefront, despite the oocytes swelling normally (**Figure 3.7 b–b′**; n = 14), again supporting the conclusion that the calcium wave is necessary for the F-actin wavefront.

To test the sufficiency of the calcium rise in the induction of an actin wavefront, we initiated a regional calcium rise via local pressure with a microneedle. To ensure that the induced calcium rise was not caused by calcium leaking in due to a damaged plasma membrane (PM), we included propidium iodide (PI) dye in the isolation buffer (IB) to indicate PM damage. We observed that regional pressure by a microneedle can induce a local calcium rise without damaging the oocyte PM (**Figure 3.7 c**). However, a calcium rise induced by such local pressure did not spread beyond the induction site or change the actin network (**Figure 3.7 c′**; n = 12). This argues that regional pressure can cause a local calcium rise, but that an additional factor(s) is required to reorganize the actin cytoskeletal network.

We therefore assessed whether sustaining a global calcium signal is sufficient to maintain the increase we observed in F-actin. To test this, we treated mature oocytes with sodium orthovanadate (Na_3VO_4), an ATPase inhibitor, dissolved into AB (**Figure 3.8 a–a′**). Upon addition of AB with Na_3VO_4, the calcium rise no longer recovered to basal levels and we found that the F-actin signal also remained elevated. These data suggest that a prolonged global calcium rise may be sufficient to maintain a higher actin signal post-activation and that there is an ATP-dependent mechanism in recovery and extrusion of calcium after activation. However, we make this suggestion with caution, as Na_3VO_4 has numerous effects on cells.

To further investigate the dynamics of actin following a calcium rise, we

observed the F-actin phenotype when mature oocytes were treated with distilled water. This treatment results in a rapid swelling of the oocyte and a calcium increase from multiple points at the cortex (**Figure 3.8 b**). Following this pattern of calcium rises, we observed a similar pattern of actin increase approximately 4 min later (**Figure 3.8 b′**). Interestingly, this assay suggests that all regions of the cortex have the potential to initiate a calcium wave that spreads through the oocyte and that stressing the system with excessive fluid uptake results in the loss of spatiotemporal control of the calcium entry and resulting actin reorganization.

Finally, we observe that in some wildtype *ex vivo* egg activation events, the calcium wave initiated from the anterior pole or from both poles (Kaneuchi et al., 2015). Consistent with our experimental manipulations of the calcium rise and subsequent actin changes, we found that the actin wavefront started from the anterior pole in all of the oocytes that showed the anterior calcium wave, and from both poles when calcium wave initiated from both poles (**Figure 3.8 c-d'**). Taken together, our data suggest that initiation of the calcium wave is necessary to induce a wavefront of F-actin reorganization, and a global but not regional calcium rise may be sufficient in maintaining the actin wave and coordinating its directionality.

5.4 Discussion

Actin plays an essential role in fertilization and egg activation in many organisms. However, its functions in these aspects of *Drosophila* reproduction have not been fully explored. In this study, we showed that F-actin disperses and become more dynamic during *Drosophila* egg activation and that this dynamic actin

cytoskeletal network is required for a normal calcium wave to occur during *ex vivo* egg activation (**Figure 3.8 e**). Moreover, the calcium wave mediates a reorganization of F-actin in a wavelike manner. This F-actin wavefront follows, requires, and has similar characteristics to the calcium wave. Together, these findings suggest a highly co-regulated calcium and actin signaling network in *Drosophila* oocytes during egg activation.

The importance of the actin cytoskeleton in egg activation

Our work demonstrates that in *Drosophila*, actin dynamics are important for the calcium rise which in turn leads to a reorganization of F-actin. Rearrangement of F-actin appears to be a common feature of oocytes undergoing egg activation. The reorganization of F-actin following exposure to osmotic pressure in zebrafish oocytes mediates the release of the cortical granules (Becker and Hart, 1999; Hart and Collins, 1991). More recent work in zebrafish has shown that the actin-binding factor, Aura, mediates this reorganization of actin and that in an Aura mutant background F-actin does not rearrange, and cortical granule exocytosis is inhibited (Eno et al., 2016). Our data are reminiscent of events in starfish, where a pharmacologically induced calcium rise results in depolymerization of surface actin and polymerization of F-actin bundles within the cytoplasm (Vasilev et al., 2012). Starfish oocytes also exhibit actin rearrangements at egg activation that are required for the calcium release at the cortex (Kyozuka et al., 2008). This calcium wave initiates a PIP_2 increase at the starfish cortex in a biphasic manner, whereas pharmacological inhibition of PIP_2 results in a delayed calcium wave and disrupted actin organization (Chun et al., 2010).

Functions of the actin wavefront

It is hypothesized that F-actin waves are essential for actin self reassembly after its initial dispersion at the cortex and are thought to mediate the polymerization of actin (Bretschneider et al., 2009; Case and Waterman, 2011). For example, pharmacological depolymerization of actin results in an increased number of actin waves in Dictyostelium (Bretschneider et al., 2009). A similar observation was made in fibroblasts, where actin waves take form of "circular dorsal ruffles," which are non-adhesive actin structures found on the dorsal side of some migrating cells (Bernitt et al., 2015, 2017; Chhabra and Higgs, 2007). Moreover, the F-actin wave is proposed to be associated with actin binding factors, including Arp2/3, myosin B, CARMIL, and coronin.

Live visualization of these factors in Dictyostelium cells have shown their enrichment at the leading edge of the F-actin wavefront (Bretschneider et al., 2009; Khamviwath et al., 2013). Together, this provides other examples of how the reorganization of F-actin can trigger F-actin waves. By analogy, the F-actin wavefront we observed during *Drosophila* egg activation might serve a similar purpose of reorganizing the actin cytoskeleton to facilitate further developmental events in embryogenesis.

Calcium and actin coregulatory networks

Our work suggests a pathway of actin-calcium interdependence as initial calcium entry is enabled at the poles, where we see a breakdown of the actin cytoskeleton at the cortex, and this calcium increase is required to generate a global reorganization in the actin population. Calcium is thought to regulate the actin cytoskeleton predominantly via actin-binding factors, including myosin, profilin, and

villin/gelsolin (reviewed in Hepler, 2016). Early experiments showed that calcium regulates muscle contractions via myosin V protein, rather than directly through the actin filaments (Szent-Györgyi, 1975). In this case, calcium binds troponin that in turn binds tropomyosin to mediate the actin-myosin contraction cycle (Lehman et al., 1994). Similarly, plants utilize the actin-myosin network for cytoplasmic streaming, and actin is again regulated by calcium signaling via myosin XI (Tominaga et al., 2012). Calcium can also control actin dynamics via profilin, an actin binding factor, which is required for F-actin polymerization (Vidali and Hepler, 2001). Experiments with profilin show that calcium inhibits F-actin polymerization by sequestering actin monomers and profilin subunits, which are no longer able to form the actin filaments (Kovar, 2000). Calcium causes depolymerization or severing of the actin cytoskeleton via villin actin binding factor and was shown to aid the organization of actin in epithelial intestinal cells (Walsh et al., 1984).

One especially interesting factor is α-actinin, an actin cross-linking protein that is a member of the spectrin family and is found primarily on F-actin filaments in non-muscle cells. α-actinin has been suggested to cross-link actin under low calcium conditions. However, when intracellular calcium rises (as in the case of a calcium wave), α-actinin releases actin filaments, thus no longer cross-linking the F-actin filaments (Jayadev et al., 2014; Prebil et al., 2016; Sjöblom et al., 2008). However, further work will be required to establish the exact connections between calcium and actin networks (Veksler and Gov, 2009).

An actin and calcium feedback loop during egg activation

One hypothesis for how actin dynamics are linked to calcium wave initiation is

through interaction with mechanosensitive channels such as TRP channels and DEG/ENaC. We recently showed that the *Drosophila* Trpm channel is required for the initial calcium influx (Hu and Wolfner, 2019), but how Trpm responds to mechanical stimuli remains to be elucidated. There are several models for how these channels are activated. One suggested cue is direct mechanical stress applied on the PM, due to physical pressure during ovulation and/or osmotic swelling of the oocyte in the oviducts. While it is possible that the Trpm channel might respond to the stress directly, it is also possible that the mechanical signal is also transduced through the actin cytoskeleton causing the channel to open, enabling an influx of calcium ions (Christensen and Corey, 2007).

We showed here that before egg activation, the cortical actin marker Moesin is less concentrated at the posterior end of the oocyte where calcium waves generally initiate and decrease in concentration at the cortex. It is possible that lack of actin rigidity is linked to calcium channel opening: The initial sparse site of actin allows calcium channels to open and leads to calcium influx, which in turn regulates the dynamic changes in actin to form a wavefront following calcium wave. The interlinked nature of these two pathways suggests a positive feedback loop that facilitates the progression and completion of the waves. This could be achieved as follows: (a) actin disperses and calcium enters the oocyte; (b) this calcium rise causes further actin dispersion through regulation of actin binding proteins; (c) more calcium then enters the activating egg which results in the complete calcium wave and actin reorganization in a wavelike manner. Overall, we propose that in *Drosophila* egg activation, actin is able to modulate the intracellular calcium rise, and calcium waves

in turn regulate the reorganization of actin.

Figure 5.1 Actin is reorganized at egg activation.

Time series of an *ex vivo* activated mature oocyte (a–c; n = 6) and *in vivo* activated egg (d; n = 4) expressing F-Tractin.tdTomato. Maximum Z-projection (a–d), three-dimensional (3D) projection at a 45° angle (a′–d′) and a single Z-plane at 20 μm depth (a″–d″) are shown for each time point. Images were acquired using an Olympus FV3000 confocal microscope. (a–a″) Before the addition of activation buffer, actin is in a smooth cortical distribution around ridges in the cortex. (b–c″) Following egg activation (3–12 min) and (27–35 min), actin is reorganized in larger, more widely distributed foci. 3D projection shows that the cortex has expanded, and that actin is no longer associated with the ridge. Single plane images show that a cortical enrichment pre-activation is lost, and that actin is not as enriched at the cortex after activation. (d–d″) *In vivo* activated eggs collected from the oviduct have a similar actin distribution as mature oocytes activated *ex vivo* (compare c–c″ to d–d″). Scale bar = 10 μm (a–d′)

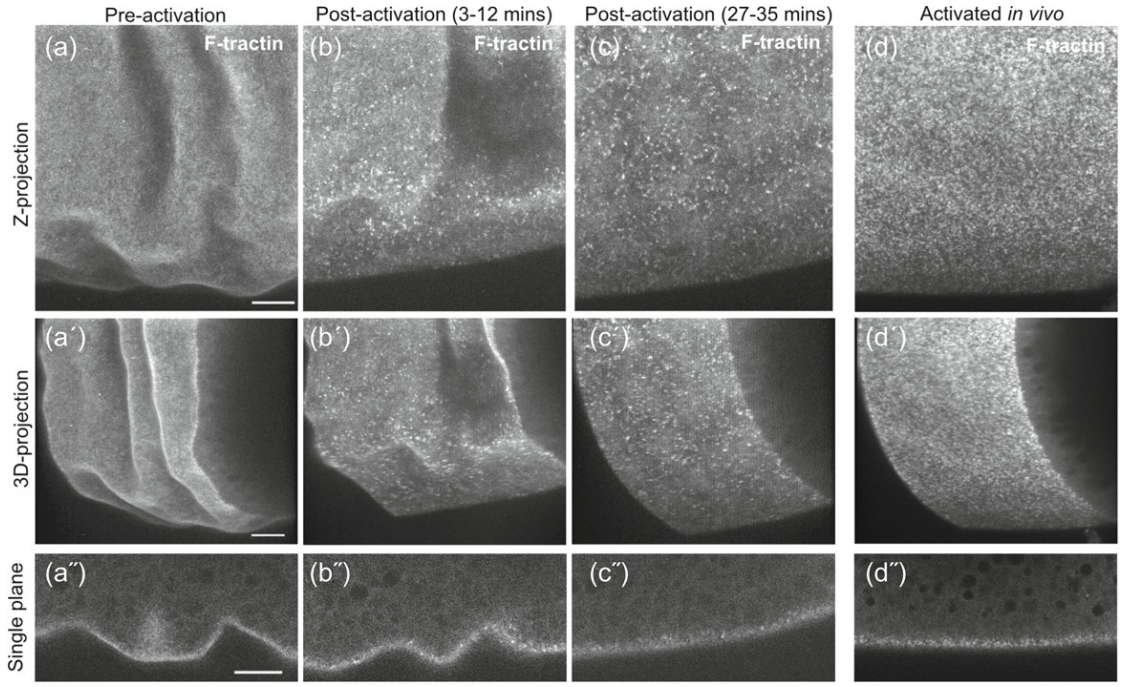
Pre-activation
Post-activation (3-12 mins)
Post-activation (27-35 mins)
Activated *in vivo*
Z-projection
3D-projection
Single plane
(a)
F-tractin
(b)
F-tractin
(c)
F-tractin
(d)
F-tractin
(a´)
(b´)
(c´)
(d´)
(a˝)
(b˝)
(c˝)
(d˝)

Figure 5.2 Actin is reorganized at egg activation and in the early embryo.

Time series of a mature oocyte activated *ex vivo* with activation buffer and an early embryo (0-30min) expressing F-Tractin.tdTomato. 3D-projection at a 60° angle (A-C) and a single Z-plane at 12μm depth (A′-C′) are shown. Images were acquired using an Olympus FV3000 confocal microscope. (A-B′) Consistent with Figure 3.1, actin is distributed around ridges in small foci prior to egg activation and is reorganized into larger more widely distributed foci after egg activation is complete (n=6). (C-C′) The early embryo (n=5) displays a similar actin distribution and the *ex vivo* and *in vivo* activated eggs (Figure 3.1 d and Figure 3.2 B). Scale bar = 10 μm (A-C′).

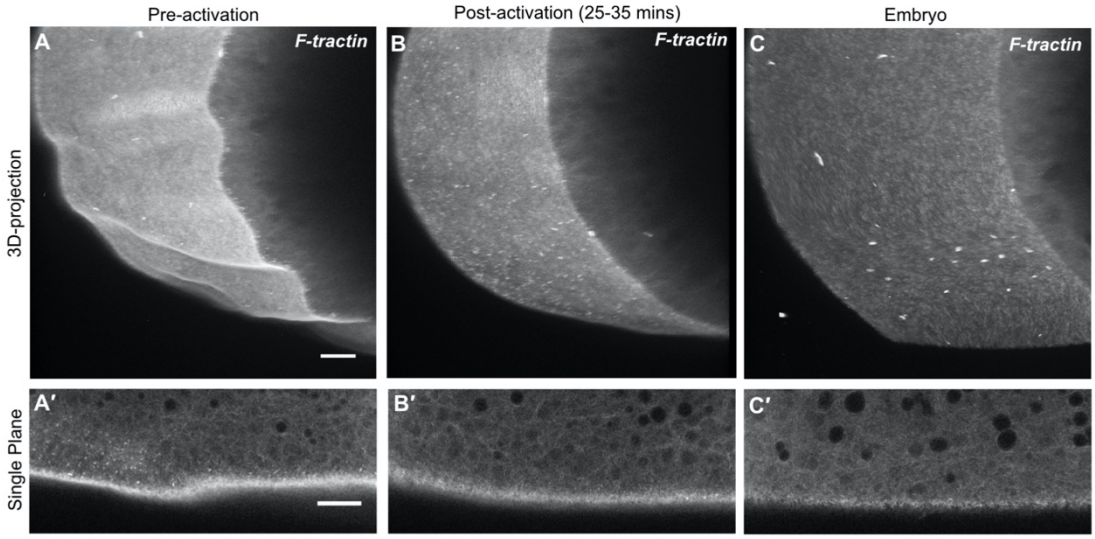
Pre-activation
Post-activation (25-35 mins)
Embryo
A
F-tractin
B
F-tractin
C
F-tractin
3D-projection
A′
B′
C′
Single Plane

Figure 5.3 A dynamic actin cytoskeleton is required for a calcium wave at egg activation.

(a–b′, g, g′) Egg chamber expressing GFP-moesin. Images were acquired using an Olympus FV3000 confocal microscope. (a, b) Fluorescence recovery after photobleaching (FRAP) of GFP-moesin before and after *ex vivo* egg activation (n = 5). GFP-moesin labeling actin at the lateral cortex is reduced to 25% of original fluorescent intensity following a bleaching step. In both Stage 14 mature egg chambers before activation (a) and after activation (b) recovery can be detected. In the unactivated oocyte, full recovery is complete at 12 min post-bleaching. However, in the activated oocyte recovery is substantially faster post-activation (14 vs. 45 s recovery halftime, n = 5). Note that movement caused by the addition of activation buffer (AB) meant that recovery could only be recorded for 1 min and 15 s postbleach. The dashed white box denotes the bleached region. (c) Graph showing calcium wave phenotypes when mature oocytes are treated with AB and the actin perturbing drugs latrunculin A, cytochalasin D, or phalloidin. A "full wave" indicates the calcium wave traversed the whole oocyte, a "partial wave" indicates that the calcium wave initiated but did not traverse the whole oocyte, and a "no wave" phenotype indicates that a calcium wave never initiated. When only AB is added, 82% of oocytes displayed full waves. The addition of latrunculin A shows a nonsignificant decrease in full waves to 72% (n = 20; p = 0.5). Mature oocytes treated with cytochalasin D or phalloidin show a significant decrease in full waves observed to 28% and 32%, respectively (n = 35 for each, Fisher's exact statistical analysis, *** p = .0001). (d) Graph showing calcium wave phenotypes when mature oocytes are treated with AB in GCaMP3 controls,

overexpression of Spire B and knockdown of scar. When Spire B is overexpressed there is a significant decrease, to 40%, in the number of activated mature oocytes that show a full calcium wave, and an increase in the number of "no wave" phenotypes to 58% (n = 12, Fisher's exact statistical analysis, $p < 0.05$). When scar is knocked down using RNAi, there were no significant changes in the calcium wave phenotype. (e) Boxplot showing the speeds of calcium entry into the mature oocyte in control (GCaMP3) and scar RNAi mature oocytes (n = 15 and n = 18). Speed of calcium entry was determined as the time taken from the addition of AB to the time of first GCaMP fluorescence detection in the oocyte. Initial calcium entry was observed by eye and confirmed through quantification of the fluorescence signal, using a threshold of a 10% increase from the oocyte background. Images were taken every 3 s. There was a significant decrease in the time taken for calcium to enter the oocyte in the scar RNAi background ($p < 0.05$). (f, f′) Stage 14 egg chambers fixed and labeled for actin with phalloidin (n = 10). More actin is detected at the cortex in a wild-type egg chamber (f) compared with a scar RNAi expressing egg chamber (f′). White arrowheads mark the lateral cortex of the egg chamber. (g, g′) In the Stage 14 egg chamber, before egg activation, GFP-moesin is less enriched at the posterior pole (g) of the oocyte (white arrowheads) as compared with elsewhere of the oocyte cortex (paired t test $p < 0.05$, n = 20). Observation of GFP-moesin at the anterior pole was challenging due to the presence of the dorsal appendages. However, in some (~40%; n = 25) oocytes Moesin is depleted compared with the lateral cortex (g′) and in these oocytes the depletion is significant (paired t test $p < 0.05$, n = 10). Single plane image (a, b, f, g). Scale bar = 10 μm (a, b), 20 μm (f, g)

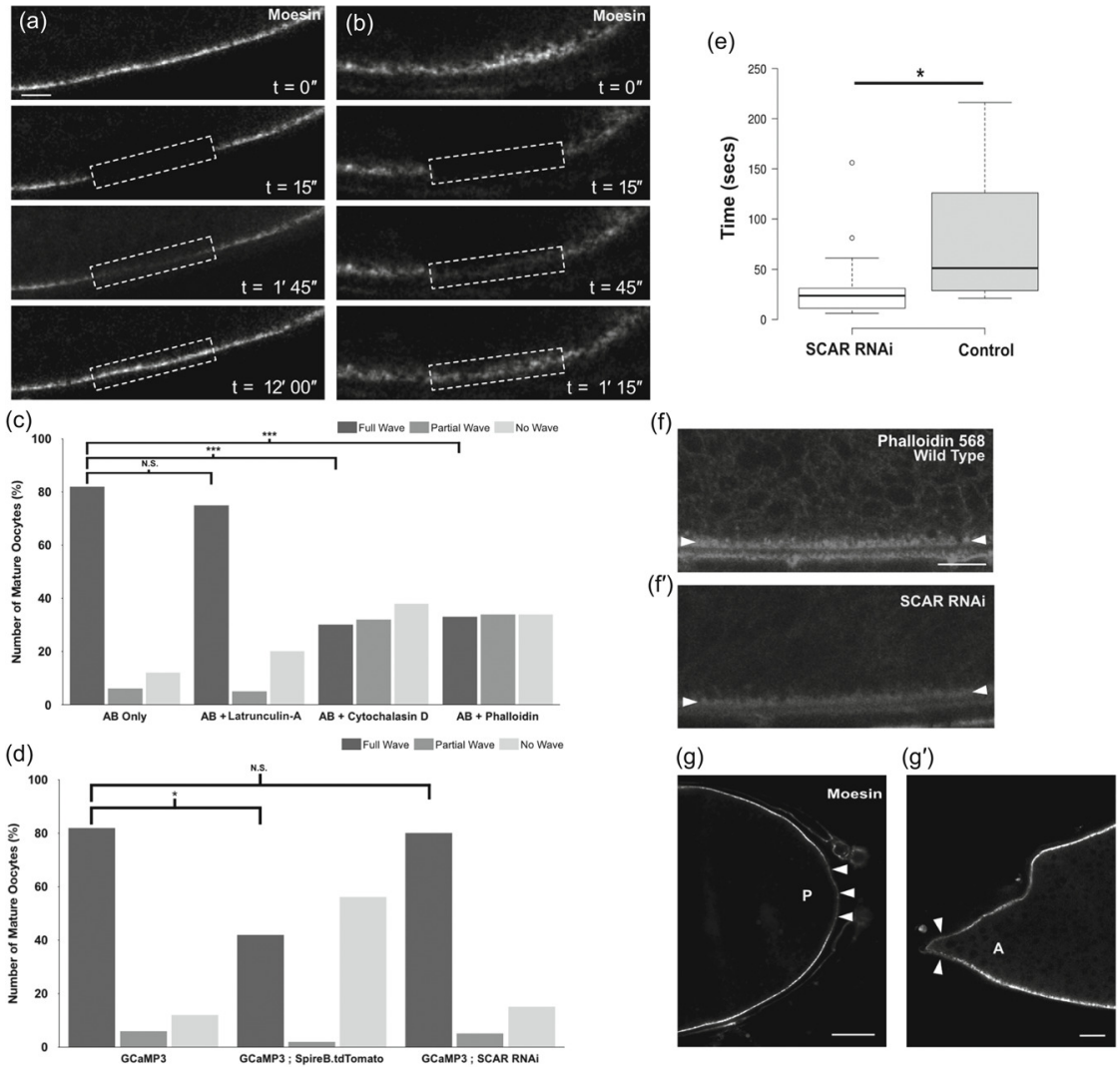
(a)
Moesin
t = 0″
t = 15″
t = 1′ 45″
t = 12′ 00″
(b)
Moesin
t = 0″
t = 15″
t = 45″
t = 1′ 15″
(e)
Time (secs)
250
200
150
100
50
0
*
SCAR RNAi
Control
(c)
Full Wave
Partial Wave
No Wave
Number of Mature Oocytes (%)
100
80
60
40
20
0
***
***
N.S.
AB Only
AB + Latrunculin-A
AB + Cytochalasin D
AB + Phalloidin
(d)
Full Wave
Partial Wave
No Wave
Number of Mature Oocytes (%)
100
80
60
40
20
0
N.S.
*
GCaMP3
GCaMP3 ; SpireB.tdTomato
GCaMP3 ; SCAR RNAi
(f)
Phalloidin 568
Wild Type
(f′)
SCAR RNAi
(g)
Moesin
P
(g′)
A

Figure 5.4 Act5C-GFP recovers more quickly after photobleaching post-egg activation.

(A-B) Egg chamber expressing Act5C-GFP Fluorescence recovery after photobleaching (FRAP) before and after *ex vivo* egg activation (n=5). Act5C-GFP at the lateral cortex is reduced to 10% of original fluorescent intensity following a bleach step. In both stage 14 mature egg chambers before activation (A) and after activation (B) recovery can be detected. In the unactivated oocyte, full recovery is complete at 5 minutes post-bleaching. However, in the activated oocyte recovery is substantially faster post-activation (20 seconds versus 41 seconds recovery halftime, n=5). Dashed white box denotes bleached region. Images were acquired using an Olympus FV3000 confocal microscope. Single plane image (A-B). Scale bar, 10μm.

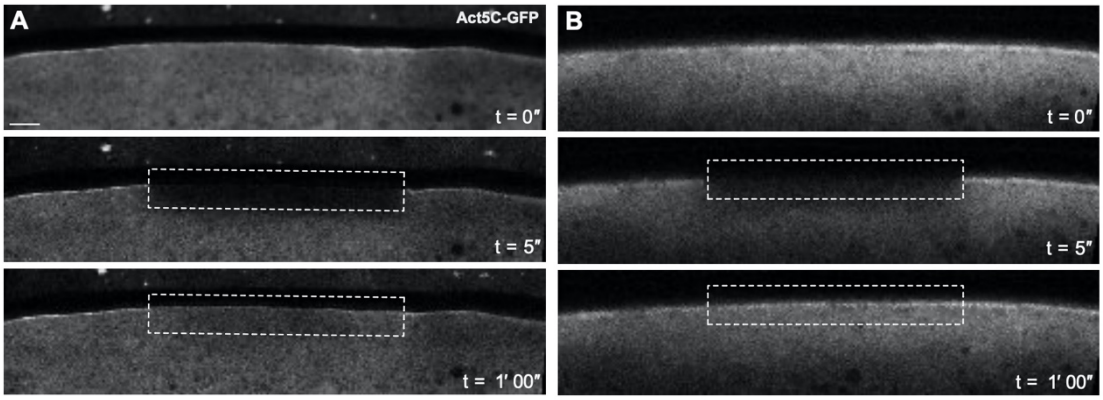
A
Act5C-GFP
t = 0″
t = 5″
t = 1′ 00″
B
t = 0″
t = 5″
t = 1′ 00″

Figure 5.5 Actin wavefront dynamics follow calcium changes at egg activation.

Time series of a mature egg chamber co-expressing GCaMP3 and F-Tractin.tdTomato (a), or only expressing F-Tractin.tdTomato (b) or Lifeact::mCherry (c). (a) At activation with activation buffer (AB) (n = 9), a calcium wave (a) initiates from the posterior pole (t = 0′) and propagates across the entire egg. A corresponding wavefront of F-tractin (a′) initiates from the posterior pole and traverses the egg. Analysis of the fluorescence intensity shows that the calcium wave initiates on average 106 s after the addition of AB (SEM = 11.5 s), traverses the whole oocyte by 267 s (SEM = 42 s) and has recovered back to its initial level by 737 s (SEM = 148.37 s). A wave of filamentous actin (F-actin) follows behind this calcium wave, initiating on average 220 s after the addition of AB (SEM = 60 s). The actin wave traverses the whole oocyte by 503 s (SEM = 72 s) and has recovered to its initial state by 829 s (SEM = 222 s). On average, the F-actin wave lags behind the calcium wave by 103 s. Images were acquired using an inverted Leica SP5 confocal microscope sequentially, with a scan time of approximately 30 s per Z-stack. (b) F-actin, labeled by F-tractin (n = 15), shows a posterior to anterior wavefront following the addition of AB (t = 0′). The wave initiates (t = 4′), propagates across the oocyte to the anterior pole (t = 10′) and recovers (t = 16′). Images were acquired using an inverted Leica SP5 confocal microscope. (c) F-actin, labeled by Lifeact (n = 10), shows a similar actin wavefront as F-tractin (b) in its initiation (t = 3′), propagation (t = 9′30″) and recovery (t = 15′). The bright fluorescence outside of the egg chamber is ovarian tissue associated with the dissection. Images were acquired using an inverted Leica SP5 confocal

microscope. Image a projection of 40 μm (a, b, c). Scale bar = 60 μm (a–c). AB, activation buffer; SEM, standard error of the mean.

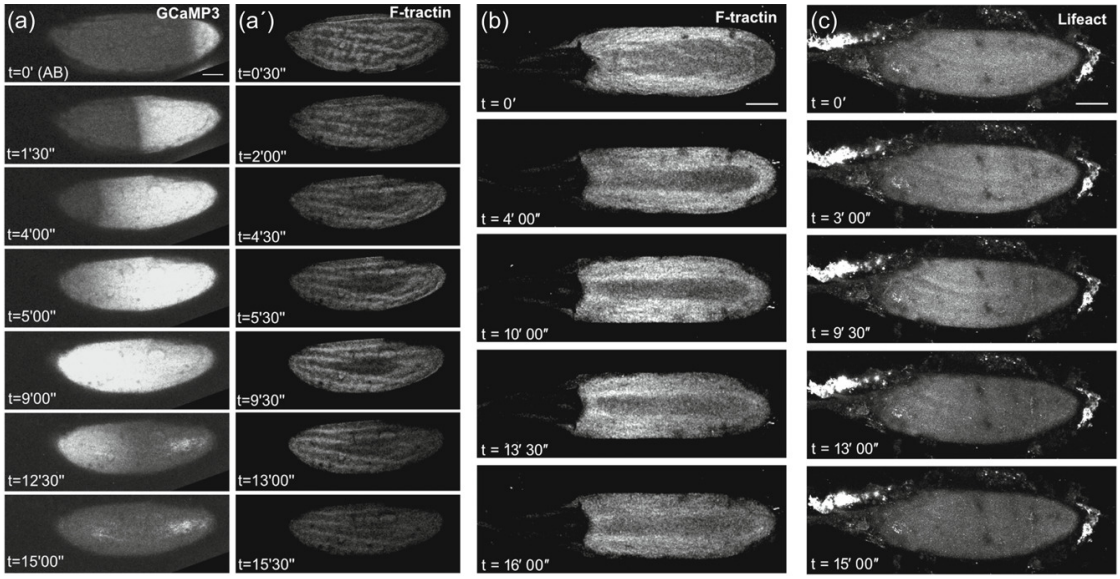
(a)
GCaMP3
t=0' (AB)
t=1'30"
t=4'00"
t=5'00"
t=9'00"
t=12'30"
t=15'00"
(a´)
F-tractin
t=0'30"
t=2'00"
t=4'30"
t=5'30"
t=9'30"
t=13'00"
t=15'30"
(b)
F-tractin
t = 0′
t = 4′ 00″
t = 10′ 00″
t = 13′ 30″
t = 16′ 00″
(c)
Lifeact
t = 0′
t = 3′ 00″
t = 9′ 30″
t = 13′ 00″
t = 15′ 00″

Figure 5.6 A wavefront of actin follows the calcium wave during egg activation.

Time series of a mature egg chamber co-expressing GCaMP3 and F-Tractin.tdTomato. (A-A′) At activation with Robb's buffer (RB) (n=4), a calcium wave (A) initiates from anterior and posterior poles and propagates across the entire egg. A corresponding wavefront of F-tractin (A′) initiates from both poles and traverses the egg. Images were acquired using a Zeiss LSM880 confocal microscope.

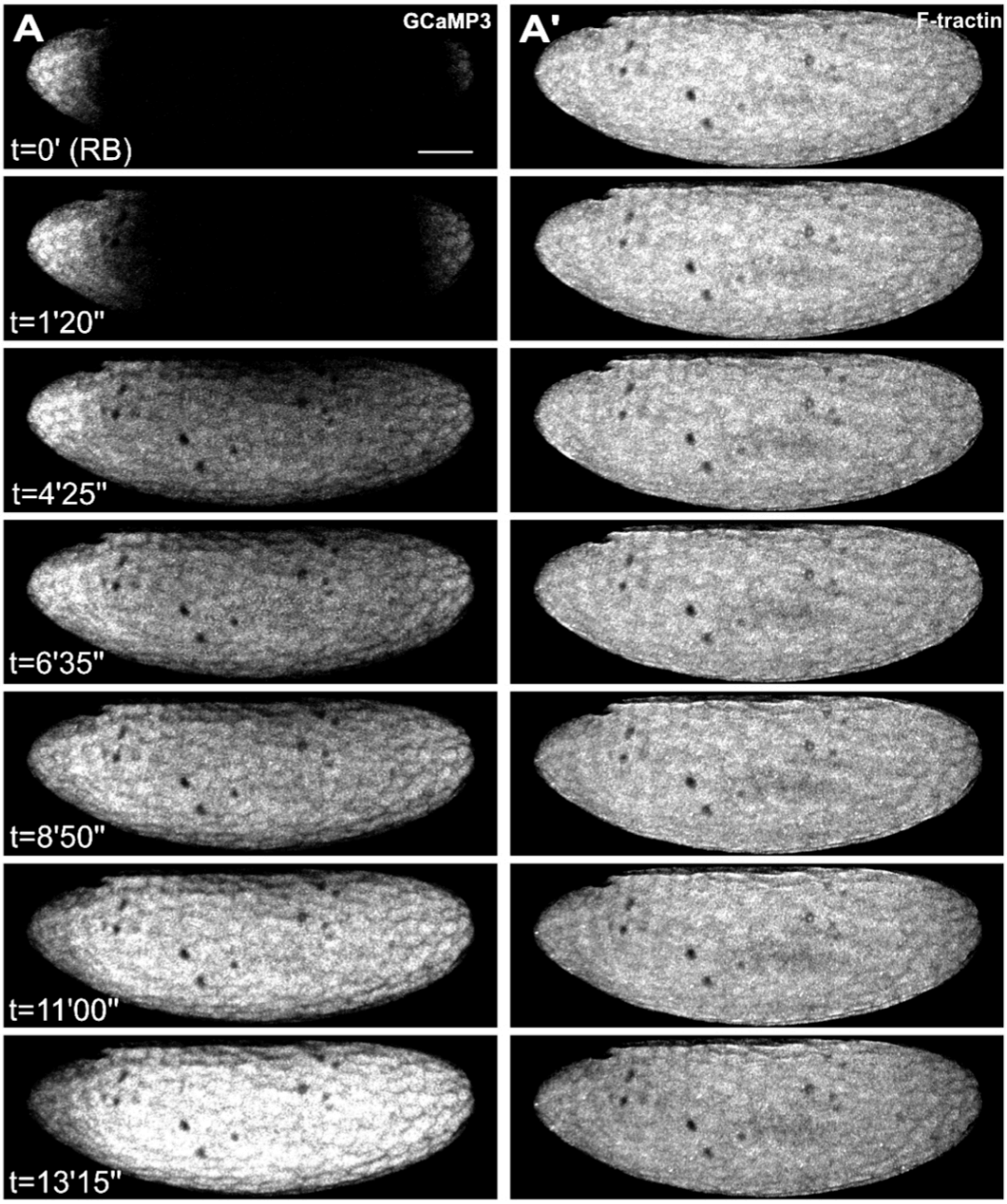
A
GCaMP3
A'
F-tractin
t=0' (RB)
t=1'20"
t=4'25"
t=6'35"
t=8'50"
t=11'00"
t=13'15"

Figure 5.7 Actin wavefront requires the calcium wave at egg activation.

Time series of mature egg chambers expressing F-Tractin.tdTomato (a) or mature egg chambers co-expressing (b, c) GCaMP3 and F-Tractin.tdTomato (b′, c′). (a) Time series of mature egg chambers expressing F-Tractin in a *sarah* mutant background (sraA108/sraA426) (n = 7). The addition of activation buffer to mature egg chambers causes an initial dispersion of cortical actin (t = 4′) but does not initiate a wavefront of filamentous actin (F-actin) (t = 15′). Images were acquired using an inverted Leica SP5 confocal microscope. (b–b′) Addition of 2-aminoethoxydiphenyl borate (a TRP and IP3 pathway inhibitor) to modified Robb's Buffer prevents initiation of the calcium wave and an F-actin wavefront is not observed (t = 13′55″; n = 14). Images were acquired using a Zeiss LSM880 confocal microscope. (c–c′) Application of pressure to the lateral cortex of the mature egg chamber induces a local increase calcium (white arrowhead, t = 0′) (n = 12). This local increase recovers over time (t = 9′30″). Application of pressure does not result in a local F-actin increase (c′) (white arrowhead, t = 0′), nor does it trigger an F-actin wavefront. Images were acquired using a Zeiss LSM880 confocal microscope. Image a projection of 40 µm (a) or 90 µm (b,c). Scale bar = 60 µm (a–c).

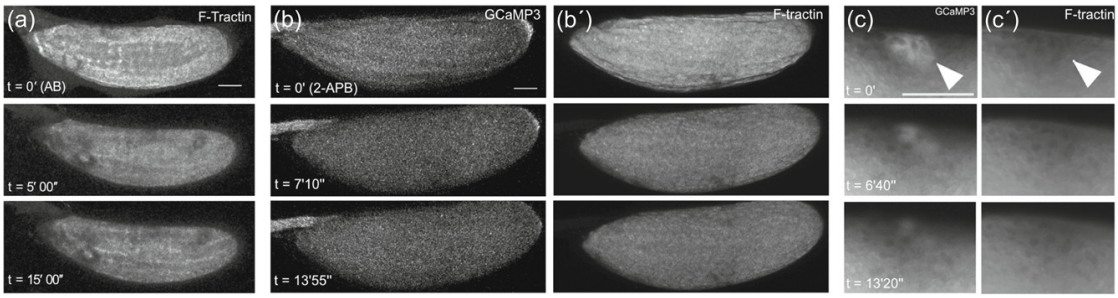
(a)
F-Tractin
t = 0' (AB)
t = 5' 00"
t = 15' 00"
(b)
GCaMP3
t = 0' (2-APB)
t = 7'10"
t = 13'55"
(b´)
F-tractin
(c)
GCaMP3
t = 0'
t = 6'40"
t = 13'20"
(c´)
F-tractin

Figure 5.8 The pattern of actin reorganization follows calcium changes.

Time series of mature egg chambers co-expressing GCaMP3 and F-Tractin.tdTomato (a, b, d) or co-expressing GCaMP3 and Lifeact::mCherry (c). (a–a′) The addition of activation buffer (AB) with sodium orthovanadate initiates a calcium wave that is sustained (t = 40′; n = 10). An increase in filamentous actin (F-actin) is similarly seen and is also maintained (t = 40′). Images were acquired using an inverted Leica SP5 confocal microscope. (b–b′) Following the addition of distilled water (DW; n = 20), the mature egg chamber undergoes a global increase in intracellular calcium (t = 0′) which slowly recovers to basal levels (t = 15′). F-actin displays an initial dispersion (t = 3′) followed by a global increase (t = 9′30″). Images were acquired using an inverted Leica SP5 confocal microscope. (c) Following the addition of AB (n = 5), the calcium wave initiates from the anterior pole (t = 0′) and is followed by the wavefront of F-actin from the same pole (t = 5′). Images were acquired using an inverted Leica SP5 confocal microscope. Following addition of modified Robb's Buffer (RB) (n = 4), the calcium wave initiates from both anterior and posterior poles (t = 0′) and traversing the oocyte (t = 4′10″). The F-actin wavefront initiates at the same sites as the calcium wave (t = 4′10″) and propagates with similar characteristics. Images were acquired using a Zeiss LSM880 confocal microscope. (e) Diagram showing the interaction between calcium and actin during *Drosophila* egg activation. Cortical actin is relatively rigid before egg activation. It is less dense near the oocyte poles, where calcium waves initiate *ex vivo*. The calcium wave that progresses through the oocyte precedes a wavefront of actin reorganization. The actin wave and the calcium wave

display similar speeds and are interdependent for propagation and completion. After completion of the calcium wave, cortical actin appears more dynamic in distribution. Actin is represented in pink and calcium in blue. The diagram was created with BioRender.com. Image a projection of 40 µm (a–c) or 90 µm (d). Scale bar = 60 µm (a–d).

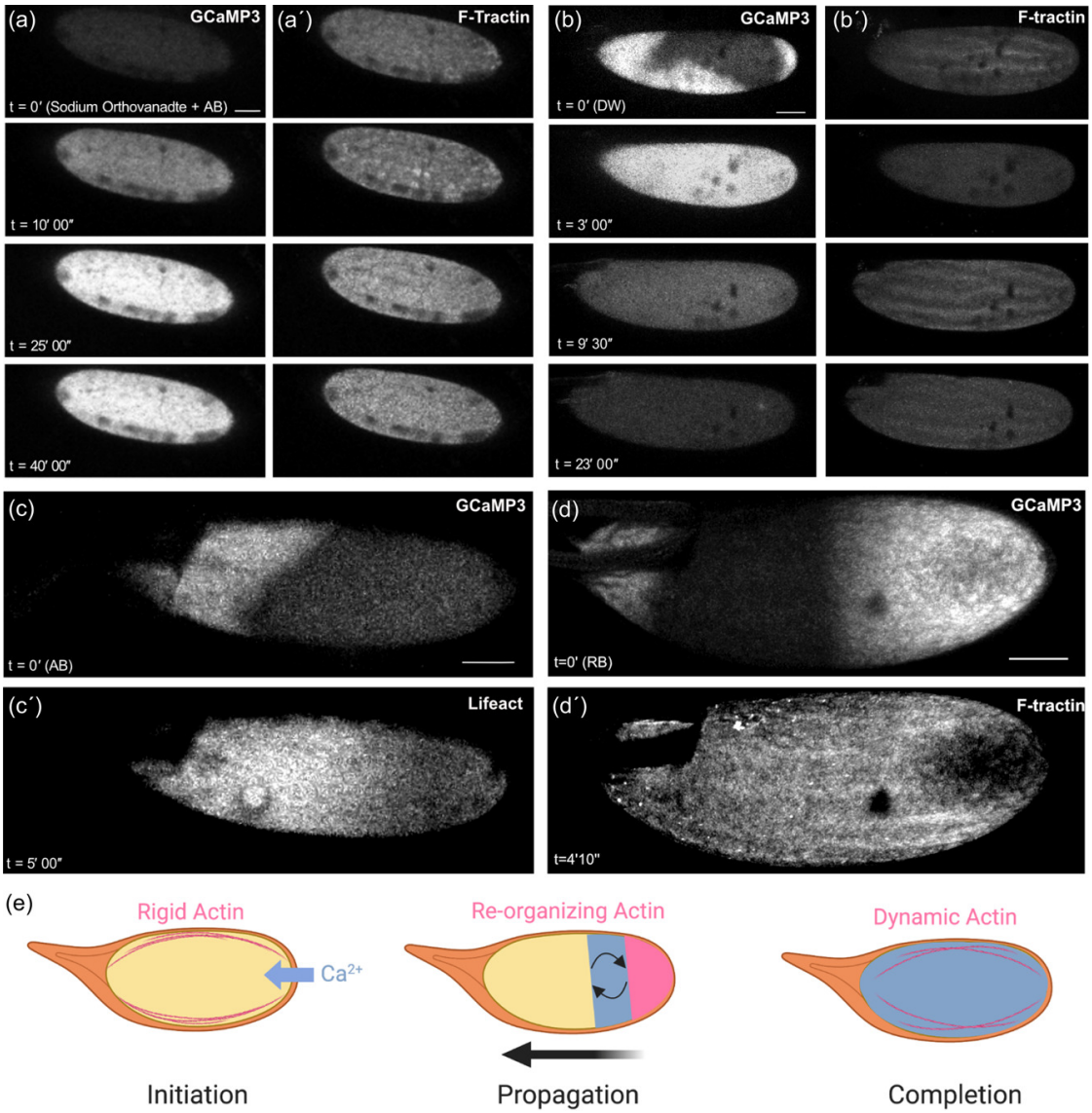
(a)
GCaMP3
t = 0′ (Sodium Orthovanadte + AB)
(a´)
F-Tractin
t = 10′ 00″
t = 25′ 00″
t = 40′ 00″
(b)
GCaMP3
t = 0′ (DW)
(b´)
F-tractin
t = 3′ 00″
t = 9′ 30″
t = 23′ 00″
(c)
GCaMP3
t = 0′ (AB)
(d)
GCaMP3
t=0′ (RB)
(c´)
Lifeact
t = 5′ 00″
(d´)
F-tractin
t=4′10″
(e)
Rigid Actin
Ca2+
Re-organizing Actin
Dynamic Actin
Initiation
Propagation
Completion

CHAPTER 6 ZINC DYNAMICS DURING DROSOPHILA OOCYTE MATURATION AND EGG ACTIVATION[4]

6.1 Introduction

Transition metals such as iron, copper, and zinc ions bound tightly within enzymatic sites play a variety of well-established structural and catalytic roles within cells (Calap-Quintana et al., 2017; Egli et al., 2003). Among them, zinc is an important inorganic regulator of processes including cell proliferation, carbohydrate metabolism and immunity. (reviewed in Frassinetti et al., 2006; Roohani et al., 2013). Zinc can persist in cells as hydrated ions, bound to small metabolites as weakly bound complex ions or bound tightly in the active sites of zinc-dependent enzymes. Recent studies indicate that fluctuations in the availability of Zn^{2+} ions occur either through ionic fluxes (Bernhardt et al., 2012) or through covalent binding to metalloregulatory proteins (Gilston et al., 2014). Thus, this element serves alongside calcium and phosphorous as an inorganic signal mediator that can activate biological switching processes. One example of zinc as an inorganic signal occurs during mammalian oocyte maturation and embryogenesis. Specifically, zinc accumulates in maturing mouse oocytes from the arrest at prophase of meiosis I to the arrest at metaphase of meiosis II (MII) (Kim et al., 2010), and this increase is dependent on maternally derived zinc transporters ZIP6 and ZIP10 (Kong et al., 2014). When mature mouse oocytes are fertilized, thus "activating" them to complete meiosis and begin

[4] This work is a collaboration with Drs. Francesca E. Duncan, Andrew B. Nowakowski, Teresa K. Woodruff and Thomas V. O'Halloran at Northwestern University and Olga A. Antipova at Argonne National Laboratory.

I contributed to designing and performing experiments, and data analysis.

embryogenesis, there is a rapid release of zinc from the oocyte (Kim et al., 2011). Such "zinc sparks" have been observed in eggs upon activation in the mouse (Kim et al., 2011; Que et al., 2014; Zhang et al., 2016), cow (Que et al., 2019), and human (Duncan et al., 2016). This zinc release is dependent on calcium oscillations during egg activation (Kim et al., 2011; Suzuki et al., 2010) and is mediated by dynamic movement and exocytosis of zinc-loaded vesicles (Que et al., 2014; Tokuhiro and Dean, 2018). The programmed loss of cellular zinc through zinc sparks is associated with resumption of the cell cycle (Kim et al., 2011) and modification of the zona pellucida to block polyspermy (Que et al., 2017b; Tokuhiro and Dean, 2018). After fertilization, regulation of zinc is required for the first mitotic divisions during embryogenesis (Kong et al., 2015). In another model organism, *C. elegans*, zinc is also required for oogenesis, meiotic progression (Hester et al., 2017) and embryo viability (Mendoza et al., 2017).

Drosophila's speed of development and excellent genetics makes it a tractable model to probe mechanisms and macromolecules of relevance to more complex systems, and its biology includes many parallels to events that occur in *Xenopus* and mammals, including in reproduction (Avila et al., 2010; Barnard et al., 2004; Bernhardt et al., 2018; Cui et al., 2008; Horner et al., 2006; Hu and Wolfner, 2019; Knapp and Sun, 2017; Mochida and Hunt, 2007; Pepling and Spradling, 2001; Takeo et al., 2010, 2006; Zhang et al., 2018a). As in other animals, *Drosophila* oocytes develop through a stepwise process of stages, 14 in this case, making it straightforward to examine zinc dynamics during oogenesis. Specifically, a cystoblast, the destined-to-differentiate daughter of a female germline stem cell, undergoes four

mitotic divisions with incomplete cytokinesis to result in a 16-cell cyst. One of the 16 cells becomes the oocyte; her 15 sisters, the nurse cells, synthesize macromolecules, organelles and other components that will be transferred into the oocyte as oogenesis progresses. Meiosis starts at early stage of oogenesis and arrests at prophase I at stage 5. This arrest lasts until stage 13 when meiosis progresses to metaphase I (MI) (von Stetina and Orr-Weaver, 2011). At later stages of oogenesis, nurse cells undergo apoptosis. The mature (stage 14) oocyte remains meiotically arrested at MI until ovulation (**Figure 6.1 A**) (reviewed in Avilés-Pagán and Orr-Weaver, 2018; Bastock and St Johnston, 2008; McLaughlin and Bratu, 2015). Then, mechanical forces due to passage into the oviduct and/or swelling of the oocyte as it takes up oviductal fluid "activate" the egg (Heifetz et al., 2001) (reviewed in Carlson, 2019; Horner and Wolfner, 2008a). As in mammals, egg activation in *Drosophila* involves a rise in internal calcium (Kaneuchi et al., 2015; York-Andersen et al., 2015), progression through meiosis, and changes in the egg's transcriptome, proteome, and envelopes (reviewed in Horner and Wolfner, 2008a; Kashir et al., 2014; Krauchunas et al., 2013; Sartain and Wolfner, 2013; Swann and Lai, 2016). The process of egg activation can be largely though not perfectly mimicked *in vitro* by submerging isolated mature oocytes in a hypotonic buffer (Horner and Wolfner, 2008b; Page and Orr-Weaver, 1997).

Given the importance of zinc dynamics during mammalian and *C. elegans* oocyte maturation and egg activation, we asked if similar processes occur in *Drosophila* as well. Interestingly, in a previous proteomic study that looked at phospho-modulation of maternal proteins during the transition from egg to embryo,

we noticed that Znt35C, the most highly expressed zinc transporter in the *Drosophila* ovary (Leader et al., 2017), undergoes phospho-state change during egg activation, suggesting that its activity might be modulated during egg activation (Zhang et al., 2018a). Znt35C regulates the biogenesis of lysosome-related zinc storage granules in *Drosophila* Malpighian tubules (Tejeda-Guzmán et al., 2018), a site of very active zinc homeostasis regulation.

To further examine the role of zinc in *Drosophila* reproduction, we first tested whether zinc is important for fertility. We observed that females fed a zinc-deficient diet had impaired fertility. This prompted us to examine the dynamics of zinc in their germline. Using synchrotron-based X-ray fluorescence microscopy (XFM), we tracked the distribution and dynamics of zinc and other transition metals throughout *Drosophila* oogenesis and egg activation. We observed that zinc is the most abundant transition metal in *Drosophila* oocytes and eggs. Total intracellular zinc levels increase during oogenesis, accompanied by formation of zinc-enriched granules in the oocyte cytoplasm. The maintenance of these zinc granules in mature oocytes is dependent on Znt35C. Upon egg activation, there is a significant decrease in intracellular zinc levels and in the presence of zinc granules in wildtype oocytes. All these observations are reminiscent of zinc dynamics seen in mammalian oocyte maturation and egg activation.

6.2 Materials and Methods

Fly strains and maintenance. All *Drosophila* strains and crosses were maintained or performed on standard yeast-glucose-agar media at 25 °C on a 12/12

light/dark cycle. When needed, 10 mM N,N,N′,N′-tetrakis(2-pyridylmethyl)-1,2-ethylenediamine (TPEN) in ethanol, 10 mM neocuproine in ethanol, 10 mM ammonium tetrathiomolybdate (TM) in water or 10mM $ZnSO_4$ in water stock solution was added to melted food to the indicated final concentration and mixed well before the food solidified. An equal volume of solvent (ethanol or water) was added to control food. All chemicals were obtained from MilliporeSigma.

Egg-laying and egg hatchability assay. Oregon-R-P2 (ORP2) wildtype flies were reared on control yeast-glucose medium, or this medium containing the indicated concentrations of TPEN (TPEN food), or medium containing TPEN and $ZnSO_4$ (TPEN rescue food). To determine how TPEN affected fertility, 3- to 5-day-old virgin females and males were mated in single pairs on TPEN food. Matings were observed and the males were removed after a single mating had completed. Females were allowed to lay eggs in the mating vial for 24 hours and were then transferred to a new vial also containing TPEN food. Females were transferred twice to new vials of TPEN food before being discarded. The number of eggs and pupae in each vial were counted. Egg hatchability was calculated by dividing the number of pupae by the number of eggs. For 3 pairs of single matings from each group, we counted the number of unhatched eggs for two days after egg-laying to calculate the number of hatched ones. Those numbers were equal to the eventual number of pupae in the selected vials, confirming the reliability of our method of calculating egg hatchability. The same procedure was followed for assays with neocuproine and TM.

DNA constructs and transgenic flies. To create a null allele of *znt35C*, we generated pU6-chiRNA constructs following protocols described on the FlyCRISPR

website (https://flycrispr.org/; Gratz et al., 2013). We generated two constructs to express sgRNAs with the following target sequences (PAM sequences are underlined): gRNA1, GGGCACGATGACAATGATCCCGG; gRNA2, GCAGATTTTCCAAGGCATCGAGG. These constructs were co-injected by Rainbow Transgenic Flies, Inc. into *nos-Cas9-attP2* embryos. We identified a chromosome carrying an edited *znt35C* gene, in which a 2 bp deletion (CCGGGATCATTGTCATCGTGCCC, deleted bases are underlined) in exon 3 caused by gRNA1 led to a frameshift in the coding sequence of Znt35C's transmembrane domains and a premature stop codon. Since this mutation is predicted to completely disrupt Znt35C's transmembrane domain, it is likely a null allele. We established a fly stock that carries the mutated allele, which we have named *znt35C*^{1}, over the CyO balancer chromosome.

X-ray fluorescence microscopy sample preparation. Oocytes were dissected in isolation buffer (IB) from the indicated female virgin flies aged on yeasted food for 3-5 days as described by (Page and Orr-Weaver, 1997). *In vitro* activated eggs were made by incubating dissected mature oocytes in Modified Robb's buffer (Hu and Wolfner, 2019) for 30 min. *In vivo* activated but unfertilized eggs were collected on a grape-juice agar plate from the indicated female flies after they had mated with spermless males (Boswell, 1985; Hu and Wolfner, 2019). We attempted to prepare oocytes for microscopy by standard methods of washing and mounting samples in standard protocol that used 100 mM ammonium acetate solution (Kim et al., 2010), but the oocytes lysed under these conditions. Alternatively, we washed oocytes and eggs with a high osmolarity buffer (400 mM sucrose) which prevents oocytes from

activating (Horner and Wolfner, 2008b). Oocytes and eggs were then transferred by forceps to a 1μL drop of 400 mM sucrose on an intact 5 mm × 5 mm silicon nitride window (Norcada). Samples were allowed to dry on a heated stage warmed to 37 °C and stored in a desiccating canister until used.

Synchrotron-based X-ray fluorescence microscopy. X-ray fluorescence microscopy (XFM) was performed at beamline 2-ID-E at the Advanced Photon Source (Argonne National Laboratory). With a single-bounce Si (111) monochromator, 10-keV X-rays were monochromatized and focused to a spot size of 1 × 1 μm using Fresnel-zone plate optics (X-radia). Raster scans were done in steps of 1 μm with 15° sample tilt to detector. Fluorescence spectra were collected with a 10 ms dwell time using a 4-element silicon drift detector (Vortex-EM). Quantification and image processing were performed with MAPS software (Vogt, 2003). The fluorescence signal was converted to a two-dimensional concentration in $\mu g/cm^2$ by fitting the spectra against the thin-film standard AXO 1X (AXO Dresden GmbH). We assumed that no elemental content was lost during sample preparation.

Statistics. One-way ANOVA tests were used to detect significant differences in levels of transition metals between wildtype and *znt35C*^{1} across oocyte stages and in egg number and egg hatchability upon TPEN, neocuproine, ammonium tetrathiomolybdate (TM) or $ZnSO_4$ treatment. Tukey's HSD test or Duncan's new multiple range test was used to identify groups that were significantly different from each other in the ANOVA tests.

6.3 Results

Dietary zinc deficiency reduces female *Drosophila* fertility

Given the importance of zinc in the mammalian and *C. elegans* oocyte, we began by testing whether zinc is essential for female fertility in *Drosophila*. We followed protocols analogous to those reported for *C. elegans* (Hester et al., 2017), where addition of the zinc chelator, N,N,N′,N′-tetrakis(2-pyridylmethyl)-1,2-ethylenediamine (TPEN), to the food at a concentration of 50 μM significantly impairs C. elegans fertility. We raised Oregon-R-P2 (ORP2; wildtype) flies on food containing 50 μM or 100 μM TPEN and assessed their fecundity and egg hatchability (percent of eggs that are able to hatch) on food containing TPEN. We tested single-pair crosses, in which one or both partners had been raised on food containing TPEN and compared them to control crosses, in which both partners had been raised on control food. Males raised on 50 or 100 μM TPEN food were not impaired in siring offspring; their mates laid normal numbers of eggs that had normal hatchability (**Figure 6.1 B-E**). Female flies raised on either 50 or 100 μM TPEN treated food exhibited reduced egg hatchability; the effect was more severe at the higher dosage of TPEN, regardless of whether their mates came from control or TPEN food (**Figure 6.1 B and D**). 50 μM TPEN treated females displayed reduced egg hatchability only beginning on day 2 post mating (**Figure 6.2 A**). To test if this was the result of residual zinc from their parents, who had been reared on untreated food and transferred to TPEN treated food after eclosion, we repeated the assay using female offspring of TPEN treated flies that themselves had been reared on TPEN treated food. We observed the same trend (**Figure 6.2 B**), suggesting that addition of 50 μM TPEN to food leads to a delayed

reduction in egg hatchability. Females raised on 50 μM TPEN laid normal numbers of eggs (**Figure 6.1 C**), whereas females raised on 100 μM TPEN produced significantly fewer eggs (**Figure 6.1 E**). All of these adverse effects on female fertility were rescued by supplementation with $ZnSO_4$ at equimolar concentrations to TPEN in the food (**Figure 6.1 B-E**), confirming the requirement of zinc for female fertility. Thus, dietary zinc is required for female *Drosophila* fertility, but does not appear to affect male fertility. Moreover, zinc insufficiency impacts both the quality and quantity of oocytes.

Since TPEN also has a high affinity for copper (Percival and Layden-Patrice, 1992), we attempted to test the effects of two copper chelators, neocuproine and ammonium tetrathiomolybdate (TM), on *Drosophila* female fertility. Unfortunately, at all concentrations tested (25 μM, 50 μM and 100 μM, based on comparative concentrations of TPEN), presence of either chelator in the medium was either toxic or semi-toxic to the flies (neocuprione) or slowed the flies' development by >3-fold (TM), indicating a negative effect on fitness. Thus, although the surviving females had lower egg-laying and hatchability than normal (reduction of 13%, 73% for 25 μM neocuprione, 41%, 88% for 50 μM neocuprione, 63%, 91% for 25 μM TM, and 52%, 95% for 50 μM TM, respectively), this cannot be considered direct effects of either chelator on the female germline; it is likely a consequence of the toxicity/negative-fitness effects of the chelator to the fly as a whole.

Zinc is the most abundant transition metal measured in *Drosophila* oocytes and activated eggs

Given the importance of zinc in mammalian and *C. elegans* gamete biology

and the effect of dietary zinc deficiency in female *Drosophila* fertility, we measured and visualized the subcellular distribution of total zinc as well as other transition elements in oocytes from ORP2 females using synchrotron-based X-ray fluorescence microscopy (XFM). We examined four groups of egg chambers and eggs throughout development: early-stage oogenesis (stages 1-8), mid/late-stage oogenesis (stages 9-13), mature oocytes (stage 14), and activated (laid, unfertilized) eggs (**Figure 6.3 A-B**). XFM data provides the content measurements of a sample through detection of element-specific X-ray emission spectra. The total amount of each element (in fmol) was calculated from data integrated along the z axis of the scans of each sample. Element distributions were represented as two-dimensional projection images with total element content measurements. We analyzed the element contents of the egg chambers (including nurse cells and oocytes) as well as the oocytes alone (for stages with clearly observable oocytes). The oocyte can be distinguished as the most posterior cell within the egg chamber. Since nurse cells dump their cytoplasm into the oocyte during late oogenesis (reviewed in Cavaliere et al., 1998), the element contents of mature oocytes and activated eggs should include those from both nurse cells and oocytes from earlier stages of oogenesis. We also attempted to quantify element concentration in scanned samples. Since the volume of egg chambers were difficult to measure due to their irregular shape, we used total element amounts in the region of interest (ROI) divided by the area of ROI as an approximate of element concentration.

Consistent with their important physiological roles, zinc, iron, and copper were the most abundant transition metals measured across all stages of oogenesis and after egg activation. Among these three, zinc was present in the highest molar amount with

5543±684 fmol in mature oocytes, compared to 2188±344 fmol of iron and 198±49 fmol of copper in mature oocytes (mean±SEM, **Figure 6.4 A**). This is analogous to the relative amounts of transition metals in mammalian oocytes and embryos (Kim et al., 2010).

Fluxes in total zinc occur during oocyte maturation and egg activation

XFM showed increases in iron, copper, and zinc content as egg chambers transitioned from early to mid/late oogenesis. Before about stage 9, there are on average 6.24±5.71 fmol of copper, 112±95 fmol of iron, and 186±178 fmol of zinc in each egg chamber. After stage 9, each egg chamber contains on average 156±36 fmol of copper, 2174±307 fmol of iron and 5045±879 fmol of zinc (mean±SEM, **Figure 6.4 A**). Interestingly, as the amount of these transition metals increased within egg chambers in mid-late oogenesis, copper, iron and zinc became more concentrated in the oocyte, relative to the associated nurse cells. In stage 9-13 egg chambers, 71.1% of copper, 51.5% of iron and 75.9% of zinc were enriched in the oocyte, on average (**Figure 6.3 A and Figure 6.5 A**).

From mid/late oogenesis stages to stage 14 and egg activation, both the amount and area concentration of iron and copper remained constant with no statistical differences in either egg chambers or oocytes alone (**Figure 6.4 A-D**). However, both the zinc content (fmol) and the zinc concentration (fmol/μm^2) underwent dynamic changes (**Figure 6.3 C-F**). When considering the entire egg chamber, zinc concentration significantly increased from stage 9-13 to stage 14 (**Figure 6.3 D**). Zinc content and concentration significantly dropped from stage 14 to activated eggs (**Figure 6.3 C-D**). When looking at the oocyte alone, zinc amount significantly

increased from stage 9-13 to stage 14 and also significantly decreased from stage 14 to activated eggs (**Figure 6.4 E**). Interestingly, oocyte zinc concentration kept dropping significantly as the oocytes progressed from stage 9-13 to stage 14 and from stage 14 to activated eggs (**Figure 6.3 F**).

Taken together, these data indicate that zinc content keeps accumulating in the egg chamber over oogenesis but decreases after egg activation. Within the egg chamber, zinc becomes more and more enriched in the oocyte over oogenesis before a significant decrease during egg activation. The reduced concentration from stage 9-13 to stage 14 mature oocyte (**Figure 6.3 F**) is possibly due to nurse cell dumping, in which the zinc-enriched oocyte cytoplasm is mixed with the nurse cell cytoplasm containing less zinc.

Zinc-enriched granules form during oocyte maturation and diminish during egg activation and Znt35C is required for their maintenance

Although copper and iron displayed generally uniform distributions within the oocyte (**Figure 6.5 A-B**), the zinc distribution became punctate over development (**Figure 6.5 A and A'**). In stage 14 mature oocytes, zinc was seen in distinct granules (**Figure 6.5 B and B'**). However, during egg activation, as intracellular zinc levels decreased, these zinc granules also decreased in number (**Figure 6.5 C and C'**). These data suggest that these granules may store zinc during oocyte maturation prior to the loss observed following egg activation. The zinc transporter Znt35C, the *Drosophila* ortholog of mammalian ZNT2/ZNT3/ZNT8, is important in the biogenesis of zinc storage granules in *Drosophila* Malpighian tubules (Tejeda-Guzmán et al., 2018). Moreover, Znt35C is the most highly expressed zinc transporter in the *Drosophila*

ovary (Leader et al., 2017) and is regulated by phosphorylation during egg activation (Zhang et al., 2018a). We investigated whether Znt35C contributes to the zinc or zinc granule dynamics that we observed during oocyte maturation and activation. We generated a *znt35C^{1}* null mutation using CRISPR/Cas9. A previously published, but unavailable, *znt35C* null mutant had been reported to be viable unless exposed to excessive zinc (Yepiskoposyan et al., 2006); our *znt35C^{1}* mutant was similarly viable on normal food. Thus, we were able to isolate oocytes at all developmental stages from homozygous *znt35C^{1}* females and subject them to XFM analysis.

znt35C^{1} egg chambers displayed accumulation of zinc from stage 1-8 to stage 9-13 of oogenesis comparable to wildtype (**Figure 6.6 A-B**). However, *znt35C^{1}* appeared to contain more zinc than wildtype in stage 9-13 when looking at both the egg chamber and the oocyte alone. This difference was statistically significant with regard to zinc concentration in egg chambers (**Figure 6.6 B**) and oocytes (**Figure 6.6 D**). However, this difference was reversed in stage 14 mature oocytes, where wildtype displayed significantly higher zinc content and concentration than *znt35C^{1}* (**Figure 6.6 A-B**). When looking at the oocyte alone, unlike that in wildtype oocytes, zinc amount in *znt35C^{1}* oocytes remained constant from stage 9-13 to stage 14 and from stage 14 to activated eggs (**Figure 6.6 C**). Zinc granules were also largely absent from *znt35C^{1}* mature oocytes (**Figure 6.6 E and E'**) or activated eggs (**Figure 6.6 F and F'**).

Taken together, our data showed that in *znt35C^{1}* mutants, zinc accumulates more in egg chambers and enriches more in oocytes compared to wildtype before stage 14. At stage 14, *znt35C^{1}* oocytes experience premature zinc loss compared to wildtype, concurrent with absence of zinc-enriched granules. The subsequent zinc

decrease during egg activation is not observed in *znt35C*^{1} mutants. Znt35C is homologous to members of the SLC30 (ZnT) family of membrane proteins, which transport zinc out of the cytosol, some of which are localized in the plasma membrane and others in intracellular compartments (reviewed in Schweigel-Röntgen, 2014). Our data are consistent with Znt35C's roles in transporting zinc out of egg chambers before oocyte maturation and/or roles in retaining zinc in mature oocytes by maintaining zinc-enriched granules.

Subcellular distribution of zinc in activated eggs

We next asked with which organelles intracellular zinc is associated in *Drosophila* oocytes and activated eggs. Centrifugation of *Drosophila* embryos can stratify its subcellular components (Tran and Welte, 2010). We attempted to centrifuge mature oocytes and activated eggs with the same protocol. All mature oocytes collapsed after centrifugation possibly due to their soft texture before activation. Thus, we were unable to determine organelle association of zinc in mature oocytes. In activated eggs centrifuged and stratified with this protocol, zinc is located at the posterior end of the eggs (**Figure 6.7 A**), which correlates with the localization of the yolk (Tran and Welte, 2010). Although we cannot conclude that zinc is located in the yolk based on overlapping localization, this observation suggested that zinc is associated with the heaviest organelles in activated eggs.

6.4 Discussion

Zinc is essential for life and necessary for reproductive functions and fertility in *C. elegans* and several mammalian species. However, the requirement for zinc in

fertility, and its levels and distributions in oocytes and after oogenesis were unknown for any arthropod, including the major model system, *Drosophila*. Here, we determined that dietary zinc is essential for *Drosophila* female fertility. This prompted us to use X-ray fluorescence microscopy to examine zinc distribution during oogenesis and egg activation. We found that zinc is the most abundant transition metal in *Drosophila* oocytes at all stages. Zinc levels increase during oogenesis, and within the egg chamber, zinc becomes concentrated in the oocyte. Mature oocytes have high levels of zinc in aggregates or granules; the latter require the zinc transporter Znt35C for their presence and maintenance. Egg activation coincides with loss of both zinc and granules from the oocyte. As discussed below, the loading of zinc into oocyte granules and the loss of zinc upon egg activation are conserved between fly and mammalian oocyte biology.

Zinc is required for female fertility in *Drosophila*

Dietary zinc is necessary for female fertility in *Drosophila*, impacting both the quality and quantity of eggs produced, suggesting the fly as a possible model for studying zinc-related subfertility. In mammalian females, zinc also plays multiple roles in oocytes across various stages. Dietary zinc depletion leads to premature germinal vesicle breakdown, spindle defects during oocyte maturation, and blocked ovulation and epigenetic programming alterations (Tian and Diaz, 2012, 2013). After fertilization, zinc deficiency further perturbs chromatin structure, reduces global transcription, and disrupts placental development during early embryogenesis (Kong et al., 2015; Tian et al., 2014). In *C. elegans* hermaphrodites, dietary zinc deficiency results in impaired oogenesis and chromosome dynamics during meiosis in the

germline, which reduces brood size and embryo viability (Hester et al., 2017; Mendoza et al., 2017). Interestingly, we did not see impairment of male fertility upon zinc-depletion in *Drosophila* males, even though in mammals zinc deficiency is associated with sperm chromatin instability and thus male infertility (Caldamone et al., 1979; Kvist et al., 1987). This observation is analogous to *C. elegans*, in which oocytes are more sensitive to zinc deprivation than sperm (Mendoza et al., 2017). It is still possible that the levels of TPEN we tested in *Drosophila*, while sufficient to impair female fertility, were too low to affect spermatogenesis. In addition, dietary zinc deficiency could also lead to impaired female fertility in a systematic and indirect way instead of through a direct impact on oogenesis. These possibilities are subjects for future studies.

Znt35C is required for the maintenance of zinc storage granules in *Drosophila* oocytes

During *Drosophila* oocyte maturation, the presence of zinc-enriched granules is maintained by zinc transporter Znt35C. *Drosophila* Znt35C mediates the biogenesis of lysosome-related zinc granules which function as the major zinc reservoir in principal Malpighian tubule epithelial cells (Tejeda-Guzmán et al., 2018). It is tempting to speculate that similar mechanisms are used in the *Drosophila* oocyte to store its high levels of zinc during maturation in preparation for zinc release upon egg activation. Consistent with this interpretation, we observed that $znt35C^{1}$ null mutant females fail to maintain high levels of zinc, or zinc granules in their mature oocytes and consequently show no decrease in zinc levels upon egg activation. These females did not display defects in egg production or hatchability (**Figure 6.8)**, however,

suggesting that the accumulation of zinc in mature oocytes is not solely (or non-redundantly) necessary for *Drosophila* fertility under zinc sufficient conditions.

In mammalian egg activation, zinc is released from zinc-loaded vesicles undergoing exocytosis after fertilization (Que et al., 2014). Given that zinc granules in wildtype *Drosophila* mature oocytes are largely absent after egg activation, they may serve similar purposes in packaging zinc for traffic out of oocytes during egg activation. It will be intriguing in this context to examine the role of the mammalian orthologs of Znt35C (ZNT2/ZNT3/ZNT8) in organizing and maintaining zinc levels in mammalian oocytes and in the mechanics of zinc release upon fertilization.

Zinc dynamics during oocyte maturation and egg activation in *Drosophila* and mammals

In multiple mammalian species, zinc levels are high in oocytes but drop dramatically during egg activation via a series of exocytotic events termed zinc sparks. (Duncan et al., 2016; Kim et al., 2011; Que et al., 2019; Zhang et al., 2016). In mice, the zinc spark occurs coordinately with and is dependent on calcium oscillations during egg activation (Kim et al., 2011) and plays multiple roles in downstream events of egg activation including resumption of cell cycle (Kim et al., 2011) and modification of the zona pellucida (Que et al., 2017b). Our observation of a decrease in zinc levels in *Drosophila* oocytes during egg activation parallels what is seen in mammals at this time, suggesting an overall analogy in phenomena, and the potential for *Drosophila* to serve as a model for dissecting zinc flux mechanisms. In mouse, mature oocytes arrest at metaphase II (MII) stage of meiosis when intracellular zinc level peaks. The zinc spark is required for release of MII arrest and completion of

meiosis (Kim et al., 2011). *Drosophila* mature oocytes arrest at metaphase I (MI) of meiosis. Meiosis also completes after egg activation. It is possible that more complex zinc fluxes occur as meiosis progress during egg activation (e.g. increase before MII and decrease afterwards, parallel to that in mouse). However, since we only examined oocyte samples before and after egg activation here, the presence of such dynamics is subject to future studies.

Interestingly, we did not see a decrease in zinc granules following *in vitro* activation. (**Figure 6.7 B and B'**); similarly, we only saw the decrease in zinc levels during egg activation *in vivo* but not after *in vitro* egg activation (**Figure 6.7 C**). There are two possible explanations for this difference between eggs activated *in vivo* and *in vitro*. It is possible that zinc release and reduction of zinc granules occurs after the 30 min window used for the *in vitro* experiments. Alternatively, *in vitro* activation is known not to be completely physiological (Horner and Wolfner, 2008b; Page and Orr-Weaver, 1997), and it may thus fail to modulate zinc levels appropriately. However, the failure of zinc changes *in vitro* to match those seen *in vivo* made it impossible for us to directly observe zinc release real-time in *Drosophila* egg activation with fluorescent zinc markers.

Our findings that zinc accumulates during *Drosophila* oogenesis, becomes concentrated in granules in the mature oocyte and eventually decreases after egg activation suggests possible conservation of zinc dynamics from *Drosophila* to those in *C. elegans* and mammals. Similar mechanisms (e.g. homologous zinc transporters) may be involved in zinc homeostasis regulation during oocyte maturation and egg activation. This strongly motivates the studies of these parallel processes from

Drosophila to *C. elegans* and mammals.

Figure 6.1 Dietary TPEN impairs female *Drosophila* fertility.

(A) Diagram of female *Drosophila* reproductive system, showing one of the pair of ovaries with enlarged view of the progressive stages in an ovariole. Meiotic stages during oogenesis are noted. Illustration created with Biorender.com. (B-E) Three-day average egg hatchability (B and D) and egg number (C and E) from single-pair crosses of females and males with either or both sexes raised in 50 μM (B-C) or 100 μM (D-E) TPEN only or TPEN + $ZnSO_4$ rescue food. Male TPEN: concentration of dietary TPEN on which the males were raised and tested. Female TPEN: concentration of TPEN added to food on which the females were raised and tested. Male $ZnSO_4$: concentration of $ZnSO_4$ added to food on which the males were raised. Female $ZnSO_4$: concentration of $ZnSO_4$ added to food on which the females were raised. n: sample size of each group. a, b, c: significance groups (significant difference of mean with $p<0.05$ between groups with different labels).

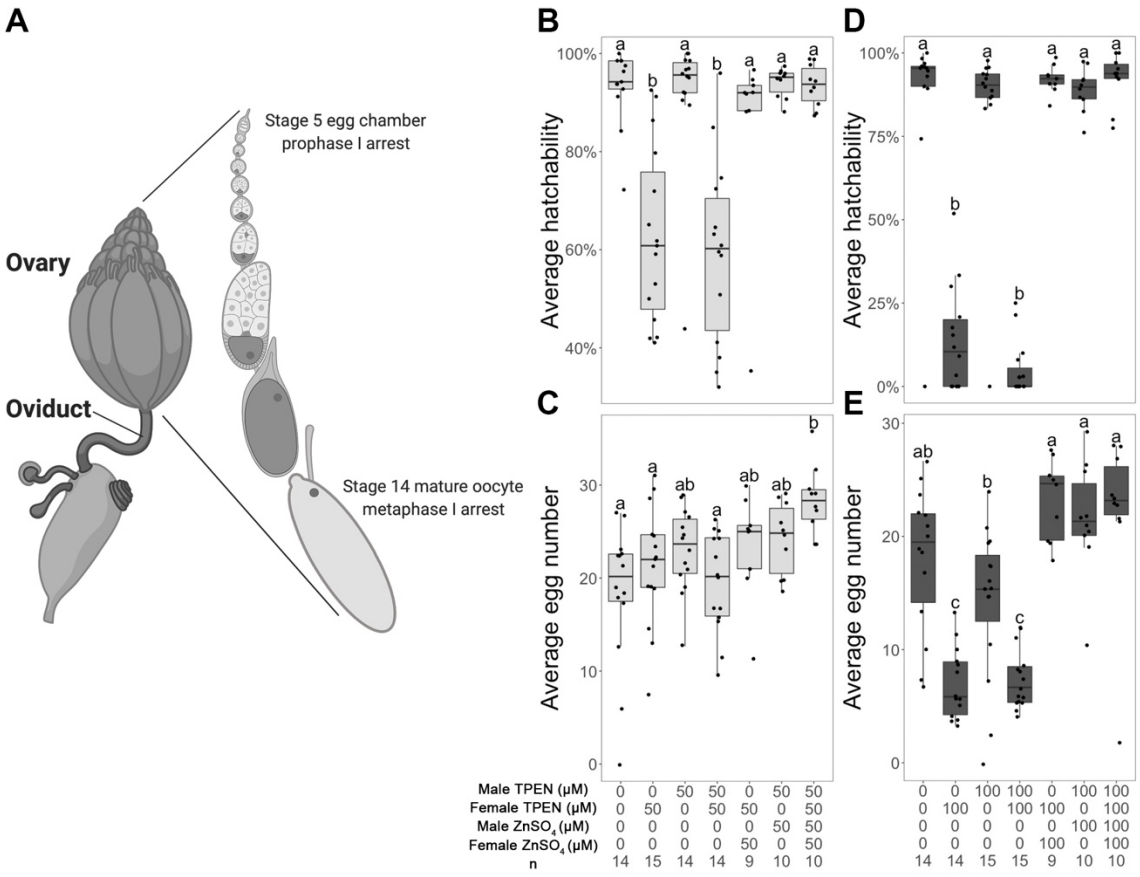
A
Stage 5 egg chamber
prophase I arrest
Ovary
Oviduct
Stage 14 mature oocyte
metaphase I arrest
B
Average hatchability
100%
80%
60%
40%
C
Average egg number
30
20
10
0
D
Average hatchability
100%
75%
50%
25%
0%
E
Average egg number
30
20
10
0
Male TPEN (μM) 0 0 50 50 0 50 50 0 0 100 100 0 100 100
Female TPEN (μM) 0 50 0 50 50 0 50 0 100 0 100 0 100 100
Male ZnSO4 (μM) 0 0 0 0 0 50 50 0 0 0 0 0 100 100
Female ZnSO4 (μM) 0 0 0 0 50 0 50 0 0 0 0 100 0 100
n 14 15 14 14 9 10 10 14 14 15 15 9 10 10

Figure 6.2 50 μM dietary TPEN reduces female *Drosophila* egg hatchability from day 2 post mating.

(A) Egg hatchability breakdown by day of Fig.1B. 50 μM dietary TPEN significantly reduces females egg hatchability starting from day 2. (B) Egg hatchability of the second generation of females reared on TPEN mated with control males reared on normal food. Egg hatchability is still significantly reduced from day 2 post mating. Male TPEN: concentration of dietary TPEN on which the males were raised and tested. Female TPEN: concentration of TPEN added to food on which the females were raised and tested. Male $ZnSO_4$: concentration of $ZnSO_4$ added to food on which the males were raised. Female $ZnSO_4$: concentration of $ZnSO_4$ added to food on which the females were raised. n: sample size of each group. a, b: significance groups (significant difference of mean with $p<0.05$ between groups with different labels).

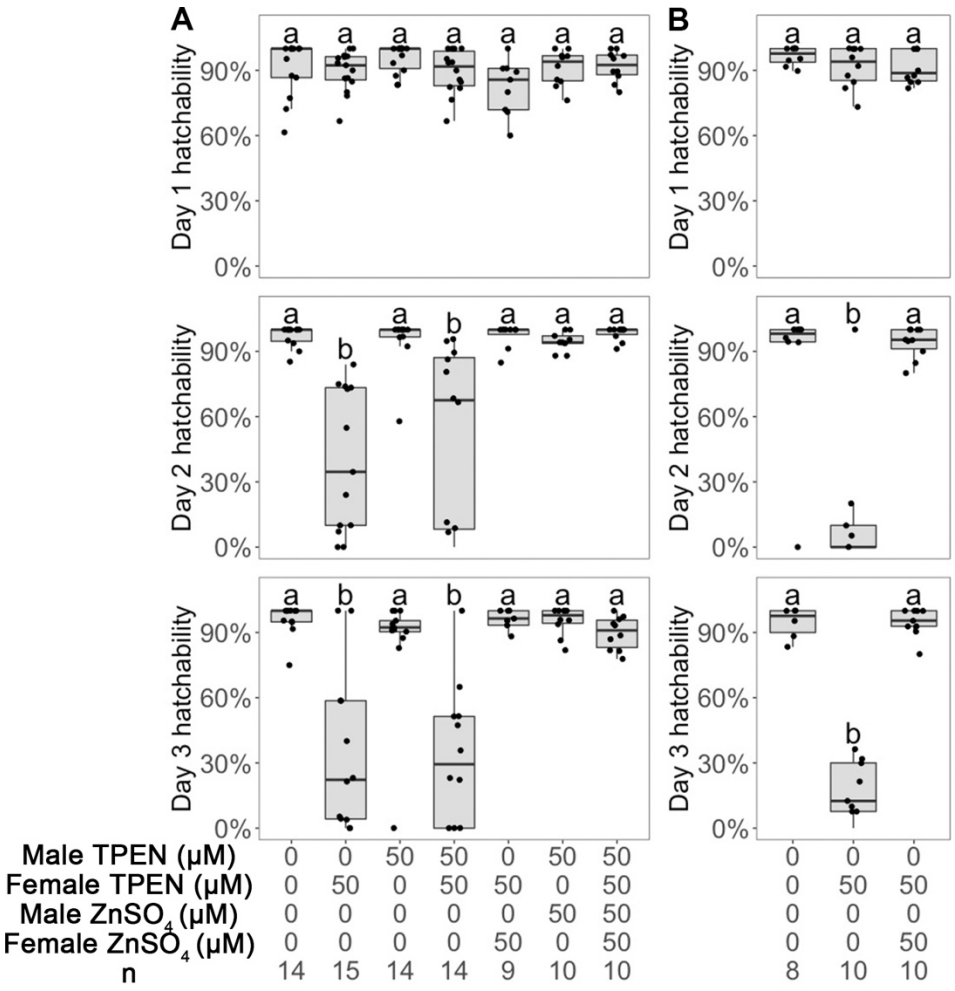
A
B
Day 1 hatchability
Day 2 hatchability
Day 3 hatchability
0%
30%
60%
90%
Male TPEN (μM) 0 0 50 50 0 50 50
Female TPEN (μM) 0 50 0 50 50 0 50
Male ZnSO4 (μM) 0 0 0 0 0 50 50
Female ZnSO4 (μM) 0 0 0 0 50 0 50
n 14 15 14 14 9 10 10
0 0 0
0 50 50
0 0 0
0 0 50
8 10 10

Figure 6.3 Zinc level and distribution changes during oocyte maturation and egg activation in wildtype *Drosophila*.

(A) Representative XFM images showing zinc distribution in egg chambers at different stages of oogenesis and egg activation. Left: an ovariole containing immature egg chambers up to stage 10. Upper right: a stage 14 mature oocyte. Lower right: an activated but unfertilized egg. Dashed lines delineate the outline of egg chambers. Dotted lines delineate the outline of oocytes in stage 9-13 egg chambers, mature oocytes and activated eggs. (B) Brightfield image of samples scanned in (A). Due to dehydration during sample preparation, morphology of these egg chambers does not completely reflect their *in vivo* state. All scale bars = 100 μM. (C-F) Total zinc content (C and E) and zinc concentration (D and F) of zinc in egg chambers (C-D) and oocytes (E-F). Stage 1-8 oocytes n=11, stage 9-13 oocytes n=15, stage 14 oocytes n=14, activated eggs n=19. a, b, c, d: significance groups (significant difference of mean with $p<0.05$ between groups with different labels).

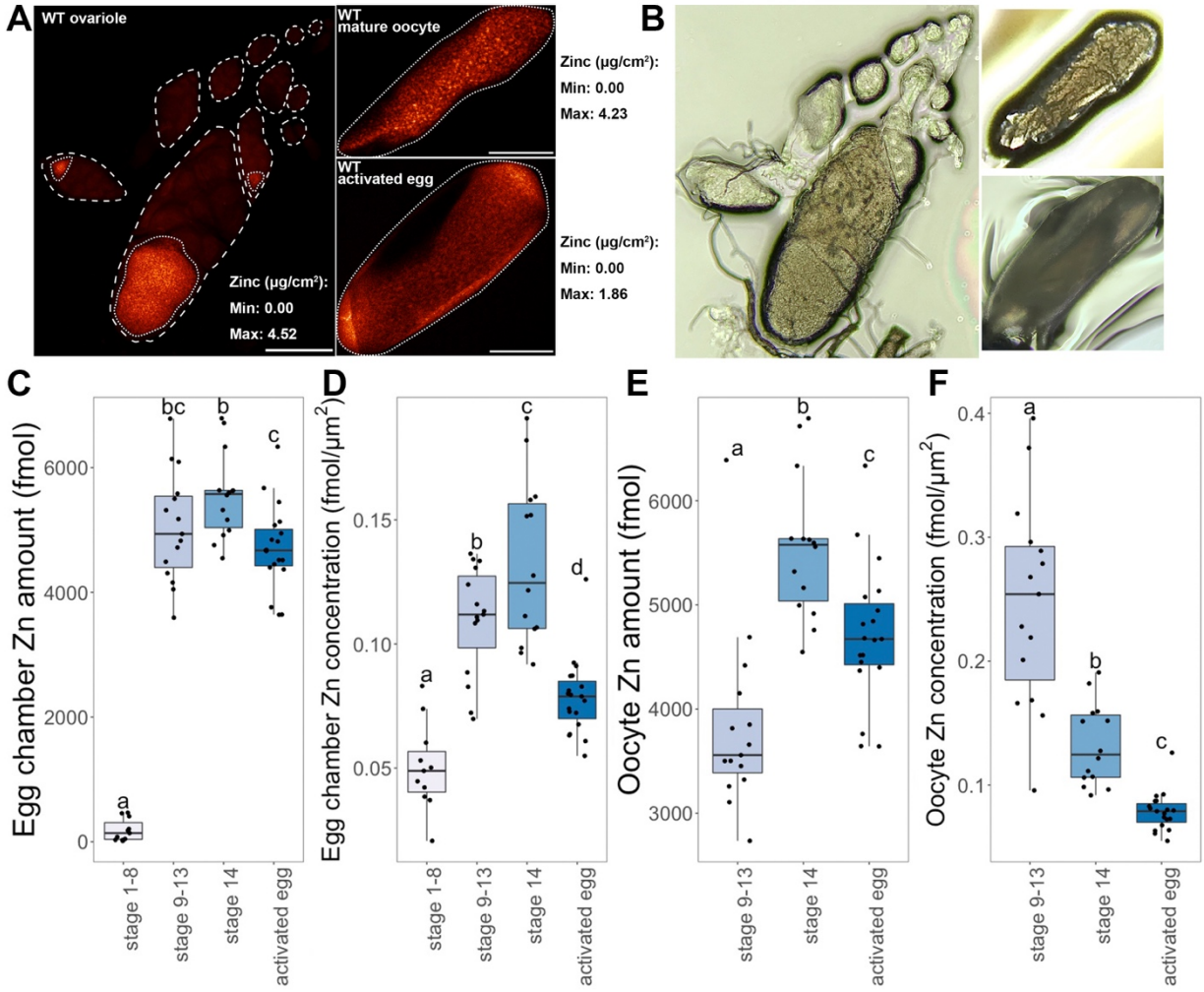
A
WT ovariole
WT
mature oocyte
WT
activated egg
Zinc (µg/cm²):
Min: 0.00
Max: 4.52
Zinc (µg/cm²):
Min: 0.00
Max: 4.23
Zinc (µg/cm²):
Min: 0.00
Max: 1.86
B
C
Egg chamber Zn amount (fmol)
D
Egg chamber Zn concentration (fmol/µm²)
E
Oocyte Zn amount (fmol)
F
Oocyte Zn concentration (fmol/µm²)
stage 1-8
stage 9-13
stage 14
activated egg

Figure 6.4 Levels of copper, iron and zinc in egg chambers and within oocytes during *Drosophila* oogenesis and egg activation.

Copper, iron and zinc are the most abundant transition metals measured during oogenesis and egg activation. The total metal content (A and C) and metal concentration (B and D) in egg chambers (A-B) and oocytes (C-D) are plotted. Stage 1-8 oocytes n=11, stage 9-13 oocytes n=15, stage 14 oocytes n=14, activated eggs n=19. a, b, c, d, e, f: significance groups (significant difference of mean with $p<0.05$ between groups with different labels).

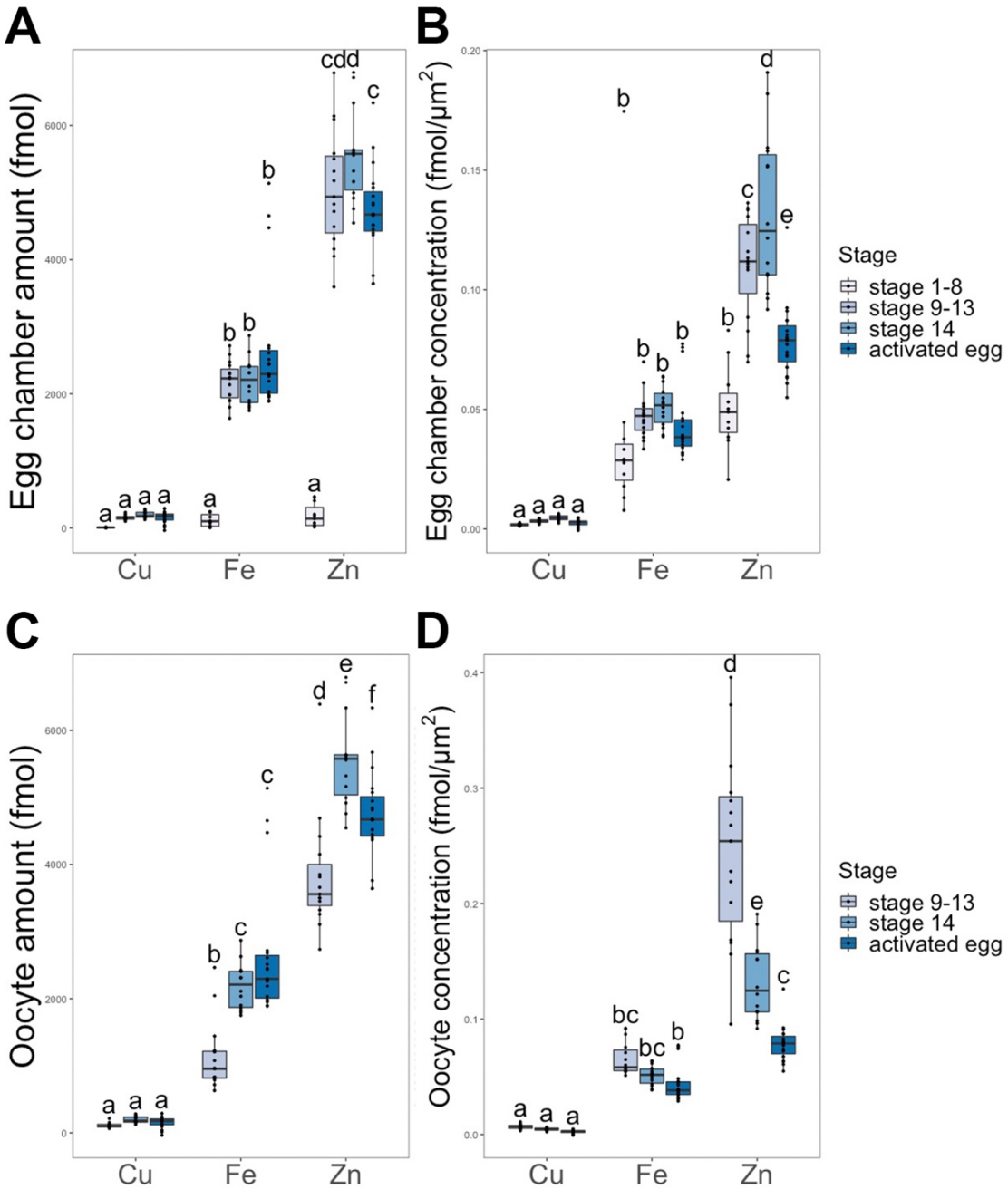
A
Egg chamber amount (fmol)
Cu
Fe
Zn
B
Egg chamber concentration (fmol/μm2)
Stage
stage 1-8
stage 9-13
stage 14
activated egg
C
Oocyte amount (fmol)
D
Oocyte concentration (fmol/μm2)

Figure 6.5 Distribution of iron, copper and zinc during oocyte maturation and egg activation in wildtype *Drosophila*.

(A-C) Representative XFM images showing iron, copper and zinc distribution in: (A) an egg chamber around stage 10. Within an egg chamber, iron, copper and zinc are all more concentrated in the oocyte (arrows); (B) a mature oocyte (stage 14). Zinc displays a more granulated distribution compared to iron and copper. Iron and copper display an even distribution. A single granule of highly concentrated iron and copper (arrows) was repeatedly observed at the anterior end of mature oocytes. The nature of this granule is unknown; (C) an activated but unfertilized egg. Zinc displays an even distribution. All samples are from ORP2 wildtype females. (A'-C') Enlarged view of zinc distribution in (A-C). Dashed squares indicate enlarged regions. All scale bars = 100 μm, insets as shown.

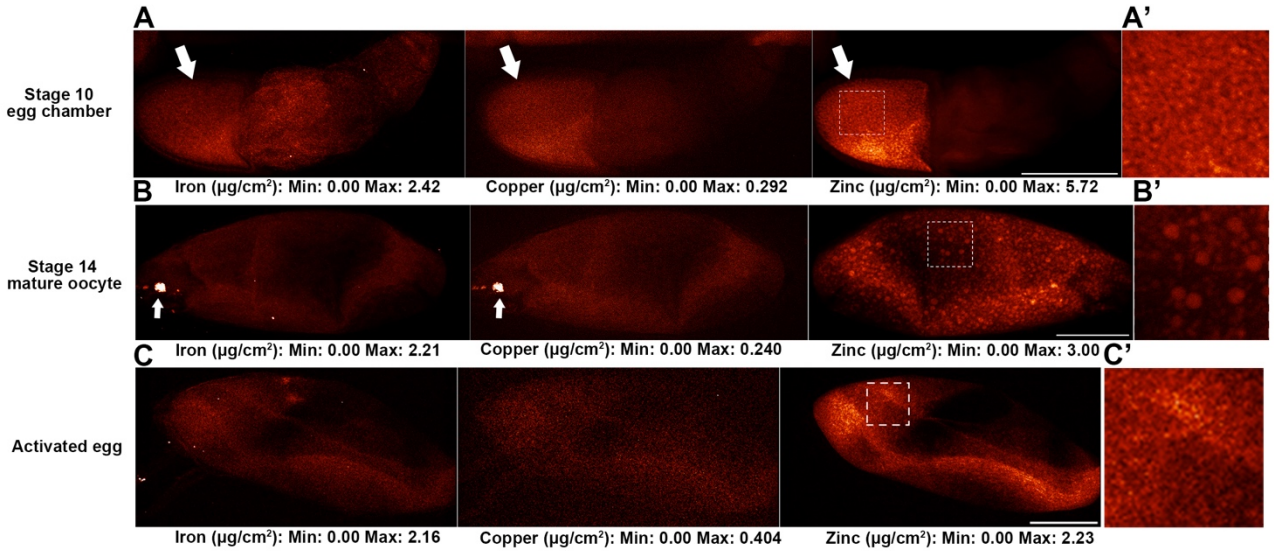
A
A'
Stage 10
egg chamber
Iron (µg/cm²): Min: 0.00 Max: 2.42
Copper (µg/cm²): Min: 0.00 Max: 0.292
Zinc (µg/cm²): Min: 0.00 Max: 5.72
B
B'
Stage 14
mature oocyte
Iron (µg/cm²): Min: 0.00 Max: 2.21
Copper (µg/cm²): Min: 0.00 Max: 0.240
Zinc (µg/cm²): Min: 0.00 Max: 3.00
C
C'
Activated egg
Iron (µg/cm²): Min: 0.00 Max: 2.16
Copper (µg/cm²): Min: 0.00 Max: 0.404
Zinc (µg/cm²): Min: 0.00 Max: 2.23

Figure 6.6 Zinc distribution and quantification over oocyte maturation and egg activation in *znt35C^{1} Drosophila*.

(A-D) The total zinc content (A and C) and zinc concentration (B and D) of zinc in each egg chamber (A-B) and oocyte (C-D) of *znt35C^{1}* compared with ORP2 wildtype. WT: ORP2 wildtype. KO: *znt35C^{1}* null mutant. Stage 1-8 oocytes WT n=11, KO n=15, stage 9-13 oocytes WT n=15, KO n =20, stage 14 oocytes WT n=14, KO n=19, activated eggs WT n=19, KO n=12. a, b, c, d, e: significance groups (significant difference of mean with $p<0.05$ between groups with different labels); (E-F) Representative XFM images showing zinc distribution in (E) a mature oocyte at stage 14; (F) an activated but unfertilized egg from *znt35C^{1}* mutant females. (E'-F') Enlarged view of (E-F). Dashed squares indicate enlarged regions. All scale bars=100 μm.

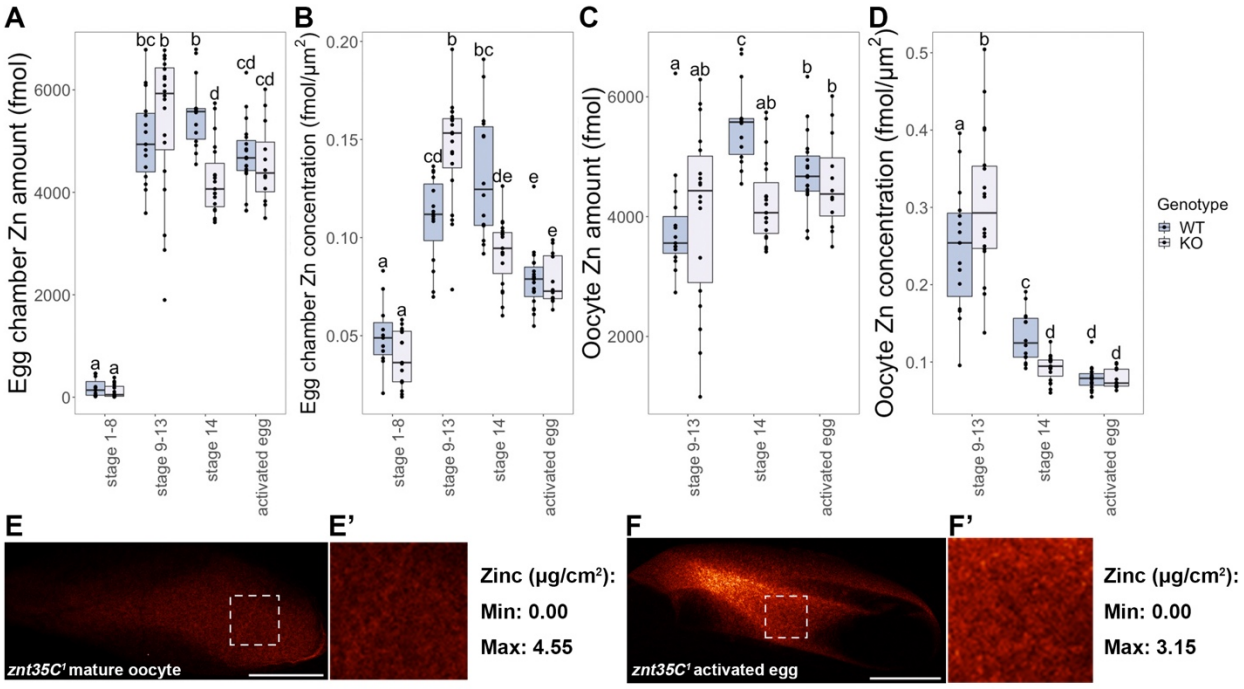
A
Egg chamber Zn amount (fmol)
B
Egg chamber Zn concentration (fmol/μm²)
C
Oocyte Zn amount (fmol)
D
Oocyte Zn concentration (fmol/μm²)
stage 1-8
stage 9-13
stage 14
activated egg
Genotype
WT
KO
E
E'
F
F'
znt35C¹ mature oocyte
znt35C¹ activated egg
Zinc (μg/cm²):
Min: 0.00
Max: 4.55
Zinc (μg/cm²):
Min: 0.00
Max: 3.15

Figure 6.7 Zinc distribution in centrifuged eggs activated *in vivo* and zinc content of eggs activated *in vitro*.

(A) Zinc accumulated at the posterior end (indicated by arrow) of *in vivo* activated eggs after centrifugation (n=3); (B) Egg activation *in vitro* did not lead to a decrease in number of zinc-enriched granules in contrast to what was seen with *in vivo* egg activation. (B') Enlarged view of (B). Dashed squares indicate enlarged regions. All scale bars = 100 μm; (C) Zinc levels in stage 14 mature oocyte, *in vivo* and *in vitro* activated eggs. Egg activation *in vitro* did not significantly reduce oocyte zinc levels in contrast to what was seen *in vivo* (stage 14 oocyte n=14, *in vivo* activated egg n=19, *in vitro* activated egg n=9). a, b: significance groups (significant difference of mean with $p<0.05$ between groups with different labels); All scale bars=100 μm.

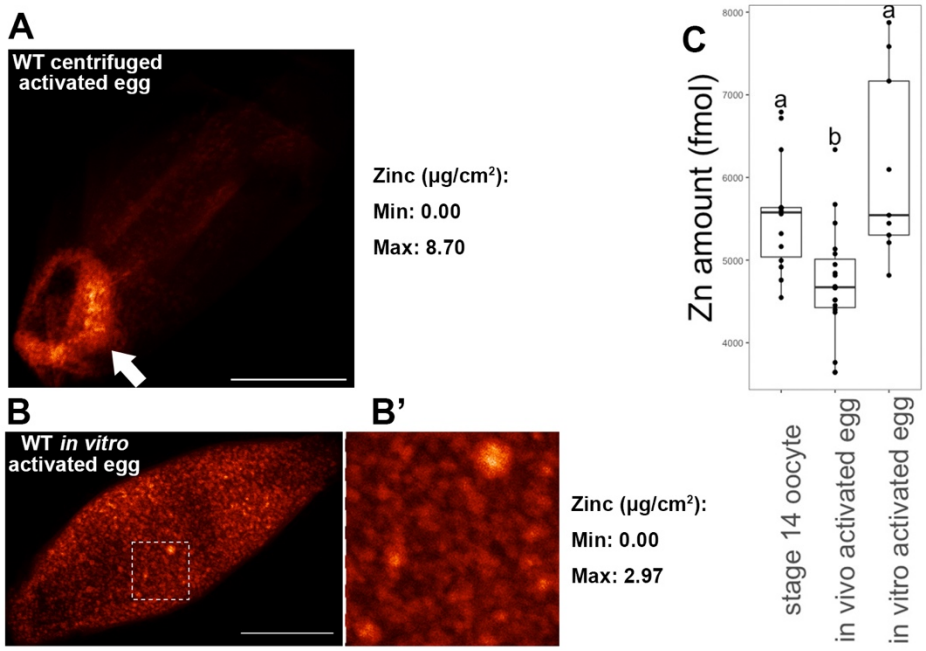
A
WT centrifuged activated egg
Zinc (µg/cm²):
Min: 0.00
Max: 8.70
B
WT in vitro activated egg
B'
Zinc (µg/cm²):
Min: 0.00
Max: 2.97
C
Zn amount (fmol)
8000
7000
6000
5000
4000
a
b
a
stage 14 oocyte
in vivo activated egg
in vitro activated egg

Figure 6.8 *znt35C^{1}* does not affect female egg production and hatchability.

Average (A) egg number and (B) hatchability over 4 days produced by control (*znt35C^{1}*/+, n=17) and *znt35C* knockout (*znt35C^{1}*/*znt35C^{1}*, n=25) females mated with ORP2 wildtype males. a: significance groups (significant difference of mean with $p<0.05$ between groups with different labels).

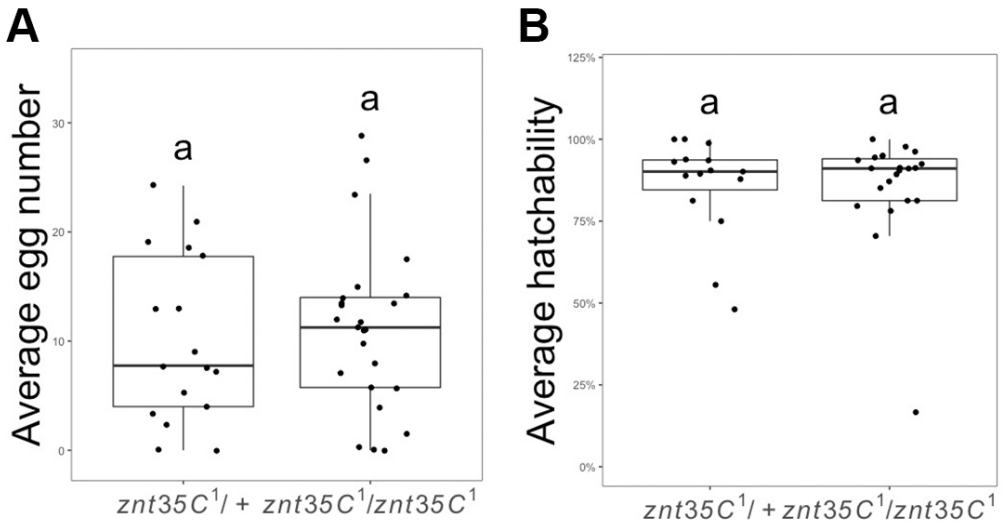
A
Average egg number
30
20
10
0
a
a
znt35C1/ +
znt35C1/znt35C1
B
Average hatchability
125%
100%
75%
50%
25%
0%
a
a
znt35C1/ +
znt35C1/znt35C1

CHAPTER 7 OPTIMIZATION OF GERMLINE-SPECIFIC CRISPR/CAS9-MEDIATED GENOME EDITING IN DROSOPHILA[5]

7.1 Introduction

Tissue-specific mutagenesis is an essential tool for characterizing functions of genes, especially when such mutations are lethal to the whole organism. Since the emergence of clustered regularly interspaced short palindromic repeats (CRISPR)-mediated genome editing methods, these have been widely used in multiple model and non-model organisms to generate heritable knockout or knockin mutations of genes or interest. This binary system utilizes a Cas (e.g. Cas9) endonuclease to cleave genomic DNA at sites determined by a synthetic single guide RNA (gRNA) to create double strand breaks (DSBs) at those sites. Such DSBs can be repaired imprecisely through non-homologous end joining (NHEJ) or precisely through homology-directed repair (HDR). Random insertions/deletions (indels), large DNA deletions, or precise DNA sequence replacements can be achieved depending on the gRNAs and repair mechanisms used (reviewed in Doudna and Charpentier, 2014; Jiang and Doudna, 2017; Ran et al., 2013).

Drosophila is a powerful model organism, given its versatile genetic manipulation tools. CRISPR-mediated genome editing methods are highly successful in this tractable system (Bassett et al., 2013; Gratz et al., 2013). A number of tissue-specific CRISPR/Cas9-mediated mutagenesis approaches have be reported in

[5] This work is a collaboration with Dr Zijing Zhang and Sarah E. Allen from Dr. Mariana F. Wolfner's lab, and Gabriel T. Koreman, Yineng Xu and Bei Wang from Dr. Chun Han's lab at Cornell University.

I contributed to performing experiments and data analysis.

Drosophila (Meltzer et al., 2019; Poe et al., 2018; Xue et al., 2014a). However, such methods have not been optimal for targeting the germline, although highly efficient editing in the germline is essential to study many reproductive related genes.

The special nature of the germline makes certain molecular mechanisms function differently from those in the soma. As a consequence, the efficiency of genetic manipulation tools can be reduced. The GAL4-UAS system has been widely used in *Drosophila* for efficient tissue-specific gene expression (Duffy, 2002). However, the application of conventional Gal4-UAS system with the standard UASt sequence in the female germline is limited due to Piwi-interacting RNAs (piRNAs) in targeting Hsp70 promoter of UASt for inhibition (DeLuca and Spradling, 2018). This has been circumvented by design of vectors optimized for the germline: UASp, which replaced the Hsp70 promoter with a transposase promoter (Rørth, 1998), and UASz, which modified the Hsp70 promoter with a synthetic untranslated region (UTR) sequence (DeLuca and Spradling, 2018). Similarly, tissue-specific CRISPR/Cas9 genome editing (Poe et al., 2018) can also have limited efficiency in the germline. Constructs specifically optimized for germline expression need to be developed for efficient CRISPR/Cas9-mediated genome editing in the germline.

The efficiency of germline editing is not a pivotal concern for conventional CRISPR/Cas9 genome editing that aims to generate mutations that will be propagated in the whole organism. Mono- or bi-allelic mutations generated in the germline of founder organisms with less-than-optimal efficiency are acceptable since homozygous mutant strains can be obtained by screening and crossing of progenies of the founders. However, efficiency is a major concern for germline-specific CRISPR/Cas9 genome

editing, whose goal is to make and phenotype mutations in the germline itself (Hu and Wolfner, 2019). Since mutations are generated in the cell lineage in which the phenotypes will be examined, bi-allelic mutations are required in a high percentage of the cells in order to reveal the mutant phenotypes of genes of interest.

Several approaches have been reported to improve CRISPR/Cas9 genome editing efficiency in the germline. For Cas9 expression, transgenes expressing Cas9 specifically in the germline were developed. Some of them put Cas9 coding sequence directly under the regulation of germline-specific promoters, such as *vasa*-Cas9 (Sebo et al., 2014) and *nos*-Cas9 (Kondo and Ueda, 2013). Some others utilize the GAL4-UAS system to achieve germline-specific Cas9 expression (Xue et al., 2014a). For gRNA expression, there has not been specific optimization in the germline yet. However, in order to ubiquitously and efficiently express multiple gRNAs to enhance editing efficiency, a number of methods have been developed, including optimizing ubiquitous promoters (Xue et al., 2014b), modifying the gRNA scaffold with a "flip and extension" (F+E) change (Chen et al., 2013), and flanking gRNA sequences with endogenous tRNAs (Port and Bullock, 2016; Xie et al., 2015). Whether these optimizations can enhance gRNA expression in the germline remains to be tested. Previous studies on CRISPR/Cas9 genome editing in the germline either requires multiple genetic components with GAL4-UAS system (Xue et al., 2014a) or requires multiple gRNA expression constructs that can only express single gRNAs (Gratz et al., 2013), which both require extensive time of embryo injection and crossing. Here, we aim to optimize germline-specific CRISPR/Cas9 editing by the use of a single cross, between *nos*-Cas9 line and a line that can efficiently express multiple gRNAs in

the germline.

Because much has already been optimized about Cas9 delivery for germline-specific editing, we focused on optimizing the gRNA expression constructs. We designed four gRNA expression constructs and placed into them sequences encoding gRNAs that target three genes with essential functions in the germline (**Table 7.1**). We integrated the constructs into the fly genome to create ubiquitous gRNA expression lines. gRNA-expressing flies were crossed with flies that carried *nos*-Cas9, which expresses Cas9 in the germline (Kondo and Ueda, 2013); progeny of this cross expressed both Cas9 and gRNA in the germline to achieve germline-specific genome editing (**Figure 1.2 B**).

The genes we targeted in our experiments were ones with known germline-expressed fertility or fecundity functions: *bag of marbles* (*bam*) (McKearin and Spradling, 1990), *centromere identifier* (*cid*) (Blower et al., 2006) and *giant nuclei* (*gnu*) (Shamanski and Orr-Weaver, 1991). *bam* and *cid* were also used in an previous study to assess germline-specific CRISPR/Cas9 genome editing (Xue et al., 2014a). Our data revealed that the most efficient construct for germline gRNA expression is the one that utilizes two separate ubiquitous promoters to drive the expression of two or more gRNAs and uses the "F+E" gRNA scaffold.

7.2 Materials and Methods

DNA constructs and transgenic flies. Components of gRNA expression constructs are described in **Figure 7.1 A**. gRNA targets of each gene are designed based on previous research (Xue et al., 2014a) (for *cid*) and efficiency scores on

Benchling software (https://benchling.com) [for *bam* (our new sequences displayed higher efficiency than Xue et al., 2014a) and *gnu*] and verified with flyCRISPR optimal target finder tools (https://flyCRISPR.com) (Gratz et al., 2014). Their sequences are as follows:

gRNA-*bam*: GCAATGAAAACGAAGATCCG;
GTTGCAAGCAATCCAAACCG;

gRNA-*cid*: GGACGCCGGACGGAGGCAGC;
GGAAAGCAAAACGCGAGCAGC;

gRNA-*gnu*: TTCGAATGTAAAAGCTTCGG;
TTCCTGCCAACGCCTCCAGT; AAAATTAGCAGAAATCCTAC;

gRNA^{1}-*gnu* and gRNA^{2}-*gnu* expressed all three gRNAs whereas gRNA^{3}-*gnu* and gRNA^{4}-*gnu* expressed the first two. These constructs were injected by Rainbow Transgenic Flies into *yw, nos- phiC31; PBac{attP-9A}* embryos. Successful transformants were isolated to establish gRNA expression fly lines.

Fly strains and maintenance. All *Drosophila* strains and crosses were maintained or performed on standard yeast-glucose-agar media at 25 °C on a 12/12 light/dark cycle. The following fly lines were obtained from Bloomington *Drosophila* Stock Center: *yw, nos-phiC31; PBac{attP-9A}* (35569), *nos-Cas9-attP2* (78782).

Fertility assay. Virgin females of the indicated genotypes were aged on yeasted food vials, males were aged on regular food vials, both for 3 to 5 d. They were then mated with Oregon-R-P2 (ORP2) wildtype males or virgin females, respectively. Matings were observed and males were removed after a single mating had completed. Females were allowed to lay eggs in the mating vial for 24 h and were

transferred to a new vial. They were transferred 3 times before being discarded. Numbers of eggs and pupae were counted. Egg hatchability was calculated by the number of pupae divided by the number of eggs (Hu and Wolfner, 2019).

Statistics. One-way ANOVA tests were used to detect significant differences in egg number and hatchability between control and germline-specific knockout flies. Tukey's HSD test was used to identify groups that were significantly different from each other in the ANOVA tests.

7.3 Results

Construct design

We tested four gRNA expression constructs (denoted as $gRNA^{1-4}$) for their efficiency in inducing expected fertility defects in germline-specific knockout flies for all three tester-genes (**Figure 7.1 A**). All four them support expression of two or more gRNAs. $gRNA^{1-2}$ utilized flanking tRNAs to facilitate multiplex gRNA expression (Port and Bullock, 2016), whereas $gRNA^{3-4}$ placed each gRNA target under its own ubiquitous promoter. $gRNA^{1}$ utilized the CR7T promoter, a ubiquitous promoter that was developed in previous studies for efficient gRNA expression (Xue et al., 2014b), $gRNA^{2}$ utilized the U6:3 promoter, a commonly used ubiquitous promoter for gRNA expression, and $gRNA^{3-4}$ utilized both of promoters, each with its own gRNA sequence. $gRNA^{1-3}$ utilized the "F+E" scaffold, a design with an A-U flip and hairpin extension on original gRNA scaffold sequence optimized for human cell lines (Chen et al., 2013), whereas $gRNA^{4}$ utilized the "2.1" scaffold, a gRNA scaffold that displayed highest efficiency in an efficiency screen in human cell lines (Grevet et al.,

2018).

Construct efficiency

Functions and expected knockout phenotypes of the three targeted genes are summarized in **Table 7.1**. We looked at three aspects of fertility to evaluate the efficiency of germline-specific knockout: (1) number and (2) hatchability (percent of eggs hatched) of eggs laid by knockout females mated with Oregon-R-P2 (ORP2) wildtype males ("female egg number" and "female hatchability", respectively), and (3) hatchability of eggs laid by ORP2 females that had mated with knockout males ("male hatchability"). Germline-specific knockout with all four constructs displayed at least some level of knockout phenotype for one or more genes, suggesting that they all worked for generating biallelic null mutations of target genes (**Figure 7.1 B-C**). However, their efficiency in generating biallelic null mutations varies, as reflected by degrees of reduction in egg number and hatchability.

bam is required for germline stem cell development in both males and females and its loss of function abolishes gametogenesis (McKearin and Spradling, 1990). Consistent with this expectation, CRISPR/Cas9 editing of bam with $gRNA^{1-3}$ almost completely eliminated female egg number, female hatchability and male hatchability (**Figure 7.1 B-D**). Of the three constructs, editing with $gRNA^{3}$ gave the fewest cases of incomplete knockout (non-zero egg number or hatchability), suggesting that it was the most efficient in generating *bam* biallelic knockouts. Due to the high efficiency of $gRNA^{3}$-*bam*, we did not further test $gRNA^{4}$ with *bam*.

cid is needed for centromere identity in meiosis (Blower et al., 2006) and its loss of function reduces male fertility (Xue et al., 2014a). Based on its known

functions, we hypothesized that *cid* loss of function will reduce female hatchability as well. In our tests of *cid* gRNAs in each of the four constructs, only CRISPR/Cas9 editing with $gRNA^3$ significantly reduced male hatchability (**Figure 7.1 B**). Editing with $gRNA^1$ did not affect female hatchability but editing with $gRNA^{2-4}$ all significantly reduced female hatchability, with $gRNA^3$ showing the greatest reduction (**Figure 7.1 D**). These data also suggest $gRNA^3$ has the highest efficiency with *cid* gRNAs.

gnu encodes a regulatory subunit of the Png kinase complex, which is maternally needed for early embryogenesis (Shamanski and Orr-Weaver, 1991). This gene is only expressed in and only affects the female germline and does not affect oogenesis. Consistent with this, CRISPR/Cas9 editing of *gnu* with all four constructs had no effect on egg number (**Figure 7.1 C**) but displayed significantly reduced female hatchability (**Figure 7.1 D**), but no effect on male hatchability. However, none showed complete elimination of hatchability and we detected no significant efficiency difference among the four constructs.

Taken together, our results consistently indicate that $gRNA^3$ is the most efficient gRNA expression construct in CRISPR/Cas9-mediated germline-specific knockout.

7.4 Discussion

CRISPR/Cas9-mediated genome editing requires specific optimization when applied to the *Drosophila* germline. Here, we examined the efficiency of four gRNA expression constructs and determined which was the most efficient for driving gRNA

expression in the *Drosophila* germline. We tested two scaffolds, two multiplex gRNA arrangements and two promoters or promoter-arrangements. We found that the highest efficiency construct was the one that utilizes two distinct ubiquitous promoters to drive the expression of two gRNAs with "F+E" scaffold. tRNA processing mechanisms and the "2.1" gRNA scaffold both improves editing efficiency in human cell lines or the *Drosophila* soma (Chen et al., 2013; Port and Bullock, 2016), but they did not show enhanced efficiency in the *Drosophila* germline.

Efficiency is key in germline-specific CRISPR/Cas9-mediated genome editing. Several approaches have been used to improve tissue-specific CRISPR/Cas9 editing:

Transgene insertion site: The insertion site of Cas9 transgene can have positional effects on its expression level, thus affecting editing efficiency (Port et al., 2014). Optimal chromosome location needs to be determined empirically.

Design of multiplex constructs: Because expressing multiple gRNAs can also increase the chance of successful editing and disruption of genes, we designed all of our constructs to support expression of two or more gRNAs. Multiplex gRNA expression driven by a single promoter with flanking tRNAs enhances genome editing efficiency in rice protoplasts (Xie et al., 2015) and in the *Drosophila* soma (Port and Bullock, 2016). However, our results indicated that this design is less effective in inducing biallelic mutations in the germline, as compared to designs in which each gRNA is driven by a promoter. Flanking tRNAs could potentially enhance gRNA efficiency by retaining them in the nucleus (Port and Bullock, 2016). However, since the tRNA-based approach relies on endogenous tRNA processing mechanisms, it is possible that the germline might be less efficient than the soma in carrying out this

processing.

gRNA scaffold: The scaffold sequence of the gRNA serves for Cas9 recognition and recruitment. Thus, scaffold efficiency can also affect genome editing efficiency. Several versions of gRNA scaffold have been designed and tested (Chen et al., 2013; Grevet et al., 2018; Stolfi et al., 2014). Here, we compared the efficiency of a "2.1" version of gRNA scaffold (Grevet et al., 2018) with that of the "F+E" gRNA scaffold (Chen et al., 2013) for germline genome editing. We found that the "2.1" gRNA scaffold did not work more efficiently than "F+E" in the *Drosophila* germline. For *cid*, "2.1" was significantly less efficient than "F+E"; for *gnu*, there was no significant efficiency difference between them.

gRNA sequences: gRNA sequences also have major impacts on genome editing efficiency. The choice of gRNA target sites can affect likelihood of potential off-target effects (Cho et al., 2014), as well as affecting RNA secondary structures and chromatin accessibility of gRNAs (Jensen et al., 2017) that will result in drastically different efficiencies. Several algorithms have been developed to assess gRNA efficiency *in silico* (Chari et al., 2017; Doench et al., 2016). Here, we showed that the efficiency of different gRNAs can be differentially sensitive to their expression construct: whereas *bam* and *cid* gRNAs consistently displayed highest efficiency with $gRNA^3$ construct (**Figure 7.1 B-D**), *gnu* gRNAs did not show significant efficiency differences among four constructs (**Figure 7.1 D**). One of the possible explanations is that specific gRNA sequences can form secondary structures with the scaffold and/or tRNAs, reducing their efficiency.

Multiple methods have been developed to enhance the efficiency of

CRISPR/Cas9-mediated genome editing, which is particularly important in tissue-specific conditions. Some methods work well in other organisms and/or tissues (Chen et al., 2013; Gandhi et al., 2017; Grevet et al., 2018; Xie et al., 2015) but may not be as applicable in the *Drosophila* germline. Our work here provides a potential optimal construct for expressing multiple gRNAs in the *Drosophila* germline.

Figure 7.1 Designs of gRNA expression constructs and their editing efficiency in the *Drosophila* germline.

(A) Four designs of gRNA expression constructs. CR7T and U6:3, ubiquitous promoters; brown bar, gRNA target sequences; magenta bar, F+E gRNA scaffold; purple bar, 2.1 gRNA scaffold; clover lines, glycine tRNA sequences. (B) 4-day average hatchability of eggs laid by ORP2 females, mated with germline-specific knockout males with indicated gene target sequences and gRNA expression constructs. (C) 4-day average number of eggs laid by germline-specific knockout females with indicated gene target sequences and gRNA expression constructs, mated with ORP2 males. (D) 4-day average hatchability of eggs laid by germline-specific knockout females with indicated gene target sequences and gRNA expression constructs, mated with ORP2 males. gRNA^3-*bam* was not significantly different from control due to small sample size (1) resulting from largely eliminated egg numbers. Significance indicators reflect comparisons with the control (*nos-Cas9-attP2*) unless between explicitly indicated pairs. ns, not significant, $p > 0.05$; **, $p < 0.01$; ***, $p < 0.001$.

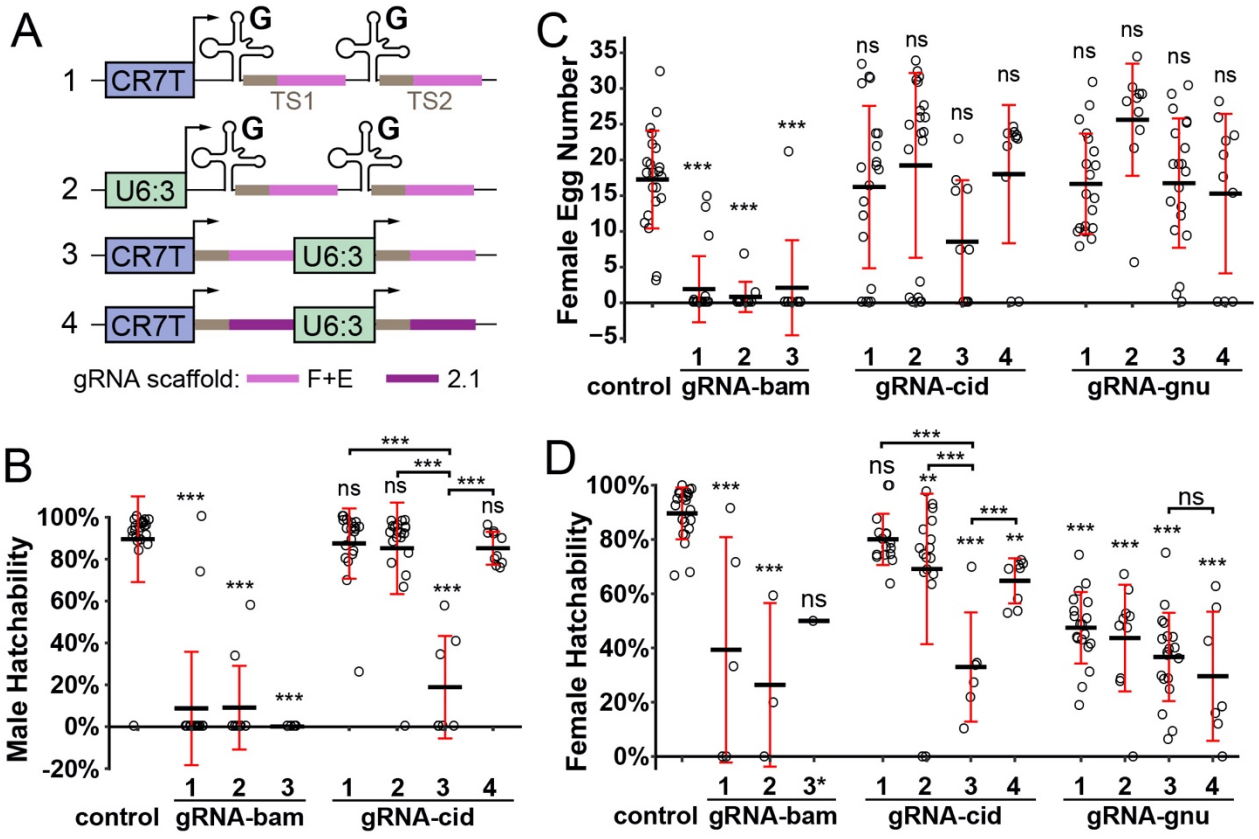
A
1
CR7T
G
G
TS1
TS2
2
U6:3
3
CR7T
U6:3
4
CR7T
U6:3
gRNA scaffold:
F+E
2.1
B
Male Hatchability
100%
80%
60%
40%
20%
0%
-20%
control
gRNA-bam
gRNA-cid
C
Female Egg Number
35
30
25
20
15
10
5
0
−5
control
gRNA-bam
gRNA-cid
gRNA-gnu
D
Female Hatchability
100%
80%
60%
40%
20%
0%
3*
control
gRNA-bam
gRNA-cid
gRNA-gnu

Table 7.1 Functions and knockout phenotypes of tested genes.

gKO: germline-specific knockout.

Target gene	**Gene function**	**Expected gKO female egg number**	**Expected gKO female egg hatchability**	**Expected gKO male fertility**
bam	Required for fate determination of germline stem cells	Reduced (McKearin and Spradling, 1990)	Reduced (McKearin and Spradling, 1990)	Reduced (McKearin and Spradling, 1990)
cid	Required for centromere identity during mitosis and meiosis	No known effect	Reduced (hypothesis based on Blower et al., 2006)	Reduced (Xue et al., 2014a)
gnu	Maternally required for the normal nuclear divisions of the syncytial embryo	No known effect	Reduced (Shamanski and Orr-Weaver, 1991)	No known effect

CHAPTER 8 THESIS SUMMARY AND PERSPECTIVES

Egg activation is a conserved process that transitions an arrested mature oocyte to a totipotent embryo once fertilized. *Drosophila* has long been a tractable genetic model to study multiple aspects of reproduction, oogenesis, embryogenesis and pattern formation. Relatively recently, *Drosophila* has been used to study egg activation. Previous studies discovered that egg activation in *Drosophila* was induced by ovulation and mechanical pressure, and included several conserved events, such as a rise of intracellular calcium in response to mechanical trigger (Kaneuchi et al., 2015; York-Andersen et al., 2015), calcineurin regulated phospho-proteome changes (Zhang et al., 2018a), and modifications to egg coverings (Petri et al., 1979). My thesis research extended the conservation of egg activation events between *Drosophila* and other species to multiple other aspects, including calcium influx mediated by Trpm channels, remodeling of cytoskeleton network, and dynamics of zinc and other transition elements during oogenesis and egg activation. These further demonstrated that *Drosophila* is a good model to elucidate molecular mechanisms of egg activation and provided tolls with which to dissect these mechanisms. Failure of egg activation underlies many cases of human infertility. The conserved processes I discovered may contribute to studies and treatment of such cases.

8.1 Regulatory mechanisms of calcium influx and phospho-proteome during *Drosophila* egg activation

My research identified Trpm as the channel mediating calcium influx during

Drosophila egg activation. Its mouse homolog TRPM7 is also involved in mediating calcium influx required for calcium oscillations during egg activation. Despite the lack of calcium waves in activating oocytes from *trpm* germline knockout females *in vitro*, I observed that these oocytes can still undergo egg activation events and even hatch (after fertilization) *in vivo*. I also observed variation in basal calcium levels of mature oocytes prior to egg activation (Hu and Wolfner, 2019). It is possible that an alternative channel contributes to increased basal level of calcium in some mature oocytes or calcium influx during egg activation *in vivo* in addition to Trpm.

An excellent candidate for this alternative channel is Piezo, a mechano-sensitive cation channel that is evolutionarily conserved from *Drosophila* to mammals. Piezo is responsible for mechanical nociception in sensory neurons (reviewed in Volkers et al., 2015; Wu et al., 2017). *Drosophila* Piezo is also capable of mediating calcium signaling in response to mechanical stimuli (He et al., 2018). According to RNAseq database, Piezo is expressed in *Drosophila* ovaries. Piezo can potentially contribute to elevating intracellular calcium levels in two ways: increasing basal calcium levels in mature oocytes prior to egg activation, and/or mediating calcium influx during egg activation *in vivo* together with Trpm. To this end, we can cross into the available *piezo* null mutant (Kim et al., 2012) our *nos*-GCaMP6m transgene (Hu and Wolfner, 2019) and examine basal calcium level by quantifying the fluorescent signal. We can also generate *trpm* and *piezo* double germline knockout females following methods described in Chapter 7 to examine its redundant role with *trpm* in mediating calcium influx during egg activation. We have designed three pairs of gRNAs targeting *piezo* and generated CR7T-gRNA1-U63-gRNA2 constructs with

them. The gRNA target sequences are as follows (PAM sequences are underlined): *piezo* gRNA-A: GCATGGTGCTCCAGCGCATCGTGG, GAACATCAAAAGGTAGACAAAGG; *piezo* gRNA-B: CATCGAATGGCTAGTGCCTGAGG, GCCAGCGCATCGTGGTGCCAGCGG; *piezo* gRNA-C: GTACGGCCGCAAAGAACAGCGTGG, AGCGTGGCCAGGCAGAACAGAGG. Efficiency of these constructs will be tested with "Cas9-LeThAL" method (Poe et al., 2018) and the optimal pair will be used for germline double knockout.

Similar approaches can be used to test Pain. Although I have found that *pain* null mutant oocytes display normal calcium wave incidence in *in vitro* egg activation, it is still possible Pain works redundantly with Trpm to mediate calcium influx since Pain is known to be mechano-sensitive (Tracey et al., 2003).

It is still not clear why calcium waves start from oocyte pole(s) during egg activation. As discussed in Chapter 3, it is most likely that terminal regions of the oocyte are molecularly different from other regions, so that special mechanisms exist at oocyte poles to allow Trpm activation only there. To this end, some candidates include cytoskeleton-related regulatory proteins. As discussed in Chapter 5, actin cytoskeleton composition is different at oocyte poles, their regulatory molecules may contribute to local activation of Trpm channels there (York-Andersen et al., 2019). Polarization of *Drosophila* oocyte during oogenesis involves transport of specific mRNAs to oocyte poles via microtubule motor proteins (Januschke et al., 2002, reviewed in Kugler and Lasko, 2014). Thus, microtubule network molecules may also be involved in Trpm local activation.

To elucidate what molecules make the oocyte poles special, one approach can be to perform proteomic analysis of the oocyte poles and waist separately. We can sever the anterior and posterior region from frozen mature oocytes, extract proteins from the poles and the waist and subject them to mass spectrometry (MS) analysis. By comparing the proteomic components and/or their phospho-state differences between the poles and the waist region of oocytes, we can identify the candidates for terminal-specific regulations. We can then generate germline mutants of those candidates using either germline-specific RNAi knockdown or CRISPR/Cas9 knockout and examine if calcium waves still initiate from poles in those mutants.

It also remains to be elucidated whether the intracellular calcium level rise is directly required for calcium dependent phosphatase (e.g. calcineurin) activity and its necessity for egg activation events to occur. Our recent proteomic study showed that activity of the calcineurin is required for phospho-state changes in maternally-provided regulators of the cell cycle, translation initiation factors, and other processes during egg activation (Zhang et al., 2018a). These changes are suggested to activate the target proteins. Given that egg activation occurred in the absence of Trpm mediated calcium influx, perhaps some of the calcineurin dependent phospho-proteome changes do not require Trpm function. To this end, we can generate *trpm* germline mutant females as described in Chapter 2 and examine the phospho-proteomes of the oocytes and activated eggs. We can then subject those oocytes and eggs to MS analysis as previously described (Zhang et al., 2018a). Analysis of phospho-peptide data this from MS and its comparison to previous studies in calcineurin knockdown mutants would reveal the impact of Trpm mediated calcium

influx on calcineurin dependent phospho-proteome changes and downstream egg activation events.

8.2 Mechanisms of calcium rises during egg activation

Despite the various triggers, a rise of intracellular free calcium level is a common feature of egg activation across species. In different species, the sources of this elevated level of calcium can differ, from solely the external environment, solely internal calcium stores, or both (reviewed in Swann and Lai, 2016). Thus, the mechanisms to introduce Ca^{2+} from the sources to the cytoplasm vary correspondingly.

In mechanisms involving influx of external calcium, Ca^{2+} enters the activating oocyte through cation channels. The involvement of TRP family cation channels is seen in both protostome and deuterostome species in which these calcium channels are identified. In *C. elegans*, TRP-3 channels are transferred from the fertilizing sperm to the oocyte to mediate calcium influx during egg activation (Takayama and Onami, 2016). In *Drosophila*, I identified Trpm as the channel mediating calcium influx in response to mechanical trigger of egg activation (Hu and Wolfner, 2019). In mouse, TRPV3 channel mediates calcium influx during parthenogenetic activation of oocytes using chemicals such as Sr^{2+} or 2-APB (Carvacho et al., 2013; Lee et al., 2016) and TRPM7 (along with $Ca_v3.2$) mediated calcium influx is required for calcium oscillations following sperm triggered egg activation (Bernhardt et al., 2018).

In some other species, through pharmaceutical inhibitor tests and deprivation of environmental calcium, it is also known that influx of extracellular calcium is

required for egg activation. However, the nature of channels mediating the influx remains unknown. In limpets, fertilization triggers egg activation and the calcium rise in this process relies solely on environmental Ca^{2+} to initiate, which most likely enters through voltage gated channels (Deguchi, 2007). In *Urechis* worm, both fertilizing sperm and intracellular pH changes are necessary for egg activation (Gould and Stephano, 1989) and by measurement, the total change in oocyte calcium level is accounted for by the influx of external calcium (Johnston and Paul, 1977).

TRP family cation channels are widespread in a great diversity of species and can respond to a variety of stimuli including mechanical pressure, voltage and pH changes (reviewed in Clapham et al., 2001; Nilius and Voets, 2005). Given their known functions of mediating calcium influx during egg activation in a wide range of species, it is tempting to speculate they are involved in calcium influx during egg activation in other species as well. Another family of ion channels of interest are voltage-gated calcium channels (VGCCs). An example of VGCC is $Ca_V3.2$, which together with TRPM7, mediates calcium entry into oocytes during both oocyte maturation and egg activation (Bernhardt et al., 2015, 2018). VGCCs are also required for meiosis resumption during egg activation of a protostome, mussel (Tomkowiak et al., 1997). TRP channels and VGCCs may evolve independently or collaboratively in their functions of mediating calcium influx during egg activation, so that one or both of them are found to play this role in both protostome and deuterostome. The presence of multiple classes of ion channels mediating calcium influx required for egg activation also raises the possibility that there may still be unknown mechanisms to mediate calcium influx in addition to the identified channels. This could explain the

observations that some egg activation events can still occur when calcium rise is blocked by inhibition of TRP channels and VGCCs in *Drosophila* and mouse (Bernhardt et al., 2018; Hu and Wolfner, 2019).

In mechanisms involving release of calcium from internal stores during egg activation, the IP_3 pathway is utilized in multiple species including nemertean worm (Stricker, 2014), fruit fly (Kaneuchi et al., 2015), sea urchin (Rakow and Shen, 1990), frog (Tokmakov et al., 2002) and mouse (Kashir et al., 2014). Although all of these organisms utilize the pathways involving IP_3 binding to its receptor IP_3R to release calcium from internal stores, they differ in upstream mechanisms. In *Xenopus*, fertilization triggers the activation of a Src-family kinase that activates PLCγ, which catalyzes the cleavage of PIP_2 to produce IP_3 (Tokmakov et al., 2002). In *Drosophila*, my research showed that Plc21C (PLCβ) is involved in linking initial calcium influx to further propagation, possibly by producing IP_3 to activate IP_3R and release calcium from stores (Chapter 4), which is required for sustaining the calcium wave propagation (Kaneuchi et al., 2015). In mouse, the fertilizing sperm delivers PLCξ to the activating oocyte to activate the IP_3 pathway (Kashir et al., 2014). These observations could be an example of "bottom-up" evolution of pathway regulation (Shearman, 2002), in which the essential and final steps of pathways emerged first and are the most conserved during evolution. Additional upstream regulatory molecules and their activation methods evolved later and divergently among species. In this case, IP_3R mediated calcium release from internal stores to increase intracellular calcium levels is this essential last step in the pathway that might have occurred first during evolution, while the use of various types of PLCs and their activation mechanisms might have

evolved later and in a lineage-specific manner.

8.3 Approaches to test potential regulators of egg activation events

In Chapter 4, we showed that Plc21C is necessary for the calcium wave during *Drosophila* egg activation. However, its null mutant oocytes did not show complete elimination of calcium waves, suggesting possible redundant mechanisms. Due to the combinatorial lethal effect of sl^{12} null allele with *nos-GCaMP6m* transgene, we were unable to determine if Sl is involved in calcium wave propagation. This pitfall can be potentially overcome by switching to a different calcium probe, *matα-GAL4-VP16 > UASp-GCaMP3*. *sl* is on X chromosome. Since sl^{12} is not lethal, we can cross it into fly lines carrying the two components of the GAL4/UAS system respectively. By generating sl^{12}; *matα-GAL4-VP16* and sl^{12};; *UAS-GCaMP3* transgenic lines and crossing them, we may be able to obtain viable homozygous sl^{12} females expressing GCaMP sensor in the germline.

In Chapter 5, we proposed α-actinin (*Actn*) as a potential mediator of the calcium-actin regulatory network. Actn can crosslink actin at low calcium concentration and release actin filaments at high calcium concentration (Jayadev et al., 2014; Prebil et al., 2016; Sjöblom et al., 2008). It may be involved in the feed-forward loop in calcium and actin waves. Related to research in Chapter 6, in addition to Znt35C, another zinc transporter, Fear-of-intimacy (*foi*), might be involved in regulation of zinc dynamics in oogenesis and egg activation as well. Foi is the second most highly expressed zinc transporter in the ovary next to Znt35C (Leader et al., 2017). It is the single ortholog of mammalian ZIP6 and ZIP10, which are required for

oocyte zinc accumulation during maturation (Kong et al., 2014). Proteomic studies in *trpm* mutant oocytes may reveal more candidates for egg activation regulation. Null mutations of both *Actn* and *foi* are homozygous lethal, so may be some other candidates from proteomic studies. It is essential to generate germline-specific mutations of these genes in order to examine their functions in oogenesis, egg activation and embryogenesis. To perturb candidate gene functions, in addition to the well-established GAL4/UAS mediated germline-specific RNAi knockdown, methods we described in Chapter 7 can also be used to generate efficient germline CRISPR/Cas9 knockout. The gRNA expression constructs also allow CRISPR/Cas9-mediated knockin. By cloning in donor sequences including homology arms into the multiple cloning site of the gRNA expression construct and integrating them altogether into the fly genome with φC31 integrase, we can achieve germline-specific CRISPR/Cas9-mediated knockin with a simple crossing between the *nos-Cas9* line and *gRNA-donor* line. This can be useful to generate desired point mutation or insert specific tags into genes of interest, especially when such modification can cause lethal effect. As a proof of principle, I have inserted a GFP tag coding sequence into either the 5' or 3' end of endogenous *trpm* gene. Although sequencing indicates successful insertion with the correct reading frame, I did not detect any GFP expression with Western blot. This is possibly due to the large gene size of *trpm* and complex splicing isoforms. However, the knockin technique itself is feasible and efficient.

To summarize, my thesis extended the conservation of egg activation events from *Drosophila* to other species. In addition to previously identified events, my work

showed or suggested the conservation in calcium rise triggers, calcium wave propagation mechanisms, cytoskeleton remodeling and zinc dynamics during egg activation. This demonstrated that *Drosophila* is a good model to disentangle the mechanisms of multiple aspects of egg activation. Findings in *Drosophila* egg activation may be applicable to other species including human, contributing to treatment of sterility due to failure of egg activation.

APPENDIX A MECHANICAL MANIPULATION OF DROSOPHILA MATURE OOCYTES[6]

A.1 Introduction

Drosophila egg activation is accompanied by a rise in intracellular free calcium levels similar to other organisms. However, this calcium rise is triggered by mechanical pressure, in contrast to the fertilization trigger used in Deuterostomes and *C. elegans*. *In vivo*, this pressure results from swelling of the oocyte due to uptake of oviductal fluid and/or to the squeezing of the oocyte by pressure from the oviduct and its musculature. *In vitro*, this pressure results from swelling of the oocyte due to hypotonicity of the buffer it is incubated in. These two types of pressure differ at least in the areas they affect: squeezing from the oviduct applies will initially only affect the posterior end of the oocyte which enters the oviduct first and initiates the calcium wave, whereas pressure from swelling of the oocyte due to osmotic conditions affects the entire oocyte. However, both of these pressures induce the calcium wave and at least some egg activation events. In order to determine what type of pressure is required for calcium wave initiation during *Drosophila* egg activation, I attempted various types of mechanical manipulation of the *Drosophila* oocyte. In investigate pressure applied by micropipette, microneedle and microfluidic chamber. Methods and experiment results of microneedle manipulation are described in Chapter 3 and

[6] The micropipette aspiration experiment was a collaboration with Dr. David Bassen from Dr. Jonathan T. Butcher's lab at Cornell University. The microfluidic chamber experiment was a collaboration with Dr. Chih-Kuan Tung from Dr. Mingming Wu's lab at Cornell University. The microneedle experiment was a collaboration with Dr. Gregory Fedorchak from Dr. Jan Lammerding's lab at Cornell University. Dr. Bassen, Dr. Tung and Dr. Fedorchak contributed to the experiment designs. I contributed to performing the experiments.

Chapter 5. Here I will document the experimental methods and results of micropipette and microfluidic chamber manipulation.

A.2 Materials and Methods

Microfluidic chamber. Chamber fabrication methods was as described in (Tung et al., 2014). The design of silicon master is described in **Figure A.1 A-B**. Fabrication of the silicon master mold was done at Cornell Nano-Scale Science and Technology Facility (CNF). The chambers were cast with Polydimethylsiloxane (PDMS). A schematic of a chamber is shown in **Figure A.1 C**. The chamber was filled with isolation buffer (IB) (Mahowald et al., 1983), and a mature oocyte dissected from *matα-GAL4-VP16 > UASp-GCaMP3* virgin females (Kaneuchi et al., 2015) was transferred into one of the wells. A silicon tube was then attached to the same well and more IB was injected into the chamber with a syringe to push the oocyte through the narrow constriction. A Metamorph fluorescence microscope with 5X lens and settings for GFP imaging was focused on the constriction to record GCaMP3 fluorescence as the oocytes squeezed through the constriction. Time series images were taken at 1 s intervals.

Micropipette aspiration. Micropipette instruments were set up as described in (Apoorva et al., 2017). Mature oocytes dissected from *matα-GAL4-VP16 > UASp-GCaMP3* virgin females were incubated in IB on a glass bottom petri-dish. The micropipette was applied to various regions of the oocytes. Vacuum pressure from the micropipette was applied incrementally via a silicone tube and calibrated by a manometer. Images were taken with a Zeiss Discovery v20 stereo microscope with 5X

lens and settings for GFP imaging.

A.3 Results

Although a calcium rise was induced once in an experiment with microfluidic chamber it was not reproducible

During ovulation *In vivo*, oocyte has to squeeze through pedicel at the base of ovaries and into an oviduct that also has a diameter smaller than the oocyte. To test whether a squeezing pressure from a narrow constriction is sufficient to induce calcium rises in *Drosophila* mature oocytes, we attempted to mimic the process of ovulation by passing mature oocytes through a narrow constriction in a microfluidic chamber. Using as reference the sizes of the oocyte and the oviduct, we designed a channel that is 250 μm wide to allow oocytes to pass through freely and a narrow constriction that is 50 μm wide to force oocytes to squeeze through and experience pressure (**Figure A.1 D**). In our experiments, the orientation of the oocyte (anterior or posterior first) when it reached the constriction was random. Oocytes were submerged in IB in the entire process, ruling out the contribution of osmotic pressure, so the only mechanical pressure applied to them in this experiment was from the constriction.

We repeated squeezing the oocytes through various tapering angles of constrictions in microfluidic chambers. However, among the 32 oocytes we tested, only one (in a chamber with tapering angle of 30°, see **Figure A.1 B**) displayed a transient calcium rise in the entire oocyte when passing through the constriction (**Figure A.1 E**). This suggested that regional mechanical pressure from passing through a narrow constriction may not be sufficient to trigger calcium rises in

Drosophila mature oocytes, or that our chamber design did not fully replicate *in vivo* dimensions and shape.

Micropipette aspiration does not induce calcium rises in *Drosophila* mature oocytes

To test whether a point aspiration pressure can induce calcium rise in *Drosophila* mature oocytes, we subject mature oocytes from *matα-GAL4-VP16 > UASp-GCaMP3* virgin females to a micropipette system, which can apply an aspirating pressure to the plasma membrane (PM) of the oocytes. Due to technical limitations, it was difficult to dock the oocyte poles to the micropipette. For 7 mature oocytes we docked a micropipette to their side and applied vacuum pressure (**Figure A.2**). None displayed elevated calcium levels as indicated by GCaMP3 signal at the site of aspiration, even with the highest pressure setting possible. This suggests that point aspiration pressure from a micropipette at the side of mature oocytes is not sufficient to induce a calcium rise.

A.4 Discussion

To determine what type of pressure is sufficient to trigger calcium rises and subsequent egg activation events in *Drosophila*, we attempted various methods of mechanical manipulation of mature oocytes and examined oocyte calcium dynamics in response to them.

It is well documented that submerging *Drosophila* mature oocytes in a hypotonic buffer, which applies a global osmotic pressure to the entire oocyte, is sufficient to trigger a complete calcium wave and several egg activation events

(Horner and Wolfner, 2008b; Kaneuchi et al., 2015; Mahowald et al., 1983; Page and Orr-Weaver, 1997; York-Andersen et al., 2015). In Chapter 3 and 5 of this thesis, I also demonstrated that a point-pressure from a microneedle can induce a regional calcium rise that does not propagate into a wave. Here, I tested two other types of pressure: point aspiration pressure from a micropipette and regional squeezing pressure from a narrow constriction in a microfluidic chamber. Neither was sufficient to trigger calcium rises or waves in mature oocytes. The fact that neither point pressing or point aspiration pressure can induce a complete calcium wave suggests that pressure applied to larger regions of the oocyte may be required to trigger a propagating calcium wave. The microfluidic chamber mimicked the pressure during ovulation and affects larger region of the oocyte. However, it still did not reproducibly induce a propagating calcium wave. It is possible that the dimensions and/or the material elasticity of the microfluidic chambers we made were different from the actual oviduct and were not sufficient to trigger the calcium wave. The dehydrated mature oocytes also take up oviductal fluid and swell *in vivo* while passing through the tight regions of the reproductive tract, whereas our microfluidic chamber experiments were done in IB, which prevents such fluid uptake and swelling. It is also possible that the swelling is the major mechanical trigger of calcium waves and egg activation. Given that calcium waves complete much faster *in vivo* than *in vitro* (Kaneuchi et al., 2015), it is possible that the squeezing pressure from the oviduct contributes to faster propagation of calcium waves. This could be tested by passing mature oocytes in hypotonic modified Robb's buffer (RB) and squeezing them through narrow constrictions while the calcium wave is still propagating. However, since calcium

waves only take ~ 5 min to complete *in vitro* and setting up the microfluidic chambers also takes time, this experiment could be difficult to set up and requires further optimization.

Figure A.1 Design of microfluidic chamber experiments.

(A) Structure of the silicon wafer used as a mold to cast microfluidic chambers. The two rows of devices are identical. The red area represents where the 250 μm protrusion is. Each device has two reservoirs where PDMS will be punched through, used to place oocytes into the device, as well as applying fluid flow to move the oocyte in the channel. The separation between the two reservoirs is mostly for the ease of operation. (B) Enlarged view of the narrow constriction. The channels will taper down to 50 μm with different angles of tapering. The lengths of the horizontal bars are 200 μm, used as markers to identify the width of the funnel. The optimal angle for tapering was unknown, so funnels with 15°, 20°, 30°, 45°, 60° were designed for testing. (C) Scheme of an experiment squeezing mature oocytes through the constriction. (D) Representative brightfield view of an oocyte entering the constriction with posterior end. (E) Time lapse images of the transient calcium wave in the oocyte passing through the constriction. Only one out 32 oocytes examined showed this response. Scale bars = 100 μm.

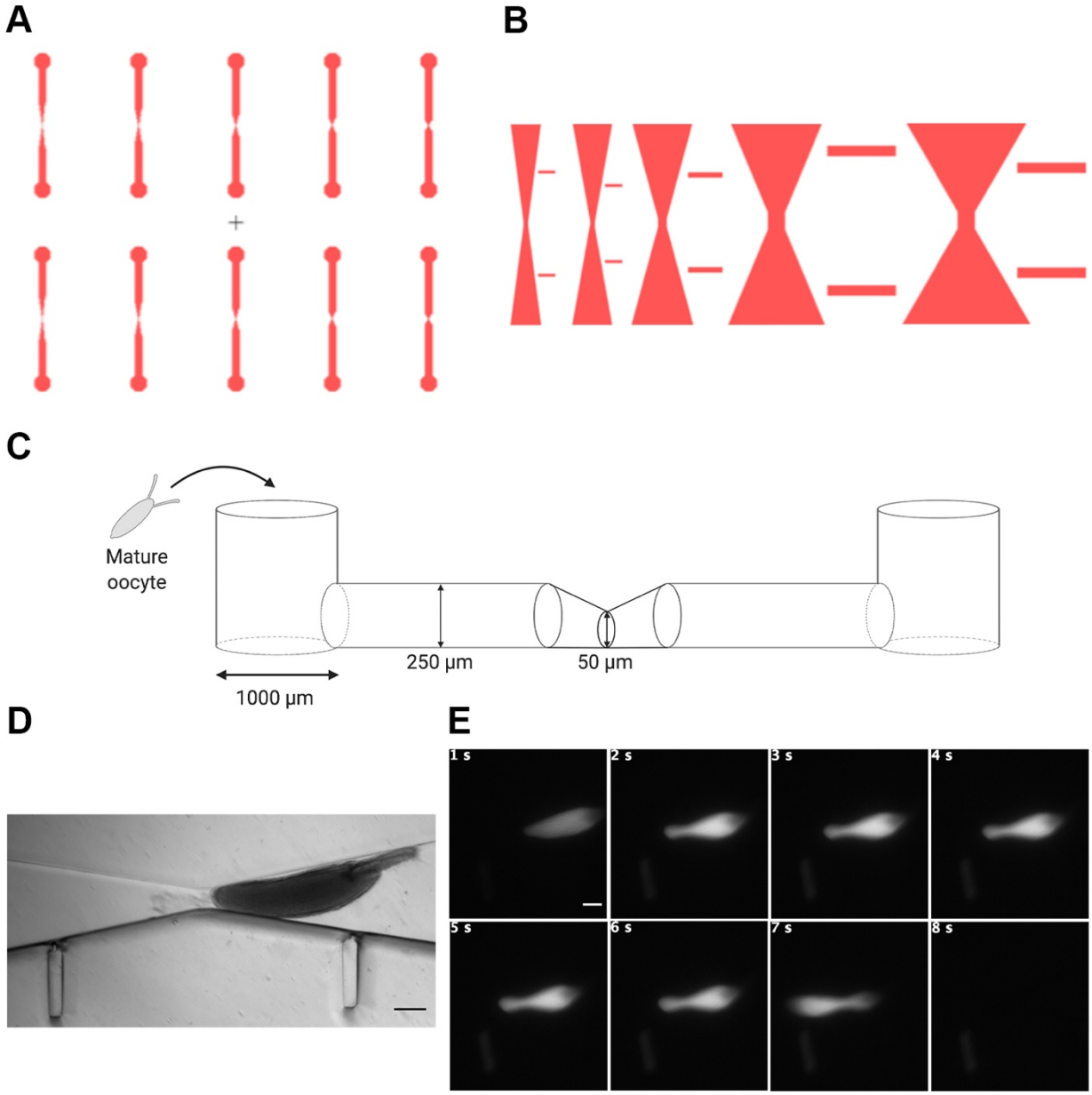
A
B
C
Mature
oocyte
250 µm
50 µm
1000 µm
D
E
1 s
2 s
3 s
4 s
5 s
6 s
7 s
8 s

Figure A.2 Micropipette aspiration of mature oocytes.

Brightfield (A) and fluorescent (B) view of a mature oocyte docked to a micropipette. No calcium rise was observed even with maximum vacuum pressure, n = 7. Scale bar = 100 μm.

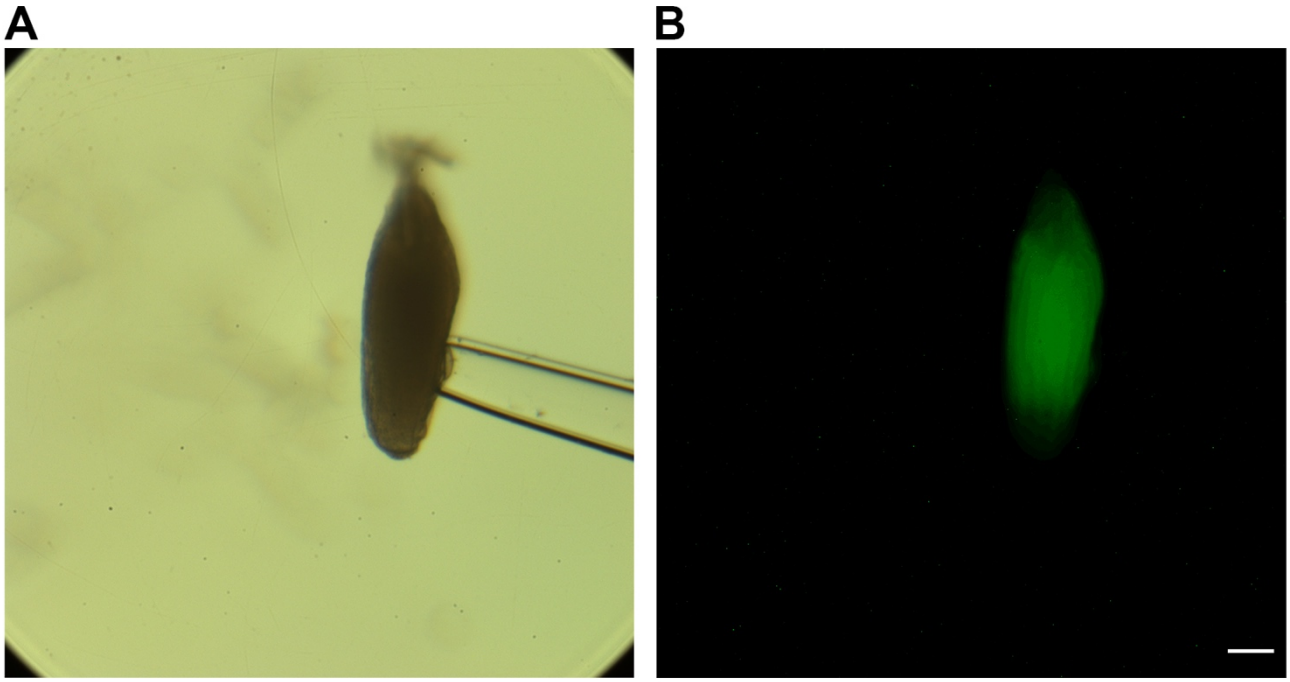
A
B

APPENDIX B STRONTIUM-INDUCED CALCIUM OSCILLATIONS DURING DROSOPHILA EGG ACTIVATION

B.1 Introduction

Previous studies revealed multiple events during egg activation that are parallel between *Drosophila* and mouse (Bernhardt et al., 2018; Cui et al., 2008; Ducibella et al., 2002; Hu and Wolfner, 2019; Kaneuchi et al., 2015; Nakanishi et al., 2006). In mouse, mature oocytes can be parthenogenetically activated with several artificial triggers instead of the sperm. Among them is replacing calcium with 5-10 mM of strontium (Sr^{2+}) in the buffer incubating mature mouse oocyte *in vitro* (Kline and Kline, 1992). Sr^{2+} enters the mouse oocyte through TRPV3 channels (Carvacho et al., 2013). This Sr^{2+} influx can induce calcium level oscillations and egg activation in these oocytes and allow embryonic development when combined with somatic cell nuclear transplantation (Wakayama et al., 1998). Since this approach to achieve mouse egg activation is independent of sperm, similar to the case in *Drosophila*, we asked if the same procedure can induce a calcium rises and egg activation in *Drosophila* as well. If so, it would reveal more mechanistic similarities in intracellular calcium level rises between *Drosophila* and mouse.

B.2 Materials and Methods

Mature oocytes were dissected from *matα-GAL4-VP16 > UASp-GCaMP3* virgin females and were activated *in vitro* as previously described (Hu and Wolfner, 2019; Kaneuchi et al., 2015). The hypotonic buffer used to activate the oocytes was switched to modified activation buffer (AB) with its 2 mM $CaCl_2$ replaced with 10

mM $SrCl_2$. A Metamorph fluorescent microscope with 5X lens and settings for GFP imaging was used to record the calcium dynamics of activating oocytes. Time series images were taken at 1 s intervals for 20 min. Oocyte fluorescence was quantified by measuring total intensity within the oocyte area using ImageJ software (Schindelin et al., 2012).

B.3 Results and Discussion

Upon replacing isolation buffer (IB) with modified AB, calcium waves initiated from one or both poles of mature oocytes, similar to those induced with unmodified AB. However, unlike the single transient calcium wave that normally sweeps through the *Drosophila* oocyte incubated in unmodified AB (Kaneuchi et al. 2015, York-Andersen et al. 2015), strontium induced repeated calcium waves that died down before completion and then repeated (**Figure B.1 A**). Quantification of the GCaMP3 fluorescence signal showed an oscillatory pattern (**Figure B.1 B**), with oscillations lasting for the entire duration of imaging (20 min) for all the oocytes tested (n = 11). In one oocyte that was imaged in the modified AB for an extended period of time, calcium oscillations lasted for over an hour.

Calcium oscillations are observed in activating mouse oocytes. The initial calcium rise is triggered by sperm derived PLCζ (reviewed in Swann and Lai, 2013), and subsequent oscillations involve expelling calcium and re-uptake of external calcium through TRPM7 and $Ca_v3.2$ channels (Bernhardt et al., 2018). 10 mM Sr^{2+} can also activate mouse oocytes, and produces calcium oscillation patterns similar to the normal ones (Carvacho et al., 2013). Despite the difference in the natural triggers,

the fact that both *Drosophila* and mouse oocytes are capable of inducing calcium oscillations in response to activation trigger suggests that although calcium rises take the form of multiple oscillations in mammals and transient single waves in most other species, the underlying calcium signaling machinery may be conserved. This machinery is capable of triggering multiple rounds of calcium uptake-expelling but might have been co-opted to do so only in mammals later in evolution. Along this line, my research, together with previous studies, has suggested a conserved Trpm – PLC – IP_3 pathway of calcium influx and wave propagation from *Drosophila* to mouse.

Figure B.1 Strontium induced calcium oscillations

(A) Representative time lapse images of calcium oscillations triggered by 10 mM Sr^{2+}, n = 11. (B) Quantification of fluorescent intensity over time in (A). Scale bar = 100 μm.

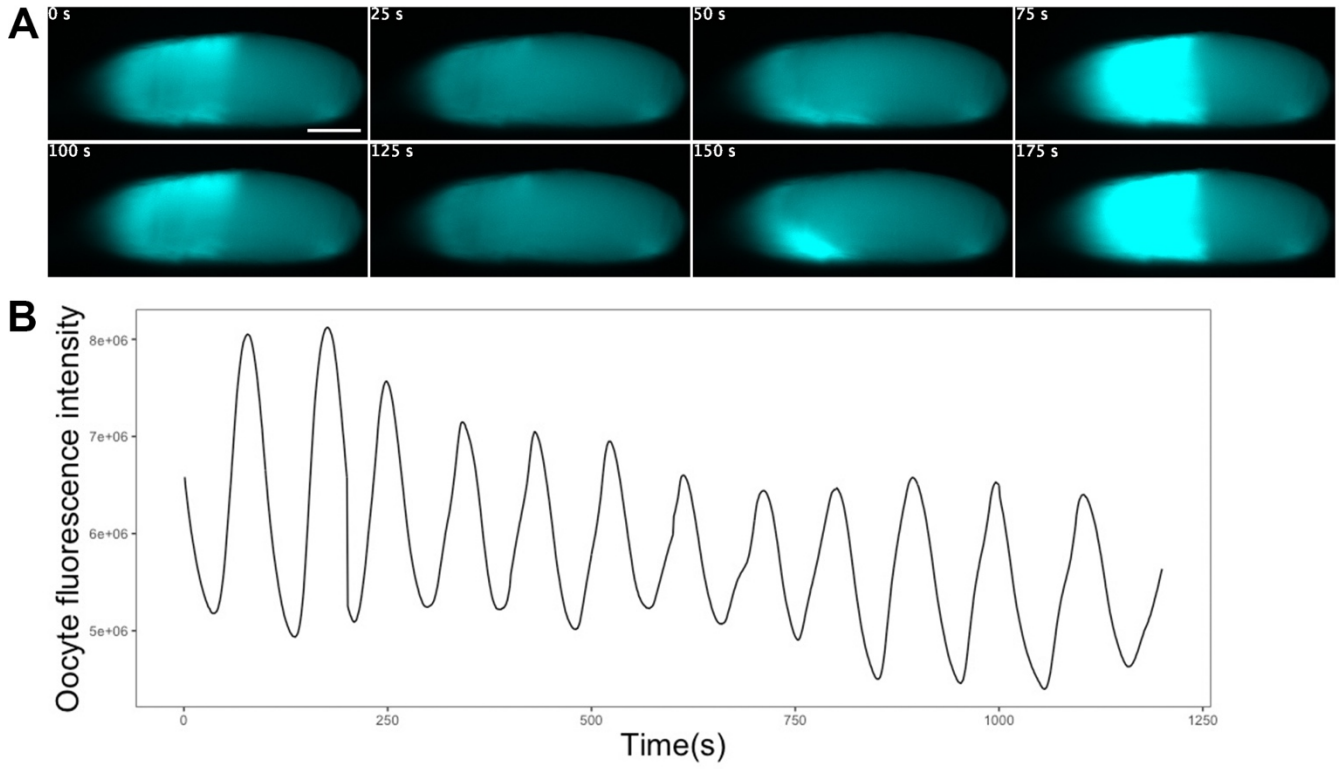
A
0 s
25 s
50 s
75 s
100 s
125 s
150 s
175 s
B
Oocyte fluorescence intensity
8e+06
7e+06
6e+06
5e+06
0
250
500
750
1000
1250
Time(s)

APPENDIX C CROSSING SCHEME FOR GENERATING TRPM GERMLINE CLONES FOR CALCIUM IMAGING

C.1 Introduction

In Chapter 2, I wished to visualize calcium wave phenotype in a *trpm* null background. Since the *trpm* null mutation is homozygous lethal (Hofmann et al., 2010), I attempted various methods to genetically disrupt *trpm* specifically in the germline. Although both germline-specific RNAi knockdown and CRISPR/Cas9-mediated knockout successful for answering the question (Hu and Wolfner, 2019), their technical limitations limited knockdown/knockout extent to over 90%. In an effort to achieve 100% knockout of *trpm* in the germline, I attempted to generate germline clones of the *trpm* null mutation, using the Flp-FRT system and ovo^D dominant female sterile technique (Chou and Perrimon, 1996) (see **1.3** and **Figure 1.2 B**). This involves generating a transgenic fly line carrying multiple special chromosomes and transgenes, including hs-Flp, ovo^D and the *trpm* null allele on homologous chromosomes carrying the same FRT site, and a germline-expressed GCaMP calcium sensor. Here I will document the crossing scheme I designed to achieve this goal. This could provide an example for future germline clone crossings.

C.2 Materials and Methods

Fly strains and maintenance. All *Drosophila* strains and crosses were maintained or performed on standard yeast-glucose-agar media at 25 °C on a 12/12 light/dark cycle. w^{1118}; $trpm^3$/CyO null mutant strain was isolated from progenies of *trpm* germline-specific knockout females (Hu and Wolfner, 2019) crossed with

Sco/CyO balancer males. It carries an 8-base deletion in exon 3 that leads to a frameshift and premature stop codon. The *nos-GCaMP6m-attP2* line is as previously described (Hu and Wolfner, 2019). The following fly lines were obtained from Bloomington *Drosophila* Stock Center: *hsFLP*; *Adv*/*CyO* (6), *FRT42B*, ovo^{D} (4434), w^{1118}; [*FRT42B,* w^{+}], *L**/CyO (1958), FM7a; TM3 (36283), T(2;3)/CyO;TM3 (2475), w^{1118} (3605).

C.3 Results and Discussion

Recombination and crossing scheme to generate *FRT42B*, $trpm^{3}$ is shown in **Figure C.1 A-B**. The following crossing scheme is shown in **Figure C.1 C**. I successfully obtained Line A and B shown in **Figure C.1 C**. However, I did not obtain any progeny from the cross between them. It is possible that multiple transgenes in one or both of the lines led to negative effects on their fertility. Thus, after a multi-generational crossing scheme, I was unable to obtain the final females that I needed for the experiment. As an alternative, I successfully created efficient *trpm* germline-specific CRISPR/Cas9 knockout females that expressed GCaMP in the germline to examine calcium wave phenotype in *trpm* homozygous knockout oocytes (Chapter 2).

Figure C.1 Crossing schemes to create *trpm* germline clones for oocyte calcium imaging.

(A) Scheme of generating *FRT42B*, $trpm^{3}$ via recombination. (B) Crossing scheme to generate a *FRT42B*, $trpm^{3}$ stable line. (C) Crossing scheme to generate *trpm* germline clones using the dominant female sterile technique. The final experimental females also express GCaMP in the germline to allow calcium wave imaging.

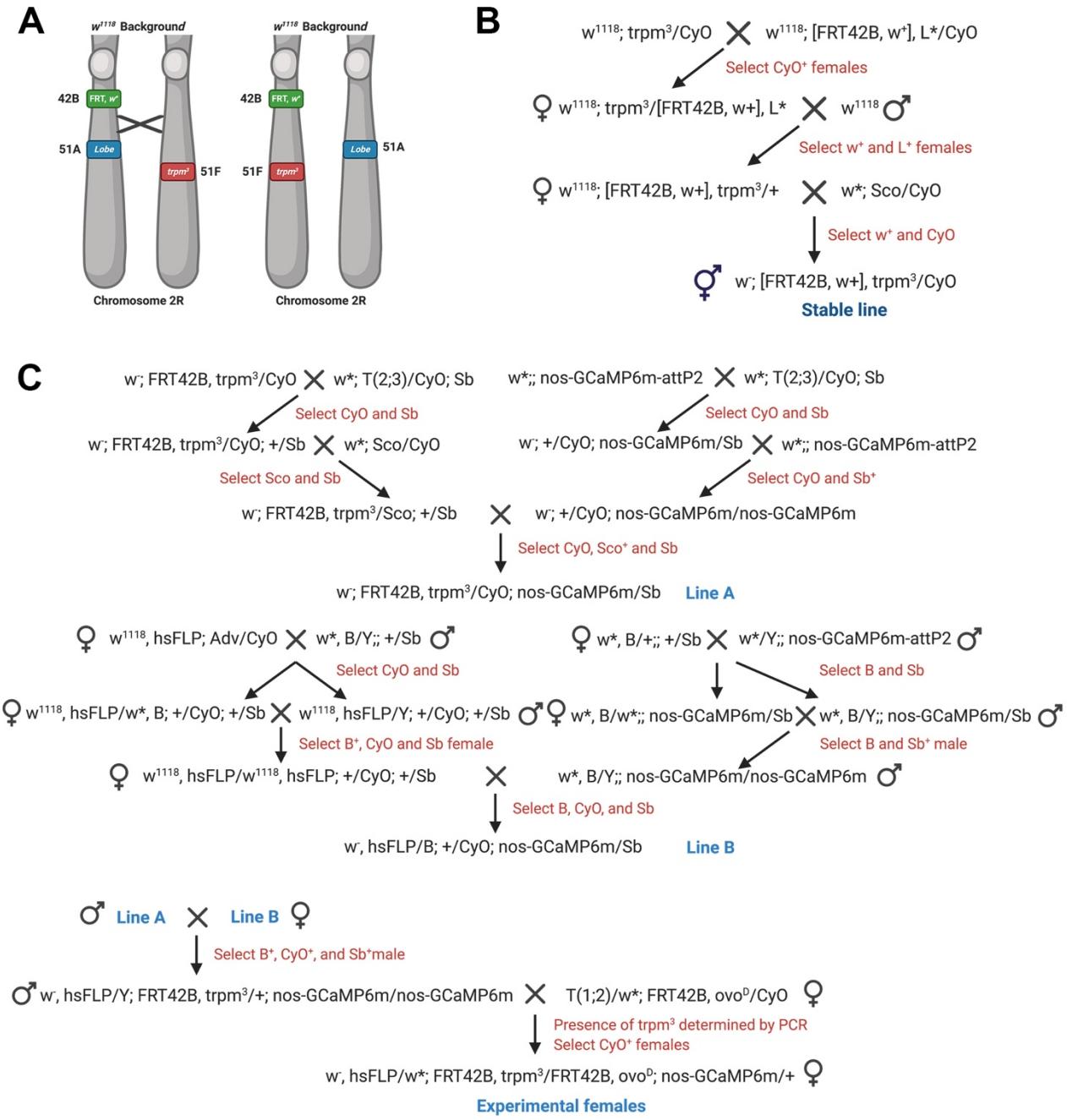
A
w1118 Background
42B
FRT, w+
51A
Lobe
trpm3
51F
Chromosome 2R
w1118 Background
42B
FRT, w+
51F
trpm3
Lobe
51A
Chromosome 2R
B
w1118; trpm3/CyO
w1118; [FRT42B, w+], L*/CyO
Select CyO+ females
w1118; trpm3/[FRT42B, w+], L*
w1118
Select w+ and L+ females
w1118; [FRT42B, w+], trpm3/+
w*; Sco/CyO
Select w+ and CyO
w-; [FRT42B, w+], trpm3/CyO
Stable line
C
w-; FRT42B, trpm3/CyO
w*; T(2;3)/CyO; Sb
Select CyO and Sb
w-; FRT42B, trpm3/CyO; +/Sb
w*; Sco/CyO
Select Sco and Sb
w-; FRT42B, trpm3/Sco; +/Sb
w*;; nos-GCaMP6m-attP2
w*; T(2;3)/CyO; Sb
Select CyO and Sb
w-; +/CyO; nos-GCaMP6m/Sb
w*;; nos-GCaMP6m-attP2
Select CyO and Sb+
w-; +/CyO; nos-GCaMP6m/nos-GCaMP6m
Select CyO, Sco+ and Sb
w-; FRT42B, trpm3/CyO; nos-GCaMP6m/Sb
Line A
w1118, hsFLP; Adv/CyO
w*, B/Y;; +/Sb
Select CyO and Sb
w1118, hsFLP/w*, B; +/CyO; +/Sb
w1118, hsFLP/Y; +/CyO; +/Sb
Select B+, CyO and Sb female
w1118, hsFLP/w1118, hsFLP; +/CyO; +/Sb
w*, B/+;; +/Sb
w*/Y;; nos-GCaMP6m-attP2
Select B and Sb
w*, B/w*;; nos-GCaMP6m/Sb
w*, B/Y;; nos-GCaMP6m/Sb
Select B and Sb+ male
w*, B/Y;; nos-GCaMP6m/nos-GCaMP6m
Select B, CyO, and Sb
w-, hsFLP/B; +/CyO; nos-GCaMP6m/Sb
Line B
Line A
Line B
Select B+, CyO+, and Sb+male
w-, hsFLP/Y; FRT42B, trpm3/+; nos-GCaMP6m/nos-GCaMP6m
T(1;2)/w*; FRT42B, ovoD/CyO
Presence of trpm3 determined by PCR
Select CyO+ females
w-, hsFLP/w*; FRT42B, trpm3/FRT42B, ovoD; nos-GCaMP6m/+
Experimental females

REFERENCES

Acquaviva, C., and Pines, J. (2006). The anaphase-promoting complex/cyclosome: APC/C. J. Cell Sci. *119*, 2401–2404.

Apoorva, F.N.U., Tian, Y.F., Pierpont, T.M., Bassen, D.M., Cerchietti, L., Butcher, J.T., Weiss, R.S., and Singh, A. (2017). Lymph node stiffness-mimicking hydrogels regulate human B-cell lymphoma growth and cell surface receptor expression in a molecular subtype-specific manner. J. Biomed. Mater. Res. Part A *105*, 1833–1844.

Avila, F.W., Sirot, L.K., LaFlamme, B.A., Rubinstein, C.D., and Wolfner, M.F. (2010). Insect Seminal Fluid Proteins: Identification and Function. Annu. Rev. Entomol. *56*, 21–40.

Avilés-Pagán, E.E., and Orr-Weaver, T.L. (2018). Activating embryonic development in *Drosophila*. Semin. Cell Dev. Biol. *84*, 100–110.

Barnard, D.C., Ryan, K., Manley, J.L., and Richter, J.D. (2004). Symplekin and xGLD-2 Are Required for CPEB-Mediated Cytoplasmic Polyadenylation. Cell *119*, 641–651.

Bassett, A.R., Tibbit, C., Ponting, C.P., and Liu, J.-L. (2013). Highly efficient targeted mutagenesis of *Drosophila* with the CRISPR/Cas9 system. Cell Rep. *4*, 220–228.

Bastock, R., and St Johnston, D. (2008). *Drosophila* oogenesis. Curr. Biol. *18*, R1082–R1087.

Becker, K.A., and Hart, N.H. (1999). Reorganization of filamentous actin and myosin-II in zebrafish eggs correlates temporally and spatially with cortical granule exocytosis. J. Cell Sci. *112 (1)*, 97–110.

Bernhardt, M.L., Kong, B.Y., Kim, A.M., O'Halloran, T. V, and Woodruff, T.K. (2012). A zinc-dependent mechanism regulates meiotic progression in mammalian oocytes. Biol. Reprod. *86*, 111–114.

Bernhardt, M.L., Zhang, Y., Erxleben, C.F., Padilla-Banks, E., McDonough, C.E., Miao, Y.-L., Armstrong, D.L., and Williams, C.J. (2015). Ca_V3. 2 T-type channels mediate Ca^{2+} entry during oocyte maturation and following fertilization. J Cell Sci *128*, 4442–4452.

Bernhardt, M.L., Stein, P., Carvacho, I., Krapp, C., Ardestani, G., Mehregan, A., Umbach, D.M., Bartolomei, M.S., Fissore, R.A., and Williams, C.J. (2018). TRPM7 and $Ca_V3.2$ channels mediate Ca^{2+} influx required for egg activation at fertilization. Proc. Natl. Acad. Sci. U. S. A. *267*, 201810422.

Bernitt, E., Koh, C.G., Gov, N., and Döbereiner, H.-G. (2015). Dynamics of Actin Waves on Patterned Substrates: A Quantitative Analysis of Circular Dorsal Ruffles. PLoS One *10*, e0115857.

Bernitt, E., Döbereiner, H.-G., Gov, N.S., and Yochelis, A. (2017). Fronts and waves of actin polymerization in a bistability-based mechanism of circular dorsal ruffles. Nat. Commun. *8*, 1–8.

Blower, M.D., Daigle, T., Kaufman, T., and Karpen, G.H. (2006). *Drosophila* CENP-A mutations cause a BubR1-dependent early mitotic delay without normal localization of kinetochore components. PLoS Genet. *2*.

Boswell, R. (1985). tudor, a gene required for assembly of the germ plasm in *Drosophila melanogaster*. Cell *43*, 97–104.

Bretschneider, T., Anderson, K., Ecke, M., Müller-Taubenberger, A., Schroth-Diez, B., Ishikawa-Ankerhold, H.C., and Gerisch, G. (2009). The Three-Dimensional Dynamics of Actin Waves, a Model of Cytoskeletal Self-Organization. Biophys. J. *96*, 2888–2900.

Brodskiy, P.A., Wu, Q., Soundarrajan, D.K., Huizar, F.J., Chen, J., Liang, P., Narciso, C., Levis, M.K., Arredondo-Walsh, N., Chen, D.Z., et al. (2019). Decoding Calcium Signaling Dynamics during *Drosophila* Wing Disc Development. Biophys. J. *116*, 725–740.

Brönner, G., and Jäckle, H. (1991). Control and function of terminal gap gene activity in the posterior pole region of the *Drosophila* embryo. Mech. Dev. *35*, 205–211.

Brown, J.B., Boley, N., Eisman, R., May, G.E., Stoiber, M.H., Duff, M.O., Booth, B.W., Wen, J., Park, S., Suzuki, A.M., et al. (2014). Diversity and dynamics of the *Drosophila* transcriptome. Nature *512*, 393–399.

Busa, W.B., and Nuccitelli, R. (1985). An elevated free cytosolic Ca^{2+} wave follows fertilization in eggs of the frog, *Xenopus laevis*. J. Cell Biol. *100*, 1325–1329.

Buszczak, M., and Cooley, L. (2000). Eggs to die for: cell death during *Drosophila* oogenesis. Cell Death Differ. *7*, 1071–1074.

Calap-Quintana, P., González-Fernández, J., Sebastiá-Ortega, N., Llorens, V.J., and Moltó, D.M. (2017). *Drosophila melanogaster* Models of Metal-Related Human Diseases and Metal Toxicity. Int. J. Mol. Sci. *18*.

Caldamone, A.A., Freytag, M.K., Cockett, A.T.K., and Cockett, T.K. (1979). Seminal zinc and male infertility. Urology *13*, 280–281.

Carlson, A.E. (2019). Mechanical stimulation activates *Drosophila* eggs via Trpm channels. Proc. Natl. Acad. Sci. *116*, 18757–18758.

Carroll Jr, E.J., and Epel, D. (1975). Isolation and biological activity of the proteases released by sea urchin eggs following fertilization. Dev. Biol. *44*, 22–32.

Carvacho, I., Lee, H., Fissore, R.A., and Clapham, D.E. (2013). TRPV3 Channels mediate strontium-induced mouse-egg activation. Cell Rep. *5*, 1375–1386.

Carvacho, I., Ardestani, G., Lee, H.C., McGarvey, K., Fissore, R.A., and Lykke-Hartmann, K. (2016). TRPM7-like channels are functionally expressed in oocytes and modulate post-fertilization embryo development in mouse. Sci. Rep. *6*, 34236.

Case, L.B., and Waterman, C.M. (2011). Adhesive F-actin Waves: A Novel Integrin-Mediated Adhesion Complex Coupled to Ventral Actin Polymerization. PLoS One *6*, e26631.

Cavaliere, V., Taddei, C., and Gargiulo, G. (1998). Apoptosis of nurse cells at the late stages of oogenesis of *Drosophila melanogaster*. Dev. Genes Evol. *208*, 106–112.

Chari, R., Yeo, N.C., Chavez, A., and Church, G.M. (2017). sgRNA Scorer 2.0: A Species-Independent Model To Predict CRISPR/Cas9 Activity. ACS Synth. Biol. *6*, 902–904.

Cheeseman, L.P., Boulanger, J., Bond, L.M., and Schuh, M. (2016). Two pathways regulate cortical granule translocation to prevent polyspermy in mouse oocytes. Nat. Commun. *7*, 13726.

Chen, B., Gilbert, L.A., Cimini, B.A., Schnitzbauer, J., Zhang, W., Li, G.-W., Park, J., Blackburn, E.H., Weissman, J.S., and Qi, L.S. (2013). Dynamic imaging of genomic loci in living human cells by an optimized CRISPR/Cas system. Cell *155*, 1479–1491.

Chhabra, E.S., and Higgs, H.N. (2007). The many faces of actin: matching assembly factors with cellular structures. Nat. Cell Biol. *9*, 1110–1121.

Cho, S.W., Kim, S., Kim, Y., Kweon, J., Kim, H.S., Bae, S., and Kim, J.-S. (2014). Analysis of off-target effects of CRISPR/Cas-derived RNA-guided endonucleases and nickases. Genome Res. *24*, 132–141.

Chou, T.B., and Perrimon, N. (1996). The autosomal FLP-DFS technique for generating germline mosaics in *Drosophila melanogaster*. Genetics *144*, 1673–1679.

Christensen, A.P., and Corey, D.P. (2007). TRP channels in mechanosensation: direct or indirect activation? Nat. Rev. Neurosci. *8*, 510–521.

Chubanov, V., Mederos Y Schnitzler, M., Meißner, M., Schäfer, S., Abstiens, K., Hofmann, T., and Gudermann, T. (2012). Natural and synthetic modulators of SK (K ca2) potassium channels inhibit magnesium-dependent activity of the kinase-coupled cation channel TRPM7. Br. J. Pharmacol. *166*, 1357–1376.

Chun, J.T., Puppo, A., Vasilev, F., Gragnaniello, G., Garante, E., and Santella, L. (2010). The Biphasic Increase of PIP2 in the Fertilized Eggs of Starfish: New Roles in Actin Polymerization and Ca^{2+} Signaling. PLoS One *5*, e14100.

Clapham, D.E., Runnels, L.W., and Strübing, C. (2001). The TRP ion channel family. Nat. Rev. Neurosci. *2*, 387–396.

Clark, K., Langeslag, M., van Leeuwen, B., Ran, L., Ryazanov, A.G., Figdor, C.G., Moolenaar, W.H., Jalink, K., and van Leeuwen, F.N. (2006). TRPM7, a novel regulator of actomyosin contractility and cell adhesion. EMBO J. *25*, 290–301.

Cooper, J.A. (1987). Effects of cytochalasin and phalloidin on actin. J. Cell Biol. *105*, 1473–1478.

Coste, B., Xiao, B., Santos, J.S., Syeda, R., Grandl, J., Spencer, K.S., Kim, S.E., Schmidt, M., Mathur, J., Dubin, A.E., et al. Piezo proteins are pore-forming subunits of mechanically activated channels. Nature *483*, 176–181.

de Cuevas, M., and Spradling, A.C. (1998). Morphogenesis of the *Drosophila* fusome and its implications for oocyte specification. Development *125*, 2781–2789.

Cui, J., Sackton, K.L., Horner, V.L., Kumar, K.E., and Wolfner, M.F. (2008). Wispy, the *Drosophila* Homolog of GLD-2, Is Required During Oogenesis and Egg

Activation. Genetics *178*, 2017–2029.

Cui, J., Sartain, C. V, Pleiss, J.A., and Wolfner, M.F. (2013). Cytoplasmic polyadenylation is a major mRNA regulator during oogenesis and egg activation in *Drosophila*. Dev. Biol. *383*, 121–131.

Cui, J., Lai, Y.W., Sartain, C. V, Zuckerman, R.M., and Wolfner, M.F. (2016). The *Drosophila* prage gene, required for maternal transcript destabilization in embryos, encodes a predicted RNA exonuclease. G3 Genes, Genomes, Genet. *6*, 1687–1693.

Dahlgaard, K., Raposo, A.A.S.F., Niccoli, T., and St Johnston, D. (2007). Capu and Spire Assemble a Cytoplasmic Actin Mesh that Maintains Microtubule Organization in the *Drosophila* Oocyte. Dev. Cell *13*, 539–553.

Deguchi, R. (2007). Fertilization causes a single Ca^{2+} increase that fully depends on Ca^{2+} influx in oocytes of limpets (Phylum Mollusca, Class Gastropoda). Dev. Biol. *304*, 652–663.

DeLuca, S.Z., and Spradling, A.C. (2018). Efficient Expression of Genes in the *Drosophila* Germline Using a UAS Promoter Free of Interference by Hsp70 piRNAs. Genetics *209*, 381–387.

Derrick, C.J., York-Andersen, A.H., and Weil, T.T. (2016). Imaging Calcium in *Drosophila* at Egg Activation. J. Vis. Exp. 54311.

Doench, J.G., Fusi, N., Sullender, M., Hegde, M., Vaimberg, E.W., Donovan, K.F., Smith, I., Tothova, Z., Wilen, C., Orchard, R., et al. (2016). Optimized sgRNA design to maximize activity and minimize off-target effects of CRISPR-Cas9. Nat. Biotechnol. *34*, 184–191.

Doudna, J.A., and Charpentier, E. (2014). The new frontier of genome engineering with CRISPR-Cas9. Science. *346*, 1258096.

Ducibella, T., Huneau, D., Angelichio, E., Xu, Z., Schultz, R.M., Kopf, G.S., Fissore, R., Madoux, S., and Ozil, J.P. (2002). Egg-to-embryo transition is driven by differential responses to Ca^{2+} oscillation number. Dev. Biol. *250*, 280–291.

Duffy, J.B. (2002). GAL4 system indrosophila: A fly geneticist's swiss army knife. Genesis *34*, 1–15.

Duncan, F.E., Que, E.L., Zhang, N., Feinberg, E.C., O'Halloran, T. V, and Woodruff,

T.K. (2016). The zinc spark is an inorganic signature of human egg activation. Sci. Rep. *6*, 24737.

Dunphy, W.G., Brizuela, L., Beach, D., and Newport, J. (1988). The *Xenopus* cdc2 protein is a component of MPF, a cytoplasmic regulator of mitosis. Cell *54*, 423–431.

Edwards, K.A., Demsky, M., Montague, R.A., Weymouth, N., and Kiehart, D.P. (1997). GFP-Moesin Illuminates Actin Cytoskeleton Dynamics in Living Tissue and Demonstrates Cell Shape Changes during Morphogenesis in*Drosophila*. Dev. Biol. *191*, 103–117.

Egli, D., Selvaraj, A., Yepiskoposyan, H., Zhang, B., Hafen, E., Georgiev, O., and Schaffner, W. (2003). Knockout of 'metal-responsive transcription factor' MTF-1 in *Drosophila* by homologous recombination reveals its central role in heavy metal homeostasis. EMBO J *22*, 100.

Eno, C., Solanki, B., and Pelegri, F. (2016). aura(mid1ip1l) regulates the cytoskeleton at the zebrafish egg-to-embryo transition. Development *143*, 1585–1599.

Fan, H.-Y., and Sun, Q.-Y. (2004). Involvement of Mitogen-Activated Protein Kinase Cascade During Oocyte Maturation and Fertilization in Mammals1. Biol. Reprod. *70*, 535–547.

Fleig, A., and Chubanov, V. (2014). TRPM7 Mammalian Transient Receptor Potential (TRP) Cation Channels: Volume I, B. Nilius, and V. Flockerzi, eds. (Berlin, Heidelberg: Springer Berlin Heidelberg), pp. 521–546.

Frassinetti, S., Bronzetti, G., Caltavuturo, L., Cini, M., and Croce, C. Della (2006). The role of zinc in life: a review. J. Environ. Pathol. Toxicol. Oncol. *25*, 597–610.

Gadella, B.M., and Evans, J.P. (2011). Membrane Fusions During Mammalian Fertilization Cell Fusion in Health and Disease. T. Dittmar, and K.S. Zänker, eds. (Dordrecht: Springer Netherlands), pp. 65–80.

Gallicano, G.I. (1995). Protein kinase M, the cytosolic counterpart of protein kinase C, remodels the internal cytoskeleton of the mammalian egg during activation. Dev. Biol. *267*, 482–501.

Gandhi, S., Piacentino, M.L., Vieceli, F.M., and Bronner, M.E. (2017). Optimization of CRISPR/Cas9 genome editing for loss-of-function in the early chick embryo. Dev.

Biol. *432*, 86–97.

Georgiev, P., Okkenhaug, H., Drews, A., Wright, D., Lambert, S., Flick, M., Carta, V., Martel, C., Oberwinkler, J., and Raghu, P. (2010). TRPM Channels Mediate Zinc Homeostasis and Cellular Growth during *Drosophila* Larval Development. Cell Metab. *12*, 386–397.

Gilston, B.A., Wang, S., Marcus, M.D., Canalizo-Hernandez, M.A., Swindell, E.P., Xue, Y., Mondragon, A., and O'Halloran, T. V (2014). Structural and mechanistic basis of zinc regulation across the E. coli Zur regulon. PLoS Biol. *12*.

González-Reyes, A., Elliott, H., and St Johnston, D. (1995). Polarization of both major body axes in *Drosophila* by gurken-torpedo signalling. Nature *375*, 654–658.

Gorczyca, D.A., Younger, S., Meltzer, S., Kim, S.E., Cheng, L., Song, W., Lee, H.Y., Jan, L.Y., and Jan, Y.N. (2014). Identification of Ppk26, a DEG/ENaC Channel Functioning with Ppk1 in a Mutually Dependent Manner to Guide Locomotion Behavior in *Drosophila*. Cell Rep. *9*, 1446–1458.

Gould, M., and Stephano, J.L. (1989). How do sperm activate eggs in Urechis (as well as in polychaetes and molluscs)? In Mechanisms of Egg Activation, (Springer), pp. 201–214.

Gratz, S.J., Cummings, A.M., Nguyen, J.N., Hamm, D.C., Donohue, L.K., Harrison, M.M., Wildonger, J., and O'Connor-Giles, K.M. (2013). Genome engineering of *Drosophila* with the CRISPR RNA-guided Cas9 nuclease. Genetics *194*, 1029–1035.

Gratz, S.J., Ukken, F.P., Rubinstein, C.D., Thiede, G., Donohue, L.K., Cummings, A.M., and O'Connor-Giles, K.M. (2014). Highly specific and efficient CRISPR/Cas9-catalyzed homology-directed repair in *Drosophila*. Genetics *196*, 961–971.

Grevet, J.D., Lan, X., Hamagami, N., Edwards, C.R., Sankaranarayanan, L., Ji, X., Bhardwaj, S.K., Face, C.J., Posocco, D.F., Abdulmalik, O., et al. (2018). Domain-focused CRISPR screen identifies HRI as a fetal hemoglobin regulator in human erythroid cells. Science. *361*, 285–290.

Gulyas, B.J. (1980). Cortical granules of mammalian eggs. In International Review of Cytology, (Elsevier), pp. 357–392.

Guo, H., Garcia-Vedrenne, A.E., Isserlin, R., Lugowski, A., Morada, A., Sun, A.,

Miao, Y., Kuzmanov, U., Wan, C., and Ma, H. (2015). Phosphoproteomic network analysis in the sea urchin Strongylocentrotus purpuratus reveals new candidates in egg activation. Proteomics *15*, 4080–4095.

Gwanyanya, A., Amuzescu, B., Zakharov, S.I., Macianskiene, R., Sipido, K.R., Bolotina, V.M., Vereecke, J., and Mubagwa, K. (2004). Magnesium-inhibited, TRPM6/7-like channel in cardiac myocytes: permeation of divalent cations and pH-mediated regulation. J. Physiol. *559*, 761–776.

Hachem, A., Godwin, J., Ruas, M., Lee, H.C., Ferrer Buitrago, M., Ardestani, G., Bassett, A., Fox, S., Navarrete, F., de Sutter, P., et al. (2017). PLCζ is the physiological trigger of the Ca^{2+} oscillations that induce embryogenesis in mammals but conception can occur in its absence. Development *144*, 2914.

Häcker, U., and Perrimon, N. (1998). DRhoGEF2 encodes a member of the Dbl family of oncogenes and controls cell shape changes during gastrulation in *Drosophila*. Genes Dev. *12*, 274–284.

Hara, M., Petrova, B., and Orr-Weaver, T.L. (2017). Control of PNG kinase, a key regulator of mRNA translation, is coupled to meiosis completion at egg activation. Elife *6*, e22219.

Harada, K., Oita, E., and Chiba, K. (2003). Metaphase I arrest of starfish oocytes induced via the MAP kinase pathway is released by an increase of intracellular pH. Development *130*, 4581–4586.

Hart, N.H., and Collins, G.C. (1991). An electron-microscope and freeze-fracture study of the egg cortex of Brachydanio rerio. Cell Tissue Res. *265*, 317–328.

Harteneck, C., Frenzel, H., and Kraft, R. (2007). N-(p-Amylcinnamoyl)anthranilic Acid (ACA): A Phospholipase A2 Inhibitor and TRP Channel Blocker. Cardiovasc. Drug Rev. *25*, 61–75.

He, L., Si, G., Huang, J., Samuel, A.D.T., and Perrimon, N. (2018). Mechanical regulation of stem-cell differentiation by the stretch-activated Piezo channel. Nature *555*, 103–106.

Heifetz, Y., Yu, J., and Wolfner, M.F. (2001). Ovulation triggers activation of *Drosophila* oocytes. Dev. Biol. *234*, 416–424.

Hepler, P.K. (2016). The Cytoskeleton and Its Regulation by Calcium and Protons. Plant Physiol. *170*, 3–22.

Hester, J., Hanna-Rose, W., and Diaz, F. (2017). Zinc deficiency reduces fertility in *C. elegans* hermaphrodites and disrupts oogenesis and meiotic progression. Comp. Biochem. Physiol. Part C Toxicol. Pharmacol. *191*, 203–209.

Hofmann, T., Chubanov, V., Chen, X., Dietz, A.S., Gudermann, T., and Montell, C. (2010). *Drosophila* TRPM channel is essential for the control of extracellular magnesium levels. PLoS One *5*.

Horne-Badovinac, S., Hill, J., Gerlach, G., Menegas, W., and Bilder, D. (2012). A screen for round egg mutants in *Drosophila* identifies tricornered, furry, and misshapen as regulators of egg chamber elongation. G3 (Bethesda). *2*, 371–378.

Horner, V.L., and Wolfner, M.F. (2008a). Transitioning from egg to embryo: Triggers and mechanisms of egg activation. Dev. Dyn. *237*, 527–544.

Horner, V.L., and Wolfner, M.F. (2008b). Mechanical stimulation by osmotic and hydrostatic pressure activates *Drosophila* oocytes in vitro in a calcium-dependent manner. Dev. Biol. *316*, 100–109.

Horner, V.L., Czank, A., Jang, J.K., Singh, N., Williams, B.C., Puro, J., Kubli, E., Hanes, S.D., Mckim, K.S., Wolfner, M.F., et al. (2006). The *Drosophila* Calcipressin Sarah Is Required for Several Aspects of Egg Activation. Med. Eng. Phys. *16*, 1441–1446.

Horvath, P., and Barrangou, R. (2010). CRISPR/Cas, the immune system of bacteria and archaea. Science. *327*, 167–170.

Hu, Q., and Wolfner, M.F. (2019). The *Drosophila* Trpm channel mediates calcium influx during egg activation. Proc. Natl. Acad. Sci. *116*, 18994–19000.

Jaffe, L. a, Giusti, a F., Carroll, D.J., and Foltz, K.R. (2001). Ca^{2+} signalling during fertilization of echinoderm eggs. Semin. Cell Dev. Biol. *12*, 45–51.

Januschke, J., Gervais, L., Dass, S., Kaltschmidt, J.A., Lopez-Schier, H., Johnston, D.S., Brand, A.H., Roth, S., and Guichet, A. (2002). Polar transport in the *Drosophila* oocyte requires Dynein and Kinesin I cooperation. Curr. Biol. *12*, 1971–1981.

Jayadev, R., Kuk, C.Y., Low, S.H., and Murata-Hori, M. (2014). Calcium sensitivity

of α-actinin is required for equatorial actin assembly during cytokinesis. Cell Cycle *11*, 1929–1937.

Jensen, K.T., Fløe, L., Petersen, T.S., Huang, J., Xu, F., Bolund, L., Luo, Y., and Lin, L. (2017). Chromatin accessibility and guide sequence secondary structure affect CRISPR-Cas9 gene editing efficiency. FEBS Lett. *591*, 1892–1901.

Jiang, F., and Doudna, J.A. (2017). CRISPR–Cas9 structures and mechanisms. Annu. Rev. Biophys. *46*, 505–529.

Johnston, R.N., and Paul, M. (1977). Calcium influx following fertilization of Urechis caupo eggs. Dev. Biol. *57*, 364–374.

Kadamur, G., and Ross, E.M. (2013). Mammalian Phospholipase C. Annu. Rev. Physiol. *75*, 127–154.

Kaneuchi, T., Sartain, C. V, Takeo, S., Horner, V.L., Buehner, N.A., Aigaki, T., and Wolfner, M.F. (2015). Calcium waves occur as *Drosophila* oocytes activate. Proc. Natl. Acad. Sci. U. S. A. *112*, 791–796.

Kashir, J., Nomikos, M., Lai, F.A., and Swann, K. (2014). Sperm-induced Ca^{2+} release during egg activation in mammals. Biochem. Biophys. Res. Commun. *450*, 1204–1211.

Katan, M. (1998). Families of phosphoinositide-specific phospholipase C: structure and function. Biochim. Biophys. Acta - Mol. Cell Biol. Lipids *1436*, 5–17.

Khamviwath, V., Hu, J., and Othmer, H.G. (2013). A Continuum Model of Actin Waves in Dictyostelium discoideum. PLoS One *8*, e64272.

Kim, A.M., Vogt, S., O'Halloran, T. V, and Woodruff, T.K. (2010). Zinc availability regulates exit from meiosis in maturing mammalian oocytes. Nat. Chem. Biol. *6*, 674.

Kim, A.M., Bernhardt, M.L., Kong, B.Y., Ahn, R.W., Vogt, S., Woodruff, T.K., and Halloran, T.V.O. (2011). Zinc Sparks are Triggered by Fertilization and Facilitate Cell Cycle Resumption in Mammalian Eggs. ACS Chem. Biol. 716–723.

Kim, S.E., Coste, B., Chadha, A., Cook, B., and Patapoutian, A. (2012). The role of *Drosophila* Piezo in mechanical nociception. Nature *483*, 209–212.

Kline, D., and Kline, J.T. (1992). Repetitive calcium transients and the role of calcium in exocytosis and cell cycle activation in the mouse egg. Dev. Biol. *149*, 80–89.

Knapp, E., and Sun, J. (2017). Steroid signaling in mature follicles is important for *Drosophila* ovulation. Proc. Natl. Acad. Sci. *114*, 699–704.

Komuro, I., Kudo, S., Yamazaki, T., Zou, Y., Shiojima, I., and Yazaki, Y. (1996). Mechanical stretch activates the stress-activated protein kinases in cardiac myocytes. FASEB J. *10*, 631–636.

Kondo, S., and Ueda, R. (2013). Highly Improved Gene Targeting by Germline-Specific Cas9 Expression in *Drosophila* Genetics *195*, 715–721.

Kong, B.Y., Duncan, F.E., Que, E.L., Kim, A.M., O'Halloran, T. V, and Woodruff, T.K. (2014). Maternally-derived zinc transporters ZIP6 and ZIP10 drive the mammalian oocyte-to-egg transition. Mol. Hum. Reprod. *20*, 1077–1089.

Kong, B.Y., Duncan, F.E., Que, E.L., Xu, Y., Vogt, S., O'Halloran, T. V, and Woodruff, T.K. (2015). The inorganic anatomy of the mammalian preimplantation embryo and the requirement of zinc during the first mitotic divisions. Dev. Dyn. *244*, 935–947.

Kovar, D.R. (2000). Maize Profilin Isoforms Are Functionally Distinct. PLANT CELL ONLINE *12*, 583–598.

Krauchunas, A.R., and Wolfner, M.F. (2013). Molecular Changes During Egg Activation (Elsevier Inc.).

Krauchunas, A.R., Horner, V.L., and Wolfner, M.F. (2012). Protein phosphorylation changes reveal new candidates in the regulation of egg activation and early embryogenesis in D. *melanogaster*. Dev. Biol. *370*, 125–134.

Krauchunas, A.R., Sackton, K.L., and Wolfner, M.F. (2013). Phospho-regulation pathways during egg activation in *Drosophila melanogaster*. Genetics *195*, 171–180.

Kronja, I., Yuan, B., Eichhorn, S.W., Dzeyk, K., Krijgsveld, J., Bartel, D.P., and Orr-Weaver, T.L. (2014). Widespread Changes in the Posttranscriptional Landscape at the *Drosophila* Oocyte-to-Embryo Transition. Cell Rep. *7*, 1495–1508.

Kubota, H.Y., Yoshimoto, Y., Yoneda, M., and Hiramoto, Y. (1987). Free calcium wave upon activation in *Xenopus* eggs. Dev. Biol. *119*, 129–136.

Kugler, J.-M., and Lasko, P. (2014). Localization, anchoring and translational control of oskar, gurken, bicoidand nanosmRNA during *Drosophila* oogenesis. Fly (Austin).

3, 15–28.

Kvist, U., Björndahl, L., and Kjellberg, S. (1987). Sperm nuclear zinc, chromatin stability, and male fertility. Scanning Microsc. *1*, 1241–1247.

Kyozuka, K., Chun, J.T., Puppo, A., Gragnaniello, G., Garante, E., and Santella, L. (2008). Actin cytoskeleton modulates calcium signaling during maturation of starfish oocytes. Dev. Biol. *320*, 426–435.

Leader, D.P., Krause, S.A., Pandit, A., Davies, S.A., and Dow, J.A.T. (2017). FlyAtlas 2: a new version of the *Drosophila melanogaster* expression atlas with RNA-Seq, miRNA-Seq and sex-specific data. Nucleic Acids Res. *46*, D809–D815.

Lee, H.C., Yoon, S.-Y., Lykke-Hartmann, K., Fissore, R.A., and Carvacho, I. (2016). TRPV3 channels mediate Ca^{2+} influx induced by 2-APB in mouse eggs. Cell Calcium *59*, 21–31.

Lehman, W., Craig, R., and Vibert, P. (1994). Ca^{2+}-induced tropomyosin movement in Limulus thin filaments revealed by three-dimensional reconstruction. Nature *368*, 65–67.

Lewit-Bentley, A., and Réty, S. (2000). EF-hand calcium-binding proteins. Curr. Opin. Struct. Biol. *10*, 637–643.

Li, K., Ma, E., Zhang, J., Zhao, Y., and Zhang, X. (2016). Combination of Gal80ts and Gal4 flexibly manipulates the expression levels of UAS transgenes in *Drosophila*. Acta Entomol. Sin. *59*, 481–488.

Lin, H., Yue, L., and Spradling, A.C. (1994). The *Drosophila* fusome, a germline-specific organelle, contains membrane skeletal proteins and functions in cyst formation. Development *120*, 947–956.

Lindsay, L.L., Hertzler, P.L., and Clark, W.H. (1992). Extracellular Mg^{2+} induces an intracellular Ca^{2+} wave during oocyte activation in the marine shrimp Sicyonia ingentis. Dev. Biol. *152*, 94–102.

Liu, J., and Maller, J.L. (2005). Calcium elevation at fertilization coordinates phosphorylation of XErp1/Emi2 by Plx1 and CaMK II to release metaphase arrest by cytostatic factor. Curr. Biol. *15*, 1458–1468.

Liu, Y.-A.Y.-S., Liu, Y.-A.Y.-S., Huang, C.-J., Yen, M.-H., Tseng, C.-T., Chien, S.,

and Lee, O.K. (2015). Mechanosensitive TRPM7 mediates shear stress and modulates osteogenic differentiation of mesenchymal stromal cells through Osterix pathway. Sci. Rep. *5*, 16522.

Luo, J., Stewart, R., Berdeaux, R., and Hu, H. (2012). Tonic Inhibition of TRPV3 by Mg^{2+} in Mouse Epidermal Keratinocytes. J. Invest. Dermatol. *132*, 2158–2165.

Mahowald, A.P., and Boswell, R.E. (1983). Germ plasm and germ cell development in invertebrates. In Current Problems in Germ Cell Differentiation/the Seventh Symposium of the British Society for Developmental Biology; Edited by A. McLaren & CC Wylie, (Cambridge [Cambridge]: Cambridge University Press, c1983.), p.

Mahowald, A.P., Goralski, T.J., and Caulton, J.H. (1983). In vitro activation of *Drosophila* eggs. Dev. Biol. *98*, 437–445.

Markoulaki, S., Matson, S., Abbott, A.L., and Ducibella, T. (2003). Oscillatory CaMKII activity in mouse egg activation. Dev. Biol. *258*, 464–474.

Maruyama, T., Kanaji, T., Nakade, S., Kanno, T., and Mikoshiba, K. (1997). 2APB, 2-Aminoethoxydiphenyl Borate, a Membrane-Penetrable Modulator of Ins(1,4,5)P3-Induced Ca^{2+} Release. J. Biochem. *122*, 498–505.

McKearin, D.M., and Spradling, A.C. (1990). bag-of-marbles: a *Drosophila* gene required to initiate both male and female gametogenesis. Genes Dev. *4*, 2242–2251.

McLaughlin, J.M., and Bratu, D.P. (2015). *Drosophila melanogaster* Oogenesis: An Overview *Drosophila* Oogenesis: Methods and Protocols. D.P. Bratu, and G.P. McNeil, eds. (New York, NY: Springer New York), pp. 1–20.

Meltzer, H., Marom, E., Alyagor, I., Mayseless, O., Berkun, V., Segal-Gilboa, N., Unger, T., Luginbuhl, D., and Schuldiner, O. (2019). Tissue-specific (ts)CRISPR as an efficient strategy for in vivo screening in *Drosophila*. Nat. Commun. *10*, 2113.

Mendoza, A.D., Woodruff, T.K., Wignall, S.M., and O'Halloran, T. V (2017). Zinc availability during germline development impacts embryo viability in *Caenorhabditis elegans*. Comp. Biochem. Physiol. Part C Toxicol. Pharmacol. *191*, 194–202.

Miao, Y.L., and Williams, C.J. (2012). Calcium signaling in mammalian egg activation and embryo development: The influence of subcellular localization. Mol. Reprod. Dev. *79*, 742–756.

Millet, B. (1988). Gadolinium ion is an inhibitor suitable for testing the putative role of stretch-activated ion channels in geotropism and thigmotropism. Biophys. J. *53*, 115a.

Mochida, S., and Hunt, T. (2007). Calcineurin is required to release *Xenopus* egg extracts from meiotic M phase. Nature *449*, 336–340.

Montell, C. (2005). *Drosophila* TRP channels. Pflugers Arch. Eur. J. Physiol. *451*, 19–28.

Nagarkar-Jaiswal, S., Lee, P.T., Campbell, M.E., Chen, K., Anguiano-Zarate, S., Gutierrez, M.C., Busby, T., Lin, W.W., He, Y., Schulze, K.L., et al. (2015). A library of MiMICs allows tagging of genes and reversible, spatial and temporal knockdown of proteins in *Drosophila*. Elife *2015*, 1–28.

Nakanishi, T., Kubota, H., Ishibashi, N., Kumagai, S., Watanabe, H., Yamashita, M., Kashiwabara, S., Miyado, K., and Baba, T. (2006). Possible role of mouse poly (A) polymerase mGLD-2 during oocyte maturation. Dev. Biol. *289*, 115–126.

Ni, J.-Q., Markstein, M., Binari, R., Pfeiffer, B., Liu, L.-P., Villalta, C., Booker, M., Perkins, L., and Perrimon, N. (2008). Vector and parameters for targeted transgenic RNA interference in *Drosophila melanogaster*. Nat. Methods *5*, 49–51.

Ni, J.-Q., Zhou, R., Czech, B., Liu, L.-P., Holderbaum, L., Yang-Zhou, D., Shim, H.-S., Tao, R., Handler, D., and Karpowicz, P. (2011). A genome-scale shRNA resource for transgenic RNAi in *Drosophila*. Nat. Methods *8*, 405–407.

Nilius, B., and Voets, T. (2005). TRP channels: a TR (I) P through a world of multifunctional cation channels. Pflügers Arch. *451*, 1–10.

Nishiyama, T., Yoshizaki, N., Kishimoto, T., and Ohsumi, K. (2007). Transient activation of calcineurin is essential to initiate embryonic development in *Xenopus laevis*. Nature *449*, 341–345.

Oh, J.S., Susor, A., and Conti, M. (2011). Protein tyrosine kinase Wee1B is essential for metaphase II exit in mouse oocytes. Science. *332*, 462–465.

Page, A.W., and Orr-Weaver, T.L. (1997). Activation of the Meiotic Divisions in *Drosophila* Oocytes. Dev. Biol. *183*, 195–207.

Pepling, M.E., and Spradling, A.C. (2001). Mouse Ovarian Germ Cell Cysts Undergo

Programmed Breakdown to Form Primordial Follicles. Dev. Biol. *234*, 339–351.
Percival, S.S., and Layden-Patrice, M. (1992). HL-60 Cells Can Be Made Copper Deficient by Incubating with Tetraethylenepentamine. J. Nutr. *122*, 2424–2429.
Petri, W.H., Mindrinos, M.N., and Lombard, M.F. (1979). Independence of vitelline membrane and chorion cross-linking in the *Drosophila melanogaster* eggshell. J. Cell Biol *83*.
Poe, A.R., Wang, B., Sapar, M.L., Ji, H., Li, K., Onabajo, T., Fazliyeva, R., Gibbs, M., Qiu, Y., Hu, Y., et al. (2018). Robust CRISPR/Cas9-Mediated Tissue Specific Mutagenesis Reveals Gene Redundancy and Perdurance in *Drosophila*. Genetics genetics.301736.2018.
Ponton, F., Chapuis, M.-P., Pernice, M., Sword, G.A., and Simpson, S.J. (2011). Evaluation of potential reference genes for reverse transcription-qPCR studies of physiological responses in *Drosophila melanogaster*. J. Insect Physiol. *57*, 840–850.
Port, F., and Bullock, S.L. (2016). Augmenting CRISPR applications in *Drosophila* with tRNA-flanked sgRNAs. Nat. Methods *13*, 852–854.
Port, F., Chen, H.-M., Lee, T., and Bullock, S.L. (2014). Optimized CRISPR/Cas tools for efficient germline and somatic genome engineering in *Drosophila* Proc. Natl. Acad. Sci. *111*, E2967 LP-E2976.
Prebil, S.D., Slapšak, U., Pavšič, M., Ilc, G., Puž, V., de Almeida Ribeiro, E., Anrather, D., Hartl, M., Backman, L., Plavec, J., et al. (2016). Structure and calcium-binding studies of calmodulin-like domain of human non-muscle α-actinin-1. Sci. Rep. 1–13.
Presler, M., Van Itallie, E., Klein, A.M., Kunz, R., Coughlin, M.L., Peshkin, L., Gygi, S.P., Wühr, M., and Kirschner, M.W. (2017). Proteomics of phosphorylation and protein dynamics during fertilization and meiotic exit in the *Xenopus* egg. Proc. Natl. Acad. Sci. *114*, E10838–E10847.
Que, E.L., Bleher, R., Duncan, F.E., Kong, B.Y., Gleber, S.C., Vogt, S., Chen, S., Garwin, S.A., Bayer, A.R., Dravid, V.P., et al. (2014). Quantitative mapping of zinc fluxes in the mammalian egg reveals the origin of fertilization-induced zinc sparks. Nat. Chem. *7*, 130.

Que, E.L., Duncan, F.E., Bayer, A.R., Philips, S.J., Roth, E.W., Bleher, R., Gleber, S.C., Vogt, S., Woodruff, T.K., and O'Halloran, T. V (2017a). Zinc sparks induce physiochemical changes in the egg zona pellucida that prevent polyspermy. Integr. Biol. *9*, 135–144.

Que, E.L., Duncan, F.E., Bayer, A.R., Philips, S.J., Roth, E.W., Bleher, R., Gleber, S.C., Vogt, S., Woodruff, T.K., O'Halloran, T. V, et al. (2017b). Zinc sparks induce physiochemical changes in the egg zona pellucida that prevent polyspermy. Integr. Biol. *9*, 135–144.

Que, E.L., Duncan, F.E., Lee, H.C., Hornick, J.E., Vogt, S., Fissore, R.A., O'Halloran, T. V, and Woodruff, T.K. (2019). Bovine eggs release zinc in response to parthenogenetic and sperm-induced egg activation. Theriogenology *127*, 41–48.

Quinlan, M.E., Heuser, J.E., Kerkhoff, E., and Dyche Mullins, R. (2005). *Drosophila* Spire is an actin nucleation factor. Nature *433*, 382–388.

Radford, S.J., and McKim, K.S. (2016). Techniques for Imaging Prometaphase and Metaphase of Meiosis I in Fixed *Drosophila* Oocytes. J. Vis. Exp. 54666.

Rakow, T.L., and Shen, S.S. (1990). Multiple stores of calcium are released in the sea urchin egg during fertilization. Proc. Natl. Acad. Sci. *87*, 9285–9289.

Ran, F.A., Hsu, P.D., Wright, J., Agarwala, V., Scott, D.A., and Zhang, F. (2013). Genome engineering using the CRISPR-Cas9 system. Nat. Protoc. *8*, 2281.

Riedl, J., Crevenna, A.H., Kessenbrock, K., Yu, J.H., Neukirchen, D., Bista, M., Bradke, F., Jenne, D., Holak, T.A., Werb, Z., et al. (2008). Lifeact: a versatile marker to visualize F-actin. Nat. Methods *5*, 605–607.

Riesgo-Escovar, J., Raha, D., and Carlson, J.R. (1995). Requirement for a phospholipase C in odor response: overlap between olfaction and vision in *Drosophila*. Proc. Natl. Acad. Sci. *92*, 2864–2868.

Roohani, N., Hurrell, R., Kelishadi, R., and Schulin, R. (2013). Zinc and its importance for human health: An integrative review. J. Res. Med. Sci. *18*, 144–157.

Rørth, P. (1998). Gal4 in the *Drosophila* female germline. Mech. Dev. *78*, 113–118.

Rothwell, W.F., and Sullivan, W. (2007). Fixation of *Drosophila* embryos. Cold Spring Harb. Protoc.

Roux, M.M., Radeke, M.J., Goel, M., Mushegian, A., and Foltz, K.R. (2008). 2DE identification of proteins exhibiting turnover and phosphorylation dynamics during sea urchin egg activation. Dev. Biol. *313*, 630–647.

Sackton, K.L., Buehner, N.A., and Wolfner, M.F. (2014). Modulation of MAPK Activities During Egg Activation in *Drosophila*. Fly (Austin). *1*, 222–227.

Santella, L., Limatola, N., and Chun, J.T. (2015). Calcium and actin in the saga of awakening oocytes This review is dedicated to Professor Ernesto Carafoli. Biochem. Biophys. Res. Commun. *460*, 104–113.

Sartain, C. V., and Wolfner, M.F. (2013). Calcium and egg activation in *Drosophila*. Cell Calcium *53*, 10–15.

Saunders, C.M., Larman, M.G., Parrington, J., Cox, L.J., Royse, J., Blayney, L.M., Swann, K., and Lai, F.A. (2002). PLCζ: a sperm-specific trigger of Ca^{2+} oscillations in eggs and embryo development. Development *129*, 3533.

Schell, M.J., Erneux, C., and Irvine, R.F. (2001). Inositol 1,4,5-Trisphosphate 3-Kinase A Associates with F-actin and Dendritic Spines via Its N Terminus. J. Biol. Chem. *276*, 37537–37546.

Schindelin, J., Arganda-Carreras, I., Frise, E., Kaynig, V., Longair, M., Pietzsch, T., Preibisch, S., Rueden, C., Saalfeld, S., Schmid, B., et al. (2012). Fiji: an open-source platform for biological-image analysis. Nat. Methods *9*, 676–682.

Schweigel-Röntgen, M. (2014). Chapter Nine - The Families of Zinc (SLC30 and SLC39) and Copper (SLC31) Transporters. In Exchangers, M.O.B.T.-C.T. in M. Bevensee, ed. (Academic Press), pp. 321–355.

Sebo, Z.L., Lee, H.B., Peng, Y., and Guo, Y. (2014). A simplified and efficient germline-specific CRISPR/Cas9 system for *Drosophila* genomic engineering. Fly (Austin). *8*, 52–57.

Shamanski, F.L., and Orr-Weaver, T.L. (1991). The *Drosophila* plutonium and pan gu genes regulate entry into S phase at fertilization. Cell *66*, 1289–1300.

Shami Shah, A., Batrouni, A.G., Kim, D., Punyala, A., Cao, W., Han, C., Goldberg, M.L., Smolka, M.B., and Baskin, J.M. (2019). PLEKHA4/kramer Attenuates Dishevelled Ubiquitination to Modulate Wnt and Planar Cell Polarity Signaling. Cell

Rep. *27*, 2157-2170.e8.

Shearman, D.C.A. (2002). The Evolution of Sex Determination Systems in Dipteran Insects Other than *Drosophila*. Genetica *116*, 25–43.

Sjöblom, B., Salmazo, A., and Djinović-Carugo, K. (2008). α-Actinin structure and regulation. Cell. Mol. Life Sci. *65*, 2688–2701.

Spracklen, A.J., Kelpsch, D.J., Chen, X., Spracklen, C.N., and Tootle, T.L. (2014a). Prostaglandins temporally regulate cytoplasmic actin bundle formation during *Drosophila* oogenesis. MBoC *25*, 397–411.

Spracklen, A.J., Fagan, T.N., Lovander, K.E., and Tootle, T.L. (2014b). The pros and cons of common actin labeling tools for visualizing actin dynamics during *Drosophila* oogenesis. Dev. Biol. *393*, 209–226.

Stark, C., Breitkreutz, B.-J., Reguly, T., Boucher, L., Breitkreutz, A., and Tyers, M. (2006). BioGRID: a general repository for interaction datasets. Nucleic Acids Res. *34*, D535–D539.

von Stetina, J.R., and Orr-Weaver, T.L. (2011). Developmental control of oocyte maturation and egg activation in metazoan models. Cold Spring Harb. Perspect. Biol. *3*, 1–19.

Stolfi, A., Gandhi, S., Salek, F., and Christiaen, L. (2014). Tissue-specific genome editing in Ciona embryos by CRISPR/Cas9. Development *141*, 4115–4120.

Stricker, S.A. (2014). Calcium signaling and endoplasmic reticulum dynamics during fertilization in marine protostome worms belonging to the phylum Nemertea. Biochem. Biophys. Res. Commun. *450*, 1182–1187.

Suzuki, T., Yoshida, N., Suzuki, E., Okuda, E., and Perry, A.C.F. (2010). Full-term mouse development by abolishing Zn^{2+}-dependent metaphase II arrest without Ca^{2+} release. Development *137*, 2659–2669.

Swann, K., and Lai, F.A. (2013). PLCζ and the initiation of Ca^{2+} oscillations in fertilizing mammalian eggs. Cell Calcium *53*, 55–62.

Swann, K., and Lai, F.A. (2016). Egg Activation at Fertilization by a Soluble Sperm Protein. Physiol. Rev. *96*, 127–149.

Szent-Györgyi, A.G. (1975). Calcium regulation of muscle contraction. Biophys. J.

15, 707–723.

Tadros, W., Goldman, A.L., Babak, T., Menzies, F., Vardy, L., Orr-Weaver, T., Hughes, T.R., Westwood, J.T., Smibert, C.A., and Lipshitz, H.D. (2007). SMAUG Is a Major Regulator of Maternal mRNA Destabilization in *Drosophila* and Its Translation Is Activated by the PAN GU Kinase. Dev. Cell *12*, 143–155.

Takayama, J., and Onami, S. (2016). The Sperm TRP-3 Channel Mediates the Onset of a Article The Sperm TRP-3 Channel Mediates the Onset of a Ca^{2+} Wave in the Fertilized *C . elegans* Oocyte. Cell Rep. *15*, 625-637.

Takeo, S., Tsuda, M., Akahori, S., Matsuo, T., and Aigaki, T. (2006). The Calcineurin Regulator Sra Plays an Essential Role in Female Meiosis in *Drosophila*. Med. Eng. Phys. *16*, 1435–1440.

Takeo, S., Hawley, R.S., and Aigaki, T. (2010). Calcineurin and its regulation by Sra/RCAN is required for completion of meiosis in *Drosophila*. Dev. Biol. *344*, 957–967.

Takeo, S., Swanson, S.K., Nandanan, K., Nakai, Y., Aigaki, T., Washburn, M.P., Florens, L., and Hawley, R.S. (2012). Shaggy/glycogen synthase kinase 3β and phosphorylation of Sarah/regulator of calcineurin are essential for completion of *Drosophila* female meiosis. Proc. Natl. Acad. Sci. *109*, 6382–6389.

Tejeda-Guzmán, C., Rosas-Arellano, A., Kroll, T., Webb, S.M., Barajas-Aceves, M., Osorio, B., and Missirlis, F. (2018). Biogenesis of zinc storage granules in *Drosophila melanogaster*. J. Exp. Biol. jeb.168419.

Theodosiou, N.A., and Xu, T. (1998). Use of FLP/FRT system to study *Drosophila* development. Methods *14*, 355–365.

Tian, X., and Diaz, F.J. (2012). Zinc Depletion Causes Multiple Defects in Ovarian Function during the Periovulatory Period in Mice. Endocrinology *153*, 873–886.

Tian, X., and Diaz, F.J. (2013). Acute dietary zinc deficiency before conception compromises oocyte epigenetic programming and disrupts embryonic development. Dev. Biol. *376*, 51–61.

Tian, X., Anthony, K., Neuberger, T., and Diaz, F.J. (2014). Preconception Zinc Deficiency Disrupts Postimplantation Fetal and Placental Development in Mice. Biol.

Reprod. *90*, 83-1.

Tilney, L.G. (1980). Actin, microvilli, and the fertilization cone of sea urchin eggs. J. Cell Biol. *87*, 771–782.

Tokmakov, A.A., Sato, K.-I., Iwasaki, T., and Fukami, Y. (2002). Src kinase induces calcium release in *Xenopus* egg extracts via PLCγ and IP3-dependent mechanism. Cell Calcium *32*, 11–20.

Tokuhiro, K., and Dean, J. (2018). Glycan-Independent Gamete Recognition Triggers Egg Zinc Sparks and ZP2 Cleavage to Prevent Polyspermy. Dev. Cell *46*, 627-640.e5.

Tominaga, M., Kojima, H., Yokota, E., Nakamori, R., Anson, M., Shimmen, T., and Oiwa, K. (2012). Calcium-induced Mechanical Change in the Neck Domain Alters the Activity of Plant Myosin XI. J. Biol. Chem. *287*, 30711–30718.

Tomkowiak, M., Guerrier, P., and Krantic, S. (1997). Meiosis reinitiation of mussel oocytes involves L-type voltage-gated calcium channel. J. Cell. Biochem. *64*, 152–160.

Tracey, W.D., Wilson, R.I., Laurent, G., and Benzer, S. (2003). painless, a *Drosophila* gene essential for nociception. Cell *113*, 261–273.

Tran, S.L., and Welte, M.A. (2010). In-vivo Centrifugation of *Drosophila* Embryos. J. Vis. Exp. 1–8.

Tung, C., Ardon, F., Fiore, A.G., Suarez, S.S., and Wu, M. (2014). Cooperative roles of biological flow and surface topography in guiding sperm migration revealed by a microfluidic model. Lab Chip *14*, 1348–1356.

Turner, H.N., Armengol, K., Patel, A.A., Himmel, N.J., Sullivan, L., Iyer, S.C., Bhattacharya, S., Iyer, E.P.R., Landry, C., Galko, M.J., et al. (2016). The TRP Channels Pkd2, NompC, and Trpm Act in Cold-Sensing Neurons to Mediate Unique Aversive Behaviors to Noxious Cold in *Drosophila*. Curr. Biol. *26*, 3116–3128.

Vasilev, F., Chun, J.T., Gragnaniello, G., Garante, E., and Santella, L. (2012). Effects of Ionomycin on Egg Activation and Early Development in Starfish. PLoS One *7*, e39231.

Veksler, A., and Gov, N.S. (2009). Calcium-Actin Waves and Oscillations of Cellular Membranes. Biophys. J. *97*, 1558–1568.

Venkatachalam, K., Long, A.A., Elsaesser, R., Nikolaeva, D., Broadie, K., and Montell, C. (2008). Motor Deficit in a *Drosophila* Model of Mucolipidosis Type IV due to Defective Clearance of Apoptotic Cells. Cell *135*, 838–851.

Vidali, L., and Hepler, P.K. (2001). Actin and pollen tube growth. Protoplasma *215*, 64–76.

Viktorinová, I., König, T., Schlichting, K., and Dahmann, C. (2009). The cadherin Fat2 is required for planar cell polarity in the *Drosophila* ovary. Development *136*, 4123–4132.

Vogt, S. (2003). MAPS : A set of software tools for analysis and visualization of 3D X-ray fluorescence data sets. J. Phys. IV *104*, 635–638.

Volkers, L., Mechioukhi, Y., and Coste, B. (2015). Piezo channels: from structure to function. Pflügers Arch. J. Physiol. *467*, 95–99.

Wakai, T., and Fissore, R.A. (2013). Ca^{2+} homeostasis and regulation of ER Ca^{2+} in mammalian oocytes/eggs. Cell Calcium *53*, 63–67.

Wakayama, T., Perry, A.C.F., Zuccotti, M., Johnson, K.R., and Yanagimachi, R. (1998). Full-term development of mice from enucleated oocytes injected with cumulus cell nuclei. Nature *394*, 369–374.

Walsh, T.P., Weber, A., Davis, K., Bonder, E., and Mooseker, M. (1984). Calcium dependence of villin-induced actin depolymerization. Biochemistry *23*, 6099–6102.

Wang, Y., and Riechmann, V. (2007). The Role of the Actomyosin Cytoskeleton in Coordination of Tissue Growth during *Drosophila* Oogenesis. Med. Eng. Phys. *17*, 1349–1355.

Weigel, D., Jürgens, G., Küttner, F., Seifert, E., and Jäckle, H. (1989). The homeotic gene fork head encodes a nuclear protein and is expressed in the terminal regions of the *Drosophila* embryo. Cell *57*, 645–658.

Weil, T.T., Forrest, K.M., and Gavis, E.R. (2006). Localization of bicoid mRNA in late oocytes is maintained by continual active transport. Dev. Cell *11*, 251–262.

Weil, T.T., Parton, R., Davis, I., and Gavis, E.R. (2008). Changes in bicoid mRNA Anchoring Highlight Conserved Mechanisms during the Oocyte-to-Embryo Transition. Curr. Biol. *18*, 1055–1061.

Wellington, A., Emmons, S., James, B., Calley, J., Grover, M., Tolias, P., and Manseau, L. (1999). Spire contains actin binding domains and is related to ascidian posterior end mark-5. Development *126*, 5267.

Wu, J., Luo, H., and Wang, H. (2013). Germline Stem Cells. Curr. Top. Dev. Biol. *102*, 97–126.

Wu, J., Lewis, A.H., and Grandl, J. (2017). Touch, tension, and transduction–the function and regulation of Piezo ion channels. Trends Biochem. Sci. *42*, 57–71.

Xiao, E., Yang, H., Gan, Y.-H., Duan, D.-H., He, L.-H., Guo, Y., Wang, S., and Zhang, Y. (2014). TRPM7 Senses Mechanical Stimulation Inducing Osteogenesis in Human Bone Marrow Mesenchymal Stem Cells. Stem Cells *33*, 615-621.

Xie, K., Minkenberg, B., and Yang, Y. (2015). Boosting CRISPR/Cas9 multiplex editing capability with the endogenous tRNA-processing system. Proc. Natl. Acad. Sci. U. S. A. *112*, 3570–3575.

Xue, Z., Wu, M., Wen, K., Ren, M., Long, L., Zhang, X., and Gao, G. (2014a). CRISPR / Cas9 Mediates Efficient Conditional Mutagenesis in *Drosophila*. G3 Genes|Genomes|Genetics *4*, 2167–2173.

Xue, Z., Ren, M., Wu, M., Dai, J., Rong, Y.S., and Gao, G. (2014b). Efficient Gene Knock-out and Knock-in with Transgenic Cas9 in *Drosophila* G3 Genes|Genomes|Genetics *4*, 925–929.

Yarmola, E.G., Somasundaram, T., Boring, T.A., Spector, I., and Bubb, M.R. (2000). Actin-Latrunculin A Structure and Function: Differential modulation of actin-binding protein function by latrunculin A. J. Biol. Chem. *275*, 28120–28127.

Yepiskoposyan, H., Egli, D., Fergestad, T., Selvaraj, A., Treiber, C., Multhaup, G., Georgiev, O., and Schaffner, W. (2006). Transcriptome response to heavy metal stress in *Drosophila* reveals a new zinc transporter that confers resistance to zinc. Nucleic Acids Res. *34*, 4866–4877.

York-Andersen, A.H., Parton, R.M., Bi, C.J., Bromley, C.L., Davis, I., and Weil, T.T. (2015). A single and rapid calcium wave at egg activation in *Drosophila*. Biol. Open *4*, 553–560.

York-Andersen, A.H., Hu, Q., Wood, B.W., Wolfner, M.F., and Weil, T.T. (2019). A

calcium-mediated actin redistribution at egg activation in *Drosophila*. Mol. Reprod. Dev. *n/a*.

Zallen, J.A., Cohen, Y., Hudson, A.M., Cooley, L., Wieschaus, E., and Schejter, E.D. (2002). SCAR is a primary regulator of Arp2/3-dependent morphological events in *Drosophila* J Cell Biol *156*, 689.

Zalokar, M. (1976). Autoradiographic study of protein and RNA formation during early development of *Drosophila* eggs. Dev. Biol. *49*, 425–437.

Zhang, N., Duncan, F.E., Que, E.L., O'Halloran, T. V, Woodruff, T.K., O'Halloran, T. V., and Woodruff, T.K. (2016). The fertilization-induced zinc spark is a novel biomarker of mouse embryo quality and early development. Sci. Rep. *6*, 22772.

Zhang, Z., Ahmed-Braimah, Y., Goldberg, M.L., and Wolfner, M.F. (2018a). Calcineurin dependent protein phosphorylation changes during egg activation in *Drosophila melanogaster*. Mol Cell Proteomics mcp.RA118.001076.

Zhang, Z., Krauchunas, A.R., Huang, S., and Wolfner, M.F. (2018b). Maternal proteins that are phosphoregulated upon egg activation include crucial factors for oogenesis, egg activation and embryogenesis in *Drosophila melanogaster*. G3 Genes, Genomes, Genet. *8*, 3005–3018.